Changes in surface solar ultraviolet (UV) radiation related to changes in atmospheric conditions over South Africa

David Jean Du Preez

UNIVERSITEIT VAN PRETORIA
UNIVERSITY OF PRETORIA
YUNIBESITHI YA PRETORIA

UNIVERSITÉ DE LA RÉUNION

Changes in surface solar ultraviolet (UV) radiation related to changes in atmospheric conditions over South Africa

By

David Jean du Preez

Submitted in fulfilment of the requirements for the degree
Doctor of Philosophy (Meteorology)
in the Faculty of Natural and Agricultural Sciences
University of Pretoria

Supervisor: Dr Caradee Y. Wright

And

Docteur és Sciences (Physique de l'atmosphere)
Sciences Technologies Santé (ED542), Physique de l'Atmosphère,
Laboratoire de l'Atmosphère et des Cyclones – LACy UMR 8105
Université de La Réunion

Supervisor: Professor Hassan Bencherif

29 June 2021

Declaration

I, David Jean du Preez declare that the thesis which I hereby submit for the degree Doctor of Philosophy (Meteorology) at the University of Pretoria and Docteur és Sciences (Physique de l'atmosphere), Université de La Réunion is my own work and has not previously been submitted by me for a degree at these or any other tertiary institution.

Signature:

Date: 29 June 2021

Ethics statement

I, David Jean du Preez, whose name appears on the title of this thesis, has obtained for the research described in this work, the applicable research ethics approval. The ethics number is NAS024/2019.

The author declares that he has observed the ethical standards required in terms of the University of Pretoria's Code of Ethics for Researchers and the Policy Guidelines for Responsible Research.

Signature:

Date: 29 June 2021

Research output

Journal articles (Lead author)

du Preez, D. J., Ajtić, J. V., Bencherif, H., Bègue, N., Cadet, J. M., & Wright, C. Y. (2019). Spring and summer time ozone and solar ultraviolet radiation variations over Cape Point, South Africa. Annales Geophysicae, 37(2), 129-141. https://doi.org/10.5194/angeo-37-129-2019

- This published journal article has contributed to Chapter 3 of this thesis.

du Preez, D. J., Bencherif, H., Bègue, N., Clarisse, L., Hoffman, R. F., & Wright, C. Y. (2020). Investigating the Large-Scale Transport of a Volcanic Plume and the Impact on a Secondary Site. Atmosphere, 11(548). https://doi.org/10.3390/atmos11050548

- This published journal article has contributed to Chapter 4 of this thesis.

du Preez, D. J., A. V. Parisi, D. A. Millar, H. Bencherif & C. Y. Wright (2020). Comparison of GOME-2 UVA Satellite Data to Ground-Based UVA Measurements in South Africa. Photochemistry and Photobiology, 96, 1342-1349. https://doi.org/10.1111/php.13308

- The findings presented in this published journal article does not form part of the research presented in this thesis.

du Preez, D.J., Bencherif, H., Portafaix, T., Lamy, K., & Wright, C.Y. (2021). Solar Ultraviolet Radiation in Pretoria and Its Relations to Aerosols and Tropospheric Ozone during the Biomass Burning Season. Atmosphere, 12(2). https://doi.org/10.3390/atmos12020132

- This published journal article has contributed to Chapter 5 of this thesis.

du Preez, D.J., Wright, C.Y., Diffey, B.L., Roomaney, R.A. & Bencherif, H. (2021). Estimation of potential keratinocyte cancer risks from excess solar UVR exposure to inform sun exposure awareness programmes. Photochem and Photobio, Under-review

- The draft manuscript submitted to the journal, Photochemistry and Photobiology has been included in Chapter 6 of this thesis.

Journal articles (co-author)

Bègue, N., L. Shikwambana, H. Bencherif, J. Pallotta, J. Du Preez, M. Ranaivombola, S. Piketh & P. Formenti (2019). Statistical analysis of the long-range transport of the 2015 Calbuco volcanic eruption from ground-based and space-borne observations. Annales Geophysicae, 38, 395 – 420. https://doi.org/10.5194/angeo-38-395-2020

- The findings presented in this published journal article does not form part of the research presented in this thesis.

Bencherif, H., N. Bègue, D. K. Pinheiro, D. J. du Preez, J. M. Cadet, F. J. da Silva Lopez, L. Shikwambana, E. Landulfo, T. Vescovini, C. Labuschagne, J. J. Silva, V. Anabor, P. F. Coheur, N. Mbatha, J. Hadji-Lazaro, V. Sivakumar & C. Clerbaux (2020). Investigating the Long-Range Transport of Aerosol Plumes Following the Amazon Fires (August 2019): A Multi-Instrumental Approach from Ground-Based and Satellite Observations. Remote Sensing, 12(3846). https://doi.org/10.3390/rs12223846

- The findings presented in this published journal article does not form part of the research presented in this thesis.

Bencherif, H., A. M. Toihir, N. Mbatha, V. Sivakumar, D. J. du Preez, N. Bègue & G. J. R. Coetzee (2020). Ozone Variability and Trend Estimates from 20-Years of Ground-Based and Satellite Observations at Irene Station, South Africa. Atmosphere, 11(1216). https://doi.org/10.3390/atmos11111216

- The findings presented in this published journal article does not form part of the research presented in this thesis.

Blesić, S. M., D. J. du Preez, D. I. Stratimirović, J. V. Ajtić, M. C. Ramotsehoa, M. W. Allen & C. Y. Wright (2020). Characterization of personal solar ultraviolet radiation

exposure using detrended fluctuation analysis. Environmental Research, 182, 108976. https://doi.org/10.1016/j.envres.2019.108976

- The findings presented in this published journal article does not form part of the research presented in this thesis.

Cadet, J.-M., H. Bencherif, D. J. du Preez, T. Portafaix, N. Sultan-Bichat, M. Belus, C. Brogniez, F. Auriol, J.-M. Metzger, K. Ncongwane, G. J. R. Coetzee & C. Y. Wright (2019). Solar UV Radiation in Saint-Denis, La Réunion and Cape Town, South Africa: 10 years Climatology and Human Exposure Assessment at Altitude. Atmosphere, 10(10), 589. https://doi.org/10.3390/atmos10100589

- The findings presented in this published journal article does not form part of the research presented in this thesis.

Teare, J., A. Mathee, N. Naicker, C. Swanepoel, T. Kapwata, Y. Balakrishna, D. J. du Preez, D. A. Millar & C. Y. Wright (2020). Dwelling Characteristics Influence Indoor Temperature and May Pose Health Threats in LMICs. Annals of global health, 86(1), 91-91. https://doi.org/10.5334/aogh.2938

- The findings presented in this published journal article does not form part of the research presented in this thesis.

Wright, C. Y., D. J. du Preez, B. S. Martincigh, M. W. Allen, D. A. Millar, B. Wernecke & S. Blesic (2020). "A Comparison of Solar Ultraviolet Radiation Exposure in Urban Canyons in Venice, Italy and Johannesburg, South Africa. Photochemistry and Photobiology, 96, 1148-1153. https://doi.org/10.1111/php.13291

Wright, C. Y., D. J. du Preez, D. A. Millar & M. Norval (2020). The Epidemiology of Skin Cancer and Public Health Strategies for Its Prevention in Southern Africa. International journal of environmental research and public health, 17(3), 1017. https://doi.org/10.3390/ijerph17031017

- The findings presented in this published journal article does not form part of the research presented in this thesis.

Wright, C. Y., M. Norval, T. Kapwata, D. J. du Preez, B. Wernecke, B. M. Tod & W. I. Visser (2019). The Incidence of Skin Cancer in Relation to Climate Change in South Africa. Atmosphere, 10(10), 634. https://doi.org/10.3390/atmos10100634

- The findings presented in this published journal article does not form part of the research presented in this thesis.

Conference abstracts

du Preez, D. J., Bègue, N., Bencherif, H., Hoffman, R. & Wright, C.Y. (2019). The long-range transport of the Puyehue-Cordon Caulle volcanic eruption over the Southern Hemisphere. 35th Annual conference of the South African Society for Atmospheric Sciences. Vanderbijlpark, South Africa.

- The poster presentation at the 2019 South African Society for Atmospheric Science Conference, presented a section of the results are presented in Chapter 4 of this thesis.

du Preez, D. J., Bencherif, H., Portafaix, T. & Wright, C.Y. (2020). The radiative effect of aerosols and tropospheric ozone over Pretoria. 36th Annual conference of the South African Society for Atmospheric Sciences. Online.

- The oral presentation at the 2020 South African Society for Atmospheric Science Conference, presented a portion of the results are presented in Chapter 5 of this thesis.

du Preez, D. J., S. M. Blesić, C. Y. Wright, D. I. Stratimirović, J. V. Ajtić, M. W. Allen & H. Bencherif (2020). Characterization of human behavior in records of personal solar ultraviolet exposure records. EGU General Assembly 2020. Online.

- The oral poster presentation at the 202 online EGU conference, presented results from the publication “Characterization of personal solar ultraviolet radiation exposure using detrended fluctuation analysis” and does not form part of the research presented in this thesis.

Summary

Solar ultraviolet radiation (UVR) that reaches the surface of the Earth varies due to changes in atmospheric parameters such as cloud cover, ozone and aerosol concentrations. Personal exposure to excessive solar UVR has significant health implications for the human population including the development of skin cancers and certain cataracts. The research presented in this thesis aimed to quantify the effects of aerosols and ozone on surface UVR as well as to estimate the keratinocyte cancer risk posed to the public due to the exposure to solar UVR.

Stratospheric ozone is the most important atmospheric constituent for the absorption of incoming solar UVR. The annual formation of the Antarctic ozone hole has been found to affect stratospheric ozone levels around the Southern Hemisphere and result in increased UVR at the surface due to the passage of the polar vortex in the austral spring and summer. The radiative effect of aerosols from volcanic eruptions and biomass burning can significantly affect surface solar UVR levels. The effects of volcanic eruptions and biomass burning may not be limited to the source region but can be observed thousands of kilometres away.

Examining low-ozone events that occurred during the spring and summer months at Cape Point in South Africa, the origins of ozone poor-air masses were determined using a dynamical transport model. The origins of ozone-poor air masses at Cape Point were found to be mainly from sub-tropical regions in the lower stratosphere (435 K – 485 K) and rarely from the polar vortex in the high stratosphere (600 K). Furthermore, these low-ozone events contributed to increased surface UVR on clear-sky days.

Investigating the effect of aerosols from a volcanic eruption and biomass burning, indicated that volcanic eruptions could affect the aerosol loading at a distant secondary location. Increases in the aerosol loading could be attributed to the dispersion on the plume which was modelled with a dispersion model and observations from satellites. Using a radiative transfer model, the radiative effect of aerosols and tropospheric ozone during the biomass burning season was determined. Aerosols during the biomass burning season have a larger radiative

effect compared to tropospheric ozone. When compared to background conditions, tropospheric ozone accounted for changes in surface UVR of less than 1% where aerosols accounted for changes in surface UVR of up to 14%.

Using a novel method to develop a “weighting factor” a risk assessment of basal cell carcinoma (BCC) and squamous cell carcinoma (SCC) was conducted for individuals of different skin phototypes. The risk assessment used hypothetical scenarios of an indoor and outdoor worker in Cape Town. The assessment found that an outdoor worker was more at risk of BCC and SCC, especially those with fairer skin types.

Having demonstrated how changes in atmospheric parameters can affect surface UVR and the keratinocyte cancer risk posed to individuals, it is important to monitor atmospheric parameters to develop appropriate sun protection information and to target at-risk population groups for skin cancer prevention campaigns.

Sommaire

Le rayonnement solaire ultraviolet (UVR) qui atteint la surface de la Terre varie en raison des changements des paramètres atmosphériques tels que la couverture nuageuse, l'ozone ou les concentrations d'aérosols. L'exposition personnelle excessive à des rayons ultraviolets solaires a des incidences importantes sur la santé de la population humaine, notamment le développement de cancers de la peau et de certaines cataractes. Les recherches présentées dans cette thèse visaient à quantifier les effets des aérosols et de l'ozone sur les UV de surface, ainsi qu'à estimer le risque de cancer des kératinocytes posé au public en raison de l'exposition aux UV solaires.

L'ozone stratosphérique est le constituant atmosphérique le plus important pour l'absorption des rayons ultraviolets solaires entrants. Il a été démontré que la formation annuelle du trou d'ozone antarctique affecte les niveaux d'ozone stratosphérique dans l'hémisphère sud et entraîne une augmentation des rayons UV à la surface en raison du passage du vortex polaire au printemps et en été austral. L'effet radiatif des aérosols des éruptions volcaniques et de brulage de la biomasse

peut affecter de manière significative les niveaux du rayonnement solaire UV de surface. Les effets des éruptions volcaniques et du brulage de la biomasse ne se limitent pas aux régions sources, mais peuvent être observés à des milliers de kilomètres.

En examinant les événements de faible niveau d'ozone survenus au printemps et en été à Cape Point en Afrique du Sud, les origines des masses d'air pauvre en ozone ont été déterminées à l'aide d'un modèle de transport dynamique. Les origines des masses d'air pauvres en ozone à Cape Point provenaient principalement des régions subtropicales de la basse stratosphère (435 K - 485 K) et rarement du vortex polaire dans la haute stratosphère (600 K). De plus, ces événements à faible abondance en ozone ont contribué à une augmentation des rayons UV de surface par ciel clair.

L'étude de l'effet des aérosols provenant d'une éruption volcanique et de brulage de la biomasse a indiqué que les éruptions volcaniques peuvent augmenter la charge en aérosols aussi bien à la source qu'au-dessus de sites secondaire éloignés. La combinaison des observations et d'un modèle de transport ont montré que l'augmentation de la charge en aérosol résulte de dispersion et transport large-échelle des panaches. À l'aide d'un modèle de transfert radiatif, l'effet radiatif des aérosols et de l'ozone troposphérique durant la saison des feux en Afrique australe a été analysé et quantifié. Les aérosols pendant la saison des feux ont un effet radiatif plus important que celui de l'ozone troposphérique. Comparé aux conditions de fond, l'ozone troposphérique représentait des changements inférieurs à 1% de l'UV de surface, alors que les aérosols représentaient des changements allant jusqu'à 14%.

À l'aide d'une nouvelle méthode d'évaluation des risques, le risque de cancer des kératinocytes de scénarios hypothétiques de travailleurs en intérieur et en plein air du Cap a été évalué pour des individus de différents phototypes. L'évaluation a révélé que les travailleurs en extérieur sont les plus exposés, en particulier ceux qui avaient des types de peau plus clairs.

En utilisant une nouvelle méthode pour développer un « facteur de pondération », une évaluation des risques de carcinome basocellulaire (BCC) et de carcinome

épidermoïde (SCC) a été réalisée pour des individus de différents phototypes de peau. L'évaluation des risques a utilisé des scénarios hypothétiques d'un travailleur à l'intérieur et à l'extérieur, dans la région du Cap. L'évaluation a révélé qu'un travailleur en plein air était plus à risque de BCC et de SCC, en particulier ceux qui avaient la peau plus claire.

Après avoir démontré comment les modifications des paramètres atmosphériques peuvent affecter les rayons UV de surface et le risque de cancer des kératinocytes pour les deux groupes d'individus, il est important de surveiller les paramètres atmosphériques pour développer des informations appropriées sur des protections solaires adaptées par groupes de populations à risque et de les prendre en compte pour l'élaboration de campagnes de prévention du cancer de la peau.

Acknowledgements

I would like to acknowledge the funding that I received from the University of Pretoria, Campus France and the National Research Foundation of South Africa. Without their funding and continuous support, this research would not have been possible.

I would further like to thank the Department of Geography, Geoinformatics and Meteorology at the University of Pretoria and the Laboratoire de l'Atmosphère et des Cyclones (LACy) at the University of Réunion for providing the resources and office workspace.

For their contributions and support during my research, I would like to thank the South African Weather Service for providing solar ultraviolet radiation data, Nelson Bègue and Thierry Portafaix for their many hours of training and guidance. To my friends and family, your continued support and interest, big or small, has been invaluable in this journey.

Lastly, to my supervisors Caradee Wright and Hassan Bencherif, I am extremely grateful for the guidance and supervision that you have provided. Your insights, knowledge and experience have been invaluable. Without you, this would not have been possible and I am extremely grateful for your support.

Table of contents

List of abbreviations

AE	Ångström Exponent
AOD	Aerosol Optical Depth
BCC	Basal Cell Carcinoma
BDC	Brewer-Dobson Circulation
CALIPSO	Cloud Aerosol-Lidar and Infrared Pathfinder Satellite Observation
COL	Cut-Off Low
DU	Dobson Unit
FLEXPART	Flexible Particle
FST	Fitzpatrick Skin Phototype
GAW	Global Atmosphere Watch
GOME	Global Ozone Monitoring Experiment
HIV	Human Immunodeficiency Virus
HYSPLIT	Hybrid Single-Particle Lagrangian Integrated Trajectory
IASI	Infrared Atmospheric Sounding Interferometer
LOTUS	Long-term Ozone Trends and Uncertainties in Stratosphere
MIMOSA	Modèle Isentrope du transport Méso-échelle de l'Ozone Stratosphérique par Advection
MIMOSA-CHIM	Modèle Isentropique du transport Méso-échelle de l'ozone stratosphérique par advection avec CHIMIE
ODS	Ozone-Depleting Substance
OMI	Ozone Monitoring Instrument
PCCVC	Puyehue-Cordon Caulle Volcanic Complex
PFR	Precision-filter Radiometer
PSC	Polar Stratospheric Cloud
PV	Potential Vorticity
QBO	Quasi-Biennial Oscillation
RAF	Radiation Amplification Factor
SAFARI	Southern African Regional Science Initiative
SAWS	South African Weather Service
SED	Standard Erythemal Dose
SCC	Squamous Cell Carcinoma
SCP	Skin Cancer Phototype

SPF	Sun Protection Factor
SSA	Single Scattering Albedo
STE	Stratosphere-Troposphere Exchange
SZA	Solar Zenith Angle
TCO	Total Column Ozone
TROPOMI	Tropospheric Monitoring Instrument
TUV	Tropospheric Ultraviolet-Visible
UVI	UV Index
UVR	Ultraviolet Radiation
VOC	Volatile Organic Compound
WMO	World Meteorological Organization

List of Figures

List of Tables

Chapter 1 Introduction

1.1 Introduction

Solar ultraviolet radiation (UVR) reaching the surface of the Earth has potentially positive and negative impacts on human health with a large percentage of the global population living in regions which experience high levels of UVR in a year (Lucas et al., 2019). Solar UVR at the surface further affects terrestrial and aquatic ecosystems (Bornman et al., 2019; Williamson et al., 2019).

The amount of solar UVR reaching the Earth's surface is influenced by several factors such as ozone, aerosols, cloud cover etc (Lerche et al., 2017) – see section 1.2. The research presented in this thesis focussed on the effects of two of these atmospheric parameters, namely ozone and aerosols, on solar UVR at the surface in South Africa. South Africa is located between 22° and 34° South of the Equator and most of the interior of the country is situated on an inland plateau at an altitude greater than 1 000 m above sea level (Figure 1-1).

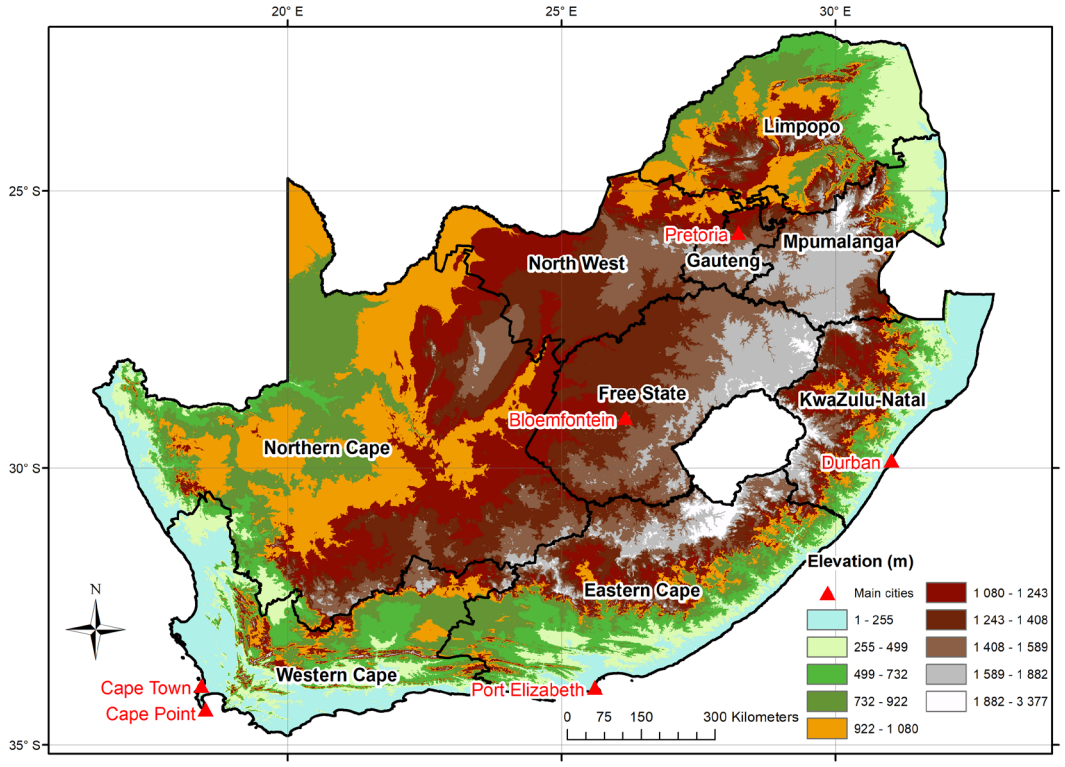

Figure 1-1. Provinces, main cities and elevation above sea-level of South Africa.

The latitude and elevation of South Africa result in high levels of surface UVR which can be experienced over large parts of the country. An analysis of surface solar UVR over South Africa found that 75% of daily noon observations can be categorised as high according to the UV Index (UVI) scale (Cadet et al., 2017). Excessive exposure to solar UVR affects human health and can result in the development of skin cancer and cataracts (Juzeniene et al., 2011; Lucas et al., 2019). In South Africa, skin cancer incidence rates are relatively high among population groups with lightly pigmented skin (Norval et al., 2014). Understanding how solar UVR is affected by various atmospheric factors and how different population groups are affected by skin cancer can improve targeted skin cancer prevention campaigns.

1.2 Solar UVR

Before the effects of ozone and aerosols on surface UVR can be investigated, it is important to understand what other factors affect surface UVR. Solar UVR is part of the electromagnetic spectrum with a wavelength band between 100 nm and 400 nm (Figure 1-2) (CCOH, 2016). Solar UVR is divided into three bands: UVA (315-400 nm), UVB (280-315 nm) and UVC (100-280 nm) due to the varying biological effects of UVR within these different bands (Madronich et al., 1998).

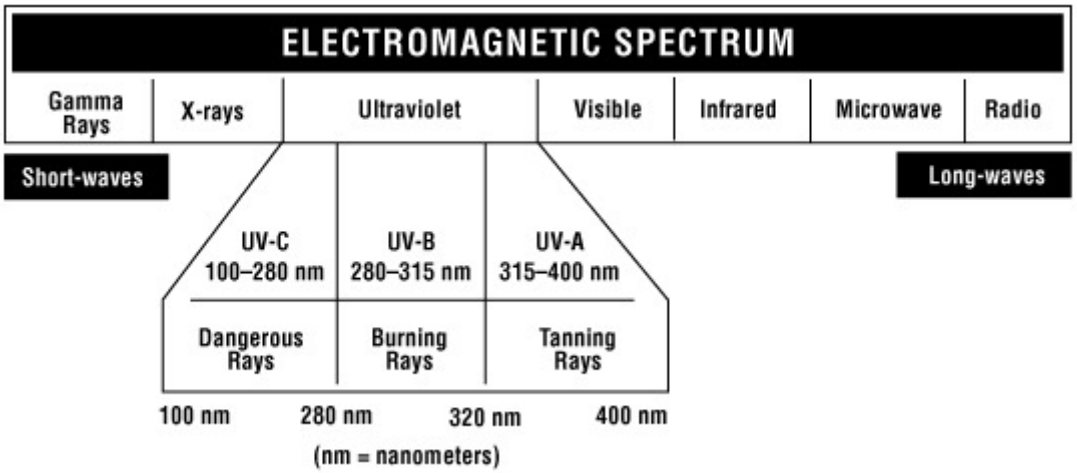

Figure 1-2. The electromagnetic spectrum and ultraviolet radiation subdivisions. (Retrieved from Canadian Centre for Occupational Health and Safety, accessed on 5 November 2020.)

UVB and UVA radiation can penetrate the atmosphere and has implications for human health. Due to the risks associated with personal exposure to solar UVR, the UVI (WHO, 2002) was developed to represent the strength of solar UVR at the

earth's surface and create public awareness. The index represents erythemally-weighted UVR (280-320 nm) and ranges between 1 and 11 (Fioletov et al., 2010) (Figure 1-3) (WHO, 2002).

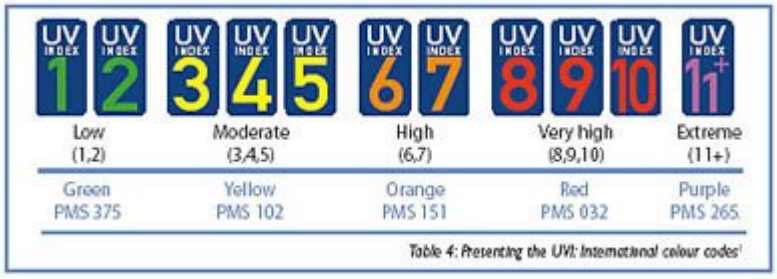

Figure 1-3. The Ultraviolet Index (UVI) values ranging from lowest to highest. (Retrieved from WHO report: Global solar UV index: a practical guide)

1.2.1 Factors affecting solar UVR at the Earth's surface

Factors affecting solar UVR at the surface vary with location, time and environmental conditions (Lerche et al., 2017). In the following subsections, several factors affecting solar UVR at the surface are discussed. These include solar zenith angle (SZA), latitude and altitude which are dependent on the specific location of a particular site.

1.2.1.1 SZA

The SZA is the angle measured from the surface between the Sun and a point directly above the observer (AmericanMeteorologicalSociety, 2019) (Figure 1-4). The SZA of the sun depends on the time of day, day of the year and geographical location (Diffey, 2002). At larger SZAs, UVR is lower as the path through the atmosphere is longer and results in more attenuation of UVR through the scattering and absorption by particles and gases in the atmosphere.

The SZA angle further influences the amount of solar UVR reaching a surface and is referred to as Lambert's Cosine Law. UVR reaching a surface at an included angle illuminates a larger area compared to UVR radiation from an orthogonal angle (Ryer, 1997).

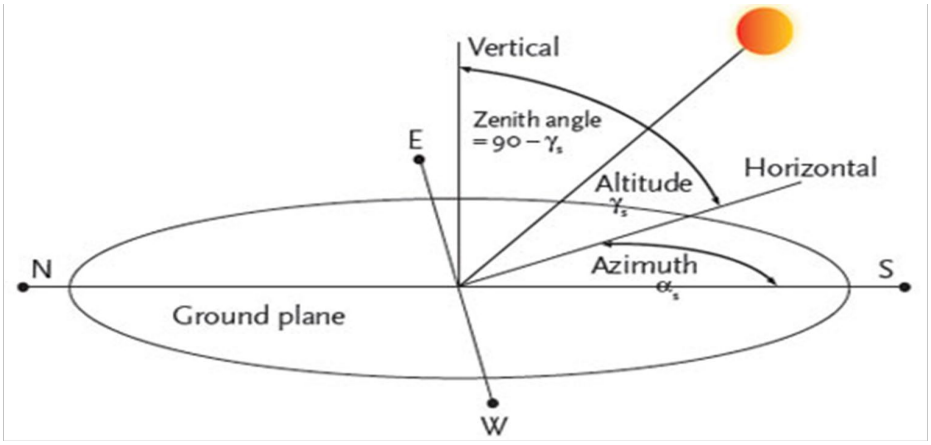

Figure 1-4. Diagram of the solar zenith angle position relative to the observer. (Retrieved from Glossary of Meteorology, American Meteorological Society, accessed 5 November 2020)

1.2.1.2 Latitude

At sites near the Equator where the minimum SZA approaches zero, UVR will be highest under clear-sky conditions (McKenzie et al., 2009). As a result, sites closer to the Equator experience higher UVR levels compared to sites closer to the poles. Therefore, comparing sites at different latitudes can result in large differences in the observed solar UVR.

1.2.1.3 Altitude

Solar UVR increases with altitude as the path that radiation has to travel through the atmosphere is shorter and therefore less scattering and absorption can occur (Sola et al., 2008). Furthermore, in high altitude regions where the surface is covered by snow and surface albedo is high may experience enhanced UVR (Kylling et al., 2000).

The composition of the atmosphere changes with altitude. As altitude increases, the composition of the atmosphere changes and pressure decreases almost exponentially due to the hydrostatic balance (Madronich, 1993). As the number of air molecules decreases, UVR can increase. This is referred to as the altitude effect and is dependent on the extinction properties of aerosols, clouds, ozone and albedo (Pfeifer et al., 2006). In the troposphere, UVR can increase between 5 - 40% per kilometre (Alexandris et

al., 1999). The absorption of UVB radiation by stratospheric ozone increases as the wavelength of solar UVR decreases (Fioletov et al., 2010).

1.2.1.4 Cloud cover

Cloud cover affects the variability of solar UVR at the surface (Bodeker et al., 1996; Calbó et al., 2005). Due to the large difference in characteristics of clouds, it is important to understand the spatial, temporal and cloud type variability that influences the amount of solar UVR at the surface (Udelhofen et al., 1999). Depending on the cloud type, position of the cloud relative to the sun and geometry, partly cloudy skies can enhance or reduce solar UVR (Bodeker et al., 1996). The effects of atmospheric ozone and aerosols on solar UVR received at the Earth's surface are described in Sections 1.3 and 1.4, respectively.

1.3 Atmospheric ozone

Atmospheric ozone is an important factor for the attenuation of incoming solar UVR. Approximately 90% of atmospheric ozone is found in the stratosphere (Figure 1-5) (Bojkov, 1995) between 16 and 50 km and is associated with high potential vorticity (PV) (Bekki et al., 2009). PV is defined as the absolute circulation of an air parcel between two isentropic levels (Holton et al., 2012). In the stratosphere, solar UVR in the UVB and UVC bands is strongly absorbed by ozone and causes surface solar UVR to sharply decrease with decreasing wavelength (Fioletov et al., 2010).

Tropospheric ozone is found between the surface and 16 km above the surface. It is a short-lived chemical pollutant that can have impacts on public health (Monks et al., 2015). In the troposphere, the air is denser which increases the photon pathlengths due to Rayleigh scattering and ozone can absorb solar UVR due to Rayleigh scattering (Brühl et al., 1989; Madronich et al., 2011).

The total amount of ozone contained in a column of air is expressed a the Total column ozone (TCO) concentration (Hegglin et al., 2015). TCO measurements are usually given in Dobson Units (DU) and one Dobson unit is the number of ozone

molecules needed to create a layer of ozone that is 0.01 mm thick at standard temperature and pressure.

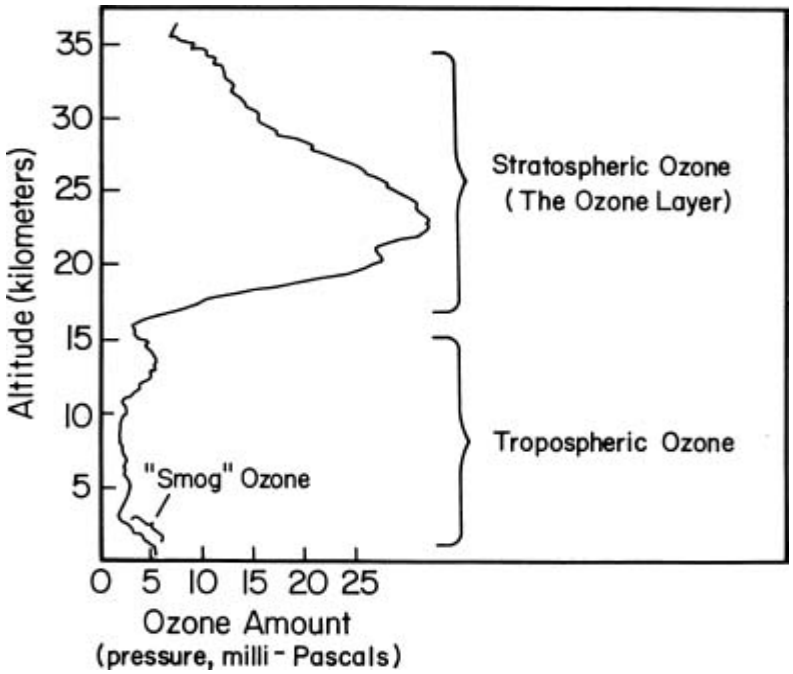

Figure 1-5. Typical ozone profile with stratospheric and tropospheric ozone ranges. (Retrieved from Scientific Ozone Assessment 1994)

In the following subsections 1.3.1 – 1.3.3, the formation of atmospheric ozone (tropospheric and stratospheric), the transport and the Antarctic ozone hole are discussed.

1.3.1 Ozone formation

The formation of stratospheric ozone is generally in equilibrium and forms through a photochemical reaction with sunlight and oxygen molecules (Hamill et al., 1991; Hegglin et al., 2015). The largest formation of stratospheric ozone occurs in the tropical stratosphere and is distributed through the atmosphere by various dynamical and chemical processes (Toihir et al., 2018; Weber et al., 2011). These processes can affect ozone concentrations in both the stratosphere and troposphere.

In the troposphere, ozone can originate from the stratosphere through stratosphere-troposphere exchange (STE) (Cooper et al., 2014) or form

through a chemical reaction involving ozone precursors in the presence of sunlight (Monks et al., 2015). These ozone precursors originate from natural and anthropogenic sources and include gaseous species such as nitrogen oxides (NOx), carbon monoxide (CO) and volatile organic compounds (VOCs) (Vakkari et al., 2014).

1.3.2 Ozone transport

Following the formation of stratospheric ozone in the subtropical stratosphere, stratospheric ozone is transported through various circulation systems. The Brewer-Dobson Circulation (BDC) (Figure 1-6) (Flury et al., 2013) refers to the circulation pattern where air masses from the troposphere enter the stratosphere in the tropics and are then moved upwards and poleward before the air masses descend in the middle and high latitudes (Butchart, 2014; Cohen et al., 2014). The BDC refers to the meridional overturning by wave-driven circulation (Cohen et al., 2014; Portafaix et al., 2003) and is responsible for the large-scale transport between the stratosphere and troposphere (Olsen et al., 2004).

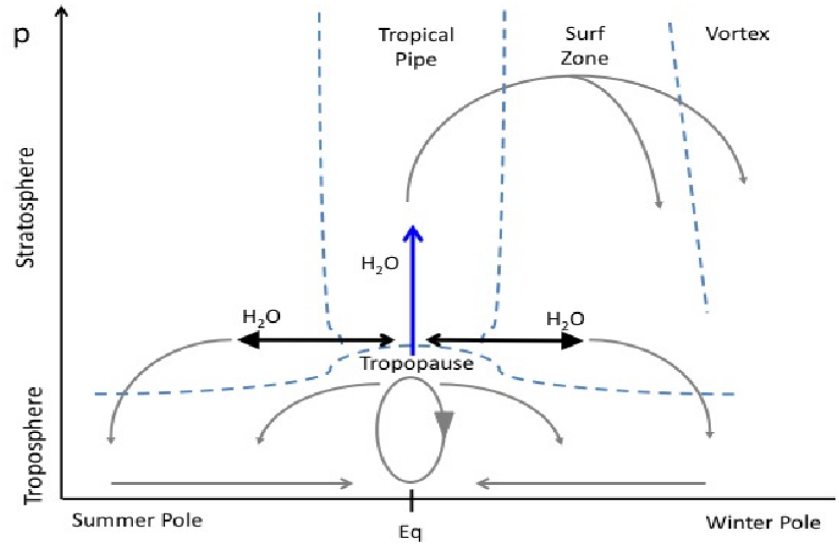

Figure 1-6. Diagram of the Brewer-Dobson Circulation. (Retrieved from Flury et. al., 2013 "Variability in the speed of the Brewer–Dobson circulation as observed by Aura/MLS")

The variability in the equatorial stratosphere is dominated by the Quasi-Biennial Oscillation (QBO). The QBO refers to the downward propagation on the easterly and westerly winds (zonal winds) averaged over 28 months (Baldwin et al., 2001; Pascoe et al., 2005). The interaction between the zonal mean flow and the equatorial planetary waves are responsible for the QBO (Plumb, 1977). The QBO affects the dynamics and chemical constitutions of the atmosphere as well as the stratospheric poleward flow of ozone outside of the tropics (Baldwin et al., 2001). Ozone concentrations in the lower stratosphere increase during the westerly phase of the QBO and decrease during the easterly phase (Kusuma et al., 2019).

While the meridional and zonal transport of stratospheric ozone can occur through the BDC and QBO, respectively. The vertical exchange of air masses and ozone between the stratosphere and troposphere can occur through STE as well. Stratosphere intrusions can transport air masses with high ozone and high PV levels to the troposphere (Mkololo et al., 2020). These stratospheric intrusions impact the chemical budget of the lower stratosphere and upper troposphere and last between 3 days and 2 weeks (Stohl et al., 2003b). In the midlatitude region, STE occurs with synoptic-scale and mesoscale processes and have been observed in tropopause folds and near the subtropical jet, polar jet and cut-off low systems (COL) (Stohl et al., 2003a). Rossby waves, QBO and cut-off lows have been shown to impact STE (Ndarana et al., 2010).

Over Southern Africa, COLs are most frequent during autumn and persist for between three to seven days. COLs play a role in STE which impacts tropospheric ozone level (Diab et al., 2004; Price et al., 1993). COL can result in STE through convection due to the deep convection associated with COLs, turbulence near the jet associated with a COL or tropopause folding (Price et al., 1993). In the Southern Hemisphere, Rossby wave breaking is a driving force between the split flow that is associated with COLs (Ndarana et al., 2010).

1.3.3 Ozone depletion

In Section 1.3, the importance of ozone in the atmosphere was described. The discovery of a region of extremely low ozone over Antarctica during the 1980s was of significant importance (Farman et al., 1985). This region of low ozone was referred to as the “Antarctica ozone hole” and is defined as an area where TCO concentrations are below 220 DU (Hegglin et al., 2015). During the austral winter over Antarctica, the ozone hole forms due to the combined effect of ozone depleting substances (ODS) and the unique meteorological conditions (Tully et al., 2011). As the polar vortex forms during autumn, air radiatively cools and Polar Stratospheric Cloud (PSC) particles develop which provides a surface on which chemical reactions can take place. During late winter, active halogen species from ODS undergo chemical reactions with sunlight and decrease ozone levels in the lower stratosphere (Klekociuk et al., 2015).

To limit the release of ODS and to slow the rate of stratospheric ozone depletion, the Montreal Protocol was adopted in 1987. Dynamical processes such as STE (Olsen et al., 2004) and the break-up of the Antarctic ozone hole during the austral spring and summer affect stratospheric ozone concentrations in the Southern Hemisphere (Ajtić et al., 2004; Bandoro et al., 2014). In Section 2.2.2, the effect of the Antarctic ozone hole on stratospheric ozone and surface UVR over the Southern Hemisphere is discussed.

1.3.4 Ozone recovery

Following the discovery of the Antarctic ozone hole and the implementation of the Montreal Protocol, atmospheric ozone levels have been monitored by various activities in the Global Atmosphere Watch (GAW) programme within the framework of the World Meteorological Organisation (WMO).

Since 2000, ODS levels in the stratosphere have been decreasing and increases of ozone in the upper stratosphere have been reported to be between approximately 2% - 4% per decade (Chipperfield et al., 2017). The lower stratosphere (13 - 24 km) is characterised by large seasonal variation in ozone. Between 60°N and 60°S, ozone in the lower stratosphere has continued

to decline (Ball et al., 2018). This negatively impacts the increase in stratospheric ozone reported above 25 km over the subtropics which has been reported in the Long-term Ozone Trends and Uncertainties in the Stratosphere (LOTUS) report (SPARC/IO3C/GAW, 2019). However, these increases in the upper stratosphere vary from region to region and the source of these increases is not clearly understood (SPARC/IO3C/GAW, 2019). Over the equatorial, tropical and subtropical regions of the Southern Hemisphere, there is a non-significant positive trend in TCO although in the 0°– 15°S region the trend is lower compared to regions south of 17°S (Toihir et al., 2018). Furthermore, tropospheric ozone has increased globally which may be responsible for the increase observed in TCO (Ball et al., 2018).

Stratospheric ozone depletion in the Southern Hemisphere has influenced atmospheric circulation patterns. The midlatitude jet has shifted poleward and has expanded the subtropical dry zone in the troposphere (Banerjee et al., 2020). This shift can be attributed to ozone depletion in the stratosphere. Temperatures in the stratosphere have decreased as ozone normally absorbs energy and heats the stratosphere. Since the early 2000s, the shift in the midlatitude jet has paused and coincided with the first detected sign of ozone recovery. Banerjee et al. are among the first authors to make this association between changes in atmospheric circulation and the Montreal Protocol (Banerjee et al., 2020; Karpechko, 2020).

Over Irene, South Africa, trends in ozone datasets have indicated that tropospheric ozone is increasing between 2.4% and 3.6% per decade (Bencherif et al., 2020; Clain et al., 2009; Thompson et al., 2014). While these increases in tropospheric ozone can slow down the decline in TCO, stratospheric ozone has continued to decline between 0.5% and 1.7% per decade (Bencherif et al., 2020).

1.4 Atmospheric aerosols

Apart from stratospheric ozone, atmospheric aerosols can attenuate incoming solar UVR and are predominantly found in the troposphere (Tesfaye et al., 2011).

Aerosols in the troposphere can impact human health and result in respiratory and cardiovascular illnesses and diseases (Pöschl, 2005).

1.4.1 Aerosol sources

The aerosol loading in the atmosphere, is affected by aerosols from natural (e.g., dust, sea salt, biomass burning, volcanoes) or anthropogenic sources (e.g., fossil fuel combustion, industry, biomass burning). These types of aerosols are referred to as primary aerosols (Haywood et al., 2000). Aerosols emitted from biomass burning or wildfires are one of the largest contributors of atmospheric aerosols (Vakkari et al., 2014) as well as volcanic eruptions which can inject large volumes of aerosols into the atmosphere (Roberts et al., 2018).

Physical and chemical processes in the atmosphere can lead to the formation of secondary aerosols from gaseous precursors (Haywood et al., 2000). Secondary aerosols include ammonium and nitrate aerosols. The formation of secondary aerosols is influenced by the release of primary aerosols from natural and anthropogenic emissions (Boucher et al., 2013).

1.4.2 The radiative effect of aerosols

Aerosols from natural or anthropogenic sources have a direct or indirect radiative effect on incoming solar UVR. The direct effect is through the scattering and absorption of solar UVR (Yu et al., 2006) while the indirect effect is the formation of clouds as aerosols act as cloud condensation nuclei (Lohmann et al., 2005) which can affect the amount of solar UVR reaching the surface.

The radiative effect of aerosols is dependent on their optical properties such as single scattering albedo (SSA), Ångström exponent (AE) and aerosol optical depth (AOD). SSA is a ratio of the scattering and extinction coefficients of aerosols (Moosmüller et al., 2018). SSA is an important factor in the radiative effect of aerosols and the impact of SSA is influenced by the AOD (Bais et al., 2002). AE is an estimate of the particle size which varies in size depending on the emission source (Eck et al., 1999) and determines the relationship between

wavelength and extinction (Schuster et al., 2006). AE values are inversely related to the size of the particle. AE values greater than one are associated with fine particles such as sulphate particles while values less than one are associated with coarse particles such as desert dust (O'Neill et al., 2001).

Furthermore, clouds and aerosols are responsible for the large variability in radiative forcing and aerosols further interact with clouds. Using effective radiative forcing which includes rapid and net forcings improve radiative forcing estimates from clouds and aerosols (IPCC, 2013).

1.4.3 Aerosol transport

Aerosols injected into the stratosphere through volcanic eruptions, biomass burning, and/or extreme wildfires can be transported across vast distances and are subjected to dynamical processes in the stratosphere (Bègue et al., 2017; Ohneiser et al., 2020). Similarly, in the troposphere where aerosols may be abundant, aerosols may be transported across oceans by prevailing winds (Diab et al., 2004). As a result, the radiative effect of aerosols is not limited to the source area but impacts the aerosol loading and solar UVR over areas downwind from the source area.

1.5 Solar UVR exposure and public health

Exposure to solar UVR by people has potential positive health impacts, such as the production of vitamin D which assists the functioning of the immune system, and negative health impacts such as sunburn (also known as erythema), skin cancer and cataracts (Lucas et al., 2019). Personal solar UVR exposure varies significantly from one individual to another due to factors such as occupation, age, personal preference of outdoor behaviour, clothing, sun protection and nature of the environment (Modenese et al., 2018; Schmalwieser et al., 2010).

Excessive exposure to UVB radiation is linked with sunburn and skin cancer while exposure to UVA radiation is linked with premature ageing of the skin (Dupont et al., 2013). Intermittent solar UVR exposure and chronic solar UVR exposure are linked to the development of basal cell carcinoma (BCC) and squamous cell carcinoma

(SCC), respectively (Watson et al., 2016). Both BCC and SCC are categorised as keratinocyte cancers (previously known as non-melanoma skin cancer). The majority of skin cancers start in the epidermis layer. BCCs start in the basal cell layer of the skin where cell continuously divide to replace the squamous cells that have worn off (Figure 1-7) while SCCs form in the epidermis (Gordon, 2013).

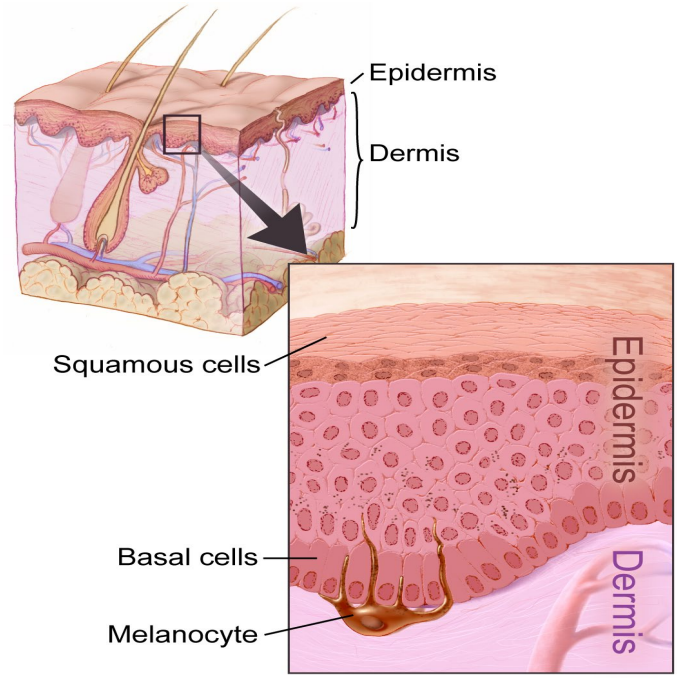

Figure 1-7. Anatomy of the human skin. (Retrieved American Cancer Association, accessed 5 November 2020)

Globally, there has been an increase in both melanoma and keratinocyte cancers (Leiter et al., 2014). The incidence of keratinocyte cancer is approximately 20 times higher than compared to melanoma, has a much lower morbidity rate compared to melanoma cancer but is associated with high treatment costs (Hay et al., 2014). The risk of melanoma skin cancer increases with age and is more common among the Caucasian population (AmericanCancerSociety). Around the globe, incidence rates have increased over the last decade with New Zealand reporting 50 cases per 100 000 persons (Apalla et al., 2017). In South Africa, the incidence of melanoma skin cancer is approximately 20 times higher in the white population compared to the Black African population (Norval et al., 2017). The incidence of melanoma skin cancer in South Africa is 4.76 per 100 000 for all people and 19.2 per 100 000 among the white population (Norval et al., 2017).

Keratinocyte cancer is 18-20 times more common than melanoma skin cancer (Apalla et al., 2017). The incidence of keratinocyte cancer varies around the world, but Australia has the highest incidence of BCC, reporting 1000 cases per 100 000 persons in 2011 with South Africa reporting 28.58 cases per 100 000 in 2012. The keratinocyte risk varies between individuals and is related to factors such as age, skin colour, gender, hair colour and prior skin cancer history influence skin cancer risk (Gordon, 2013; Thieden et al., 2004).

As mentioned in Section 1.1, South Africa experiences high solar UVR levels throughout the year. An improved understanding of the factors that affect surface solar UVR as well as identifying population groups at risk of developing skin cancer, for example, by using risk assessment tools (Diffey, 1992; Vishvakarman et al., 2003) can lead to improved decision-making and initiatives to raise public awareness of the dangers associated with excessive sun exposure.

1.6 Problem statement

How do atmospheric factors such as aerosols and stratospheric ozone affect surface solar UVR and what are the possible keratinocyte cancer risks associated with personal exposure to solar UVR in South Africa?

1.7 Rationale of the study

Due to the high levels of solar UVR observed over South Africa, the population living in South Africa may be vulnerable to the negative health risks associated with excessive solar UVR. Improving our understanding of the relationship between stratospheric ozone and solar UVR as well the radiative effect of aerosols on solar UVR may contribute to an improved understanding of solar UVR levels at the surface. Such data may also be used as input into an appropriate radiative transfer model to project levels of solar UVR, for example, for early warning of days expected to have high solar UVR levels. Furthermore, understanding which individuals have the highest keratinocyte cancer risks can help identify at-risk population groups and improve public awareness campaigns for skin cancer prevention.

1.8 Aim and objectives

The aim of this study was to investigate whether changes in aerosols and/or ozone parameters result in anomalous surface solar UVR measurements over South Africa.

The objectives of this study were:

1. To investigate the relationship between solar UVB radiation and stratospheric ozone on clear-sky days and to identify solar UVB radiation anomalies resulting from changes in stratospheric ozone.

2. To investigate the impact of a volcanic plume on aerosols, using AOD and the impact on surface UVB radiation at a secondary site.

3. To investigate the impact of tropospheric aerosols and tropospheric ozone on observed and modelled surface solar UVR levels during the biomass burning season.

4. To perform a keratinocyte cancer risk assessment for the working adults living in the City of Cape Town, South Africa.

1.9 Thesis outline

In Chapter 1, a brief introduction of the study is provided. This includes the rationale, aim and objectives of the study.

Chapter 2 provides a literature review on the factors that affect surface solar UVR as well as the impact that personal exposure to solar UVR has on public health.

Chapter 3 and Chapter 4 are related to Objectives 1 and 2, respectively, and focus on the relationships between atmospheric aerosols and ozone on solar UVR received at the earth's surface.

In Chapter 5, the radiative effect of tropospheric aerosols and tropospheric ozone during the biomass burning season are assessed as set out in Objective 3.

Chapter 6 is related to Objective 4 and focuses on the public health impact associated with excessive personal exposure to solar UVR. A keratinocyte cancer risk assessment was performed for indoor and outdoor adult workers living in Cape Town, South Africa.

Chapter 7 provides a summary of the results presented for each objective as well as an overall conclusion. In this Chapter, the strengths and limitations of the study are discussed as well as recommendations for future research.

The following Chapter provides a review of the factors that affect surface solar UVR and the impacts that exposure to solar UVR has on public health.

1.10 References

Ajtić, J., Connor, B. J., Lawrence, B. N., Bodeker, G. E., Hoppel, K. W., Rosenfield, J. E., & Heuff, D. N. (2004). Dilution of the Antarctic ozone hole into southern midlatitudes, 1998–2000. *Journal of Geophysical Research: Atmospheres, 109*(D17). doi:10.1029/2003jd004500

Alexandris, D., Varotsos, C., Ya Kondratyev, K., & Chronopoulos, G. (1999). On the altitude dependence of solar effective UV. *Physics and Chemistry of the Earth, Part C: Solar, Terrestrial & Planetary Science, 24*(5), 515-517. doi:10.1016/S1464-1917(99)00082-3

AmericanCancerSociety. Retrieved from https://www.cancer.org/cancer/melanoma-skin-cancer/about/key-statistics.html

AmericanMeteorologicalSociety. (2019). Glossary of Meteorology. Retrieved from http://glossary.ametsoc.org/wiki/Solar_zenith_angle

Apalla, Z., Lallas, A., Sotiriou, E., Lazaridou, E., & Ioannides, D. (2017). Epidemiological trends in skin cancer. *Dermatology practical & conceptual, 7*(2), 1. doi:10.5826/dpc.0702a01

Bais, A., Kazantzidis, A., Kazadzis, S., Balis, D., Zerefos, C., & Meleti, C. (2002). *Effects of aerosol optical depth and single scattering albedo on surface UV irradiance* (Vol. 4482): SPIE.

Baldwin, M. P., Gray, L. J., Dunkerton, T. J., Hamilton, K., Haynes, P. H., Randel, W. J., Holton, J. R., Alexander, M. J., Hirota, I., Horinouchi, T., Jones, D. B. A., Kinnersley, J. S., Marquardt, C., Sato, K., & Takahashi, M. (2001). The quasi-biennial oscillation. *Reviews of Geophysics, 39*(2), 179-229. doi:10.1029/1999rg000073

Ball, W. T., Alsing, J., Mortlock, D. J., Staehelin, J., Haigh, J. D., Peter, T., Tummon, F., Stübi, R., Stenke, A., Anderson, J., Bourassa, A., Davis, S. M., Degenstein, D., Frith, S., Froidevaux, L., Roth, C., Sofieva, V., Wang, R., Wild, J., Yu, P., Ziemke, J. R., & Rozanov, E. V. (2018). Evidence for a continuous decline in lower stratospheric ozone offsetting ozone layer recovery. *Atmospheric Chemistry and Physics, 18*(2), 1379-1394. doi:10.5194/acp-18-1379-2018

Bandoro, J., Solomon, S., Donohoe, A., Thompson, D. W. J., & Santer, B. D. (2014). Influences of the Antarctic Ozone Hole on Southern Hemispheric Summer Climate Change. *Journal of Climate, 27*, 6245-6264. doi:10.1175/JCLI-D-13-00698.1

Banerjee, A., Fyfe, J. C., Polvani, L. M., Waugh, D., & Chang, K.-L. (2020). A pause in Southern Hemisphere circulation trends due to the Montreal Protocol. *Nature, 579*(7800), 544-548. doi:10.1038/s41586-020-2120-4

Bègue, N., Vignelles, D., Berthet, G., Portafaix, T., Payen, G., Jégou, F., Benchérif, H., Jumelet, J., Vernier, J. P., Lurton, T., Renard, J. B., Clarisse, L., Duverger, V., Posny, F., Metzger, J. M., & Godin-Beekmann, S. (2017). Long-range transport of stratospheric aerosols in the Southern Hemisphere following the 2015 Calbuco eruption. *Atmospheric Chemistry and Physics, 17*(24), 15019-15036. doi:10.5194/acp-17-15019-2017

Bekki, S., & Lefevre, F. (2009). Stratospheric ozone: History and concepts and interactions with climate. *EPJ Web of Conferences, 1*, 113-136. doi:10.1140/epjconf/e2009-00914-y

Bencherif, H., Toihir, A. M., Mbatha, N., Sivakumar, V., du Preez, D. J., Bègue, N., & Coetzee, G. J. R. (2020). Ozone Variability and Trend Estimates from 20-Years of Ground-Based and Satellite Observations at Irene Station, South Africa. *Atmosphere, 11*(1216). doi:10.3390/atmos11111216

Bodeker, G. E., & McKenzie, R. L. (1996). An algorithm for inferring surface UV irradiance including cloud effects. *Journal of Applied Meteorology, 35*, 1860-1877.

Bojkov, R. D. (1995). The international ozone assessment-1994. *WMO, 44*.

Bornman, J. F., Barnes, P. W., Robson, T. M., Robinson, S. A., Jansen, M. A. K., Ballaré, C. L., & Flint, S. D. (2019). Linkages between stratospheric ozone, UV radiation and climate change and their implications for terrestrial ecosystems. *Photochemical & Photobiological Sciences, 18*(3), 681-716. doi:10.1039/C8PP90061B

Boucher, O., Randall, D., Artaxo, P., Bretherton, C., Feingold, G., Forster, P., Kerminen, V.-M., Kondo, Y., Liao, H., & Lohmann, U. (2013). Clouds and aerosols. In *Climate change 2013: the physical science basis. Contribution of Working Group I to the Fifth Assessment Report of the Intergovernmental Panel on Climate Change* (pp. 571-657): Cambridge University Press.

Brühl, C., & Crutzen, P. J. (1989). On the disproportionate role of tropospheric ozone as a filter against solar UV-B radiation. *Geophysical Research Letters, 16*(7), 703-706. doi:10.1029/GL016i007p00703

Butchart, N. (2014). The Brewer-Dobson circulation. *Reviews of Geophysics, 52*(2), 157-184. doi:10.1002/2013RG000448

Cadet, J.-M., Bencherif, H., Portafaix, T., Lamy, K., Ncongwane, K., Coetzee, G. J. R., & Wright, C. Y. (2017). Comparison of Ground-Based and Satellite-Derived Solar UV Index Levels at Six South African Sites. *International Journal of Environmental Research and Public Health, 14*(11), 1384. doi:10.3390/ijerph14111384

Calbó, J., & González, J. A. (2005). Empirical studies of cloud effects on UV radiation: A review. *Reviews of Geophysics, 43*(2). doi:10.1029/2004RG000155

CCOH. (2016). Ultraviolet Radiation. Retrieved from https://www.ccohs.ca/oshanswers/phys_agents/ultravioletradiation.html

Chipperfield, M. P., Bekki, S., Dhomse, S., Harris, N. R. P., Hassler, B., Hossaini, R., Steinbrecht, W., Thiéblemont, R., & Weber, M. (2017). Detecting recovery of the stratospheric ozone layer. *Nature, 549*(7671), 211-218. doi:10.1038/nature23681

Clain, G., Baray, J.-L., Delmas, R., Diab, R., de Bellevue, J. L., Keckhut, P., Posny, F., Metzger, J.-M., & Cammas, J.-P. (2009). Tropospheric ozone climatology at two Southern Hemisphere tropical/subtropical sites,(Reunion Island and Irene, South Africa) from ozonesondes, LIDAR, and in situ aircraft measurements. *Atmospheric Chemistry and Physics*.

Cohen, N. Y., Gerber, E. P., & Bühler, O. (2014). What Drives the Brewer–Dobson Circulation? *Journal of the Atmospheric Sciences, 71*(10), 3837-3855. doi:10.1175/jas-d-14-0021.1

Cooper, O. R., Parrish, D. D., Ziemke, J., Cupeiro, M., Galbally, I. E., Gilge, S., Horowitz, L., Jensen, N. R., Lamarque, J.-F., & Naik, V. (2014). Global distribution and trends of

tropospheric ozone: An observation-based review. *Elementa: Science of the Anthropocene*. doi:10.12952/journal.elementa.000029
Diab, R. D., Thompson, A. M., Mari, K., Ramsay, L., & Coetzee, G. J. R. (2004). Tropospheric ozone climatology over Irene, South Africa, from 1990 to 1994 and 1998 to 2002. *Journal of Geophysical Research, 109*(D20301). doi:10.1029/2004JD004793
Diffey, B. L. (1992). Stratospheric ozone depletion and the risk of non-melanoma skin cancer in a British population. *Physics in medicine & biology, 37*(12), 2267.
Diffey, B. L. (2002). Sources and measurement of ultraviolet radiation. *Methods, 28*, 4-13.
Dupont, E., Gomez, J., & Bilodeau, D. (2013). Beyond UV radiation: A skin under challenge. *International Journal of Cosmetic Science, 35*(3), 224-232. doi:10.1111/ics.12036
Eck, T. F., Holben, B. N., Reid, J. S., dubovik, O., Smirnov, A., O'neill, N. T., Slutsker, I., & Kinne, S. (1999). Wavelength dependence of the optical depth of biomass burning, urban, and desert dust aerosols. *Journal of Geophysical Research: Atmospheres, 104*(D24), 31333-31349. doi:10.1029/1999jd900923
Farman, J. C., Gardiner, B. G., & Shanklin, J. D. (1985). Large losses of total ozone in Antarctica reveal seasonal ClOx/NOx interaction. *Nature, 315*(6016), 207-210. doi:10.1038/315207a0
Fioletov, V., Kerr, J. B., & Fergusson, A. (2010). The UV Index: Definition, Distribution and Factors Affecting it. *Canadian journal of public health, 101*(4), I5-I9. doi:10.1007/BF03405303
Flury, T., Wu, D. L., & Read, W. G. (2013). Variability in the speed of the Brewer–Dobson circulation as observed by Aura/MLS. *Atmospheric Chemistry and Physics, 13*(9), 4563-4575. doi:10.5194/acp-13-4563-2013
Gordon, R. (2013). Skin Cancer: An Overview of Epidemiology and Risk Factors. *Seminars in Oncology Nursing, 29*(3), 160-169. doi:10.1016/j.soncn.2013.06.002
Hamill, P., & TOON, O. (1991). Polar stratospheric clouds and the ozone hole. *Physics today, 44*(12), 34-42.
Hay, R. J., Johns, N. E., Williams, H. C., Bolliger, I. W., Dellavalle, R. P., Margolis, D. J., Marks, R., Naldi, L., Weinstock, M. A., Wulf, S. K., Michaud, C., J.L. Murray, C., & Naghavi, M. (2014). The Global Burden of Skin Disease in 2010: An Analysis of the Prevalence and Impact of Skin Conditions. *Journal of Investigative Dermatology, 134*(6), 1527-1534. doi:10.1038/jid.2013.446
Haywood, J., & Boucher, O. (2000). Estimates of the direct and indirect radiative forcing due to tropospheric aerosols: A review. *Reviews of Geophysics, 38*(4), 513-543. doi:10.1029/1999RG000078
Hegglin, M. I., Fahey, D. W., McFarland, M., Montzka, S. A., & Nash, E. R. (2015). *Twenty Questions and Answers About the Ozone Layer: 2014 Update-Scientific Assessment of Ozone Depletion: 2014*.
Holton, J., & Hakim, G. (2012). An Introduction to Dynamic Meteorology 5th edition. In (pp. 110-115). USA: Academic Press.
IPCC. (2013). Climate Change 2013: The Physical Science Basis. Contribution of Working Group I to the Fifth Assessment Report of the Intergovernmental Panel on Climate Change T. F. Stocker, D. Qin, G. K. Plattner, M. Tignor, S. K. Allen, J. Boschung, A. Nauels, Y. Xia, B. V., & P. M. Midgley (Eds.). available at: https://www.ipcc.ch/report/ar5/wg1/
Juzeniene, A., Brekke, P., Dahlback, A., Andersson-Engels, S., Reichrath, J., Moan, K., Holick, M. F., Grant, W. B., & Moan, J. (2011). Solar radiation and human health. *Reports on Progress in Physics, 74*(6), 066701. doi:10.1088/0034-4885/74/6/066701
Karpechko, A. Y. (2020). Jet stream stops shifting as the ozone layer recovers. *Nature, 579*(7800), 500-501.
Klekociuk, A., Krummel, P. B., Tully, M. B., Gies, H. P., Alexander, S. P., Fraser, P. J., Henderson, S. I., Javorniczky, J., Shanklin, J. D., & Schofield, R. (2015). The Antarctic ozone hole during 2013. *Australian Meteorological and Oceanographic Journal, 65*(2), 247-266.

Kusuma, L., Lubis, S. W., & Setiawan, S. (2019). Unprecedented Quasi-Biennial Oscillation (QBO) disruption in 2015-2016: Implications for tropical waves and ozone. *IOP Conference Series: Earth and Environmental Science, 284*, 012016. doi:10.1088/1755-1315/284/1/012016

Kylling, A., Dahlback, A., & Mayer, B. (2000). The effect of clouds and surface albedo on UV irradiances at a high latitude site. *Geophysical Research Letters, 27*(9), 1411-1414.

Leiter, U., Eigentler, T., & Garbe, C. (2014). Epidemiology of Skin Cancer. In J. Reichrath (Ed.), *Sunlight, Vitamin D and Skin Cancer* (pp. 120-140). New York, NY: Springer New York.

Lerche, C., Philipsen, P., & Wulf, H. (2017). UVR: sun, lamps, pigmentation and vitamin D. *Photochemical & Photobiological Sciences, 16*(3), 291-301. doi:10.1039/C6PP00277C

Lohmann, U., & Feichter, J. (2005). Global indirect aerosol effects: a review. *Atmospheric Chemistry and Physics, 5*(3), 715-737. doi:10.5194/acp-5-715-2005

Lucas, R. M., Yazar, S., Young, A. R., Norval, M., de Gruijl, F. R., Takizawa, Y., Rhodes, L. E., Sinclair, C. A., & Neale, R. E. (2019). Human health in relation to exposure to solar ultraviolet radiation under changing stratospheric ozone and climate. *Photochemical & Photobiological Sciences, 18*(3), 641-680. doi:10.1039/C8PP90060D

Madronich, S. (1993). The Atmosphere and UV-B Radiation at Ground Level. In A. R. Young, J. Moan, L. O. Björn, & W. Nultsch (Eds.), *Environmental UV Photobiology* (pp. 1-39). Boston, MA: Springer US.

Madronich, S., McKenzie, R. L., Björn, L. O., & Caldwell, M. M. (1998). Changes in biologically active ultraviolet radiation reaching the Earth's surface. *Journal of photochemistry and photobiology B: Biology, 46*(1), 5-19. doi:10.1016/S1011-1344(98)00182-1

Madronich, S., Wagner, M., & Groth, P. (2011). Influence of Tropospheric Ozone Control on Exposure to Ultraviolet Radiation at the Surface. *Environmental Science & Technology, 45*(16), 6919-6923. doi:10.1021/es200701q

McKenzie, R. L., Liley, J. B., & Björn, L. O. (2009). UV radiation: balancing risks and benefits. *Photochemistry and Photobiology, 85*(1), 88-98. doi:10.1111/j.1751-1097.2008.00400.x

Mkololo, T., Mbatha, N., Sivakumar, V., Bègue, N., Coetzee, G., & Labuschagne, C. (2020). Stratosphere–Troposphere Exchange and O3 Variability in the Lower Stratosphere and Upper Troposphere over the Irene SHADOZ Site, South Africa. *Atmosphere, 11*(6), 586. doi:10.3390/atmos11060586

Modenese, A., Korpinen, L., & Gobba, F. (2018). Solar radiation exposure and outdoor work: an underestimated occupational risk. *International Journal of Environmental Research and Public Health, 15*(10), 2063. doi:10.3390/ijerph15102063

Monks, P. S., Archibald, A. T., Colette, A., Cooper, O., Coyle, M., Derwent, R., Fowler, D., Granier, C., Law, K. S., Mills, G. E., Stevenson, D. S., Tarasova, O., Thouret, V., von Schneidemesser, E., Sommariva, R., Wild, O., & Williams, M. L. (2015). Tropospheric ozone and its precursors from the urban to the global scale from air quality to short-lived climate forcer. *Atmospheric Chemistry and Physics, 15*(15), 8889-8973. doi:10.5194/acp-15-8889-2015

Moosmüller, H., & Sorensen, C. M. (2018). Single scattering albedo of homogeneous, spherical particles in the transition regime. *Journal of Quantitative Spectroscopy and Radiative Transfer, 219*, 333-338. doi:10.1016/j.jqsrt.2018.08.015

Ndarana, T., & Waugh, D. W. (2010). The link between cut-off lows and Rossby wave breaking in the Southern Hemisphere. *Quarterly Journal of the Royal Meteorological Society, 136*(649), 869-885. doi:10.1002/qj.627

Norval, M., Kellett, P., & Wright, C. Y. (2014). The incidence and body site of skin cancers in the population groups of South Africa. *Photodermatology, photoimmunology & photomedicine, 30*(5), 262-265. doi:10.1111/phpp.12106262

Norval, M., & Wright, C. Y. (2017). The Epidemiology of Cutaneous Melanoma in the White and Black African Population Groups in South Africa. BTI - Cutaneous Melanoma: Etiology and Therapy. In *Cutaneous Melanoma: Etiology and Therapy*. Brisbane: Codon Publications.

O'Neill, N. T., Eck, T. F., Holben, B. N., Smirnov, A., Dubovik, O., & Royer, A. (2001). Bimodal size distribution influences the variation of Angstrom derivatives in spectral and optical depth space. *Journal of Geophysical Research: Atmospheres, 106*(D9), 9787-9806. doi:10.1029/2000jd900245

Ohneiser, K., Ansmann, A., Baars, H., Seifert, P., Barja, B., Jimenez, C., Radenz, M., Teisseire, A., Floutsi, A., Haarig, M., Foth, A., Chudnovsky, A., Engelmann, R., Zamorano, F., Bühl, J., & Wandinger, U. (2020). Smoke of extreme Australian bushfires observed in the stratosphere over Punta Arenas, Chile, in January 2020: optical thickness, lidar ratios, and depolarization ratios at 355 and 532 nm. *Atmospheric Chemistry and Physics, 20*(13), 8003-8015. doi:10.5194/acp-20-8003-2020

Olsen, M. A., Schoeberl, M. R., & Douglass, A. R. (2004). Stratosphere-troposphere exchange of mass and ozone. *Journal of Geophysical Research: Atmospheres, 109*(D24). doi:10.1029/2004jd005186

Pascoe, C. L., Gray, L. J., Crooks, S. A., Juckes, M. N., & Baldwin, M. P. (2005). The quasi-biennial oscillation: Analysis using ERA-40 data. *Journal of Geophysical Research: Atmospheres, 110*(D8). doi:10.1029/2004jd004941

Pfeifer, M., Koepke, P., & Reuder, J. (2006). Effects of altitude and aerosol on UV radiation. *Journal of Geophysical Research: Atmospheres, 111*(D1). doi:10.1029/2005JD006444

Plumb, R. A. (1977). The Interaction of Two Internal Waves with the Mean Flow: Implications for the Theory of the Quasi-Biennial Oscillation. *Journal of Atmospheric Sciences, 34*(12), 1847-1858. doi:10.1175/1520-0469(1977)034<1847:Tiotiw>2.0.Co;2

Portafaix, T., Morel, B., Bencherif, H., Baldy, S., Godin-Beekmann, S., & Hauchecorne, A. (2003). Fine-scale study of a thick stratospheric ozone lamina at the edge of the southern subtropical barrier. *Journal of Geophysical Research: Atmospheres, 108*(D6). doi:10.1029/2002jd002741

Pöschl, U. (2005). Atmospheric Aerosols: Composition, Transformation, Climate and Health Effects. *Angewandte Chemie International Edition, 44*(46), 7520-7540. doi:10.1002/anie.200501122

Price, J. D., & Vaughan, G. (1993). The potential for stratosphere-troposphere exchange in cut-off-low systems. *Quarterly Journal of the Royal Meteorological Society, 119*(510), 343-365. doi:10.1002/qj.49711951007

Roberts, T. J., Vignelles, D., Liuzzo, M., Giudice, G., Aiuppa, A., Coltelli, M., Salerno, G., Chartier, M., Couté, B., Berthet, G., Lurton, T., Dulac, F., & Renard, J. B. (2018). The primary volcanic aerosol emission from Mt Etna: Size-resolved particles with SO2 and role in plume reactive halogen chemistry. *Geochimica et Cosmochimica Acta, 222*, 74-93. doi:10.1016/j.gca.2017.09.040

Ryer, A. (1997). *The Light Measurement Handbook*. Peadbody, USA: International Light Inc.

Schmalwieser, A. W., Enzi, C., Wallisch, S., Holawe, F., Maier, B., & Weihs, P. (2010). UV exposition during typical lifestyle behavior in an urban environment. *Photochemistry and Photobiology, 86*(3), 711-715. doi:10.1111/j.1751-1097.2010.00714.x

Schuster, G. L., Dubovik, O., & Holben, B. N. (2006). Angstrom exponent and bimodal aerosol size distributions. *Journal of Geophysical Research: Atmospheres, 111*(D7). doi:10.1029/2005jd006328

Sola, Y., Lorente, J., Campmany, E., De Cabo, X., Bech, J., Redaño, A., Martínez-Lozano, J., Utrillas, M., Alados-Arboledas, L., & Olmo, F. (2008). Altitude effect in UV radiation during the Evaluation of the Effects of Elevation and Aerosols on the Ultraviolet Radiation 2002 (VELETA-2002) field campaign. *Journal of Geophysical Research: Atmospheres, 113*(D23). doi:10.1029/2007JD009742

SPARC/IO3C/GAW. (2019). SPARC/IO3C/GAW Report on Long-term Ozone Trends and Uncertainties in the Stratosphere I. Petropavlovskikh, S. Godin-Beekmann, D. Hubert, R. Damadeo, B. Hassler, & V. Sofieva (Eds.), SPARC Report No. 9, GAW Report No. 241, WCRP-17/2018, doi:10.17874/f899e57a20b, available at: https://www.sparc-climate.org/publications/sparc-reports/

Stohl, A., Bonasoni, P., Cristofanelli, P., Collins, W., Feichter, J., Frank, A., Forster, C., Gerasopoulos, E., Gäggeler, H., James, P., Kentarchos, T., Kromp-Kolb, H., Krüger, B., Land, C., Meloen, J., Papayannis, A., Priller, A., Seibert, P., Sprenger, M., Roelofs, G. J., Scheel, H. E., Schnabel, C., Siegmund, P., Tobler, L., Trickl, T., Wernli, H., Wirth, V., Zanis, P., & Zerefos, C. (2003a). Stratosphere-troposphere exchange: A review, and what we have learned from STACCATO. *Journal of Geophysical Research: Atmospheres, 108*(D12). doi:10.1029/2002JD002490

Stohl, A., Wernli, H., James, P., Bourqui, M., Forster, C., Liniger, M. A., Seibert, P., & Sprenger, M. (2003b). A New Perspective of Stratosphere–Troposphere Exchange. *Bulletin of the American Meteorological Society, 84*(11), 1565-1574. doi:10.1175/bams-84-11-1565

Tesfaye, M., Sivakumar, V., Botai, J., & Mengistu Tsidu, G. (2011). Aerosol climatology over South Africa based on 10 years of Multiangle Imaging Spectroradiometer (MISR) data. *Journal of Geophysical Research: Atmospheres, 116*(D20). doi:10.1029/2011jd016023

Thieden, E., Philipsen, P. A., Heydenreich, J., & Wulf, H. C. (2004). UV radiation exposure related to age, sex, occupation, and sun behavior based on time-stamped personal dosimeter readings. *Archives of dermatology, 140*(2), 197-203. doi:10.1001/archderm.140.2.197

Thompson, A. M., Balashov, N. V., Witte, J. C., Coetzee, J. G. R., Thouret, V., & Posny, F. (2014). Tropospheric ozone increases over the southern Africa region: bellwether for rapid growth in Southern Hemisphere pollution? *Atmospheric Chemistry and Physics, 14*(18), 9855-9869. doi:10.5194/acp-14-9855-2014

Toihir, A. M., Portafaix, T., Sivakumar, V., Bencherif, H., Pazmiño, A., & Bègue, N. (2018). Variability and trend in ozone over the southern tropics and subtropics. *Annales Geophysicae, 36*(2), 381-404. doi:10.5194/angeo-36-381-2018

Tully, M., Klekociuk, A., Alexander, S., Dargaville, R., Deschamps, L., Fraser, P., Gies, H., Henderson, S., Javorniczky, J., & Krummel, P. (2011). The Antarctic ozone hole during 2008 and 2009. *Australian Meteorological and Oceanographic Journal, 61*(1), 77. doi:10.22499/2.6101.007

Udelhofen, P. M., Gies, P., Roy, C., & Randel, W. J. (1999). Surface UV radiation over Australia, 1979-1992: Effects of ozone and cloud cover changes on variations of UV radiation. *Journal of Geophysical Research, 104*, 135-159.

Vakkari, V., Kerminen, V.-M., Beukes, J. P., Tiitta, P., van Zyl, P. G., Josipovic, M., Venter, A. D., Jaars, K., Worsnop, D. R., Kulmala, M., & Laakso, L. (2014). Rapid changes in biomass burning aerosols by atmospheric oxidation. *Geophysical Research Letters, 41*(7), 2644-2651. doi:10.1002/2014gl059396

Vishvakarman, D., & Wong, J. (2003). Description of the use of a risk estimation model to assess the increased risk of non-melanoma skin cancer among outdoor workers in Central Queensland, Australia. *Photodermatology, photoimmunology & photomedicine, 19*(2), 81-88. doi:10.1034/j.1600-0781.2003.00012.x

Watson, M., Holman, D. M., & Maguire-Eisen, M. (2016). Ultraviolet Radiation Exposure and Its Impact on Skin Cancer Risk. *Seminars in Oncology Nursing, 32*(3), 241-254. doi:10.1016/j.soncn.2016.05.005

Weber, M., Dikty, S., Burrows, J. P., Garny, H., Dameris, M., Kubin, A., Abalichin, J., & Langematz, U. (2011). The Brewer-Dobson circulation and total ozone from seasonal to decadal time scales. *Atmospheric Chemistry and Physics, 11*(21), 11221-11235. doi:10.5194/acp-11-11221-2011

WHO. (2002). Global solar UV index: a practical guide (Eds.). available at: https://www.unep.org/resources/report/global-solar-uv-index-practical-guide

Williamson, C. E., Neale, P. J., Hylander, S., Rose, K. C., Figueroa, F. L., Robinson, S. A., Häder, D.-P., Wängberg, S.-Å., & Worrest, R. C. (2019). The interactive effects of stratospheric ozone depletion, UV radiation, and climate change on aquatic ecosystems. *Photochemical & Photobiological Sciences, 18*(3), 717-746. doi:10.1039/C8PP90062K

Yu, H., Kaufman, Y. J., Chin, M., Feingold, G., Remer, L. A., Anderson, T. L., Balkanski, Y., Bellouin, N., Boucher, O., Christopher, S., DeCola, P., Kahn, R., Koch, D., Loeb, N., Reddy, M. S., Schulz, M., Takemura, T., & Zhou, M. (2006). A review of measurement-based assessments of the aerosol direct radiative effect and forcing. *Atmospheric Chemistry and Physics, 6*(3), 613-666. doi:10.5194/acp-6-613-2006

Chapter 2 Literature review

2.1 Introduction – A South African perspective

The African continent experiences high surface UVR levels throughout the year and South Africa is no exception (Lucas et al., 2016). During the summer months, surface UVR levels over the interior of the country often exceed 11 UVI, part of the 'extreme' category on the UVI scale (Wright et al., 2020).

Over South Africa, stratospheric ozone reaches an annual maximum during spring and decreases over the summer months when solar UVR is at a maximum (Diab et al., 1992). Stratospheric ozone levels over South Africa are affected by dynamical processes such as STE, BDC and ozone transported from the tropics or polar vortex (Semane et al., 2006). These dynamical processes can result in decreases in stratospheric ozone which can potentially influence surface UVR. Studies investigating STE over Irene, Pretoria have shown that tropospheric ozone can be enhanced by STE, most notably during the winter and spring months at a height of approximately 9 km above ground level (Mkololo et al., 2020). The increase in tropospheric ozone due to STE during the spring season is minimal as it is similar to that found in emission reports (Mkololo et al., 2020).

Large parts of South Africa are affected by the seasonal biomass burning in different regions. This biomass burning can increase the aerosol loading in the atmosphere, particularly during the spring and summer months (Tesfaye et al., 2011). During the spring and summer months when UVR is high, changes in atmospheric parameters such as ozone and aerosols can impact the amount of UVR at the surface.

Aerosols from volcanic eruptions have the potential to impact the local aerosol loading at secondary sites. Over central Africa, the long-range transport of volcanic aerosols from the Nyamuragira and Nyiragongo volcanoes in the Democratic Republic of the Congo has been identified as a source of sulphates in the Amazon basin (Saturno et al., 2018) while aerosols from the 2011 Nabro eruption were transported to Asia and the middle east (Clarisse et al., 2014). Studies have shown

that volcanic eruptions in South America can affect the aerosol loading in Southern African due to the long-range transport of aerosols (Bègue et al., 2019; Bègue et al., 2020; Shikwambana et al., 2018).

The changes in solar UVR caused by changes in atmospheric parameters such as ozone and aerosols are important to understand due to the public health impacts associated with exposure to solar UVR. This is particularly important in South Africa, which has one of the highest skin cancer prevalence rates worldwide among the fair skin population groups (Norval et al., 2014) and where and the cost of treating skin cancer has been estimated to be high (Gordon et al., 2016). Since skin cancer related to sun exposure is essentially a preventable disease, it is important to understand how atmospheric parameters influence UVR at the surface and the health risks associated with exposure to UVR, to guide behaviour and sun protection awareness messages.

In this section, a literature review of previous research is presented in line with the objectives set out in Chapter 1 and the results are presented in Chapter 3 - 6 of this thesis. The following section focuses on ozone and solar UVR.

2.2 Ozone and the absorption of UV radiation

Solar UVR in the UVB and UVC bands is strongly absorbed by stratospheric ozone resulting in decreased UVR at the surface (Fioletov et al., 2010). Most of the radiation in the solar UVA band reaches the Earth's surface and some solar radiation in the UVB band reaches the surface depending on stratospheric ozone concentrations.

2.2.1 Relationship between UVR and Ozone

Given the important role that stratospheric ozone plays in absorbing UVR, it is important to understand how changes in stratospheric ozone affect surface UVR. Furthermore, the variability in surface UVR corresponds to the opposite trends in atmospheric ozone, particularly under clear-sky conditions (Basher et al., 1994). The variability in surface UVR caused by the presence of clouds, as described in Section 1.2.1.4, the inverse relationship between ozone and

UVR is best studied under clear-sky conditions. The clear-sky conditions can be identified using cloud-cover observations, data from sky cameras and algorithms that examine the radiometric curves to determine the presence of clouds (Bodeker et al., 1996; Cadet et al., 2020).

The relationship between ozone and surface UVR has been described as an inverse and non-linear relationship in several studies (Guarnieri et al., 2004; Herman et al., 1998). Apart from the influence of cloud cover, the SZA has been highlighted as an important factor when investigating the relationship between ozone and surface UVR (Bodhaine et al., 1997; Guarnieri et al., 2004; McKenzie et al., 1991; Prause et al., 2002; Prause et al., 1999).

The relationship between solar UVR and TCO is demonstrated in the analytical formula (Equation 1) used to calculated clear-sky UVI. The transmission of UVA and UVB radiation through the atmosphere is accounted for by including the TCO and SZA (Madronich, 2007). The clear-sky UVI can be calculated as follows:

$$UVI \sim 12.5\mu_0^{2.42}(\Omega/300)^{-1.23} \qquad \textit{Equation 1}$$

Where μ_0 is the cosine of the SZA and Ω is total column ozone.

To quantify how changes in TCO affect surface UVR, the radiation amplification factor (RAF) can be used (Equation 2). The RAF describes the percentage increase in erythemal UVR for a 1% decrease in TCO (McKenzie et al., 1991) and accounts for larger changes in TCO which affect erythemal UVR through the power-law relation (Booth et al., 1994). The RAF can be calculated as follows:

$$RAF = -\left(\frac{\Delta E}{E}\right) / \left(\frac{\Delta O_3}{O_3}\right) \qquad \textit{Equation 2}$$

Where E and O_3 are irradiances and total ozone and ΔE and ΔO_3 are the respective changes in each.

As the factors affecting surface UVR vary with place and time, there is not an applicable RAF for the entire world. Massen et. al., (2013) found that RAF varies between 0.79 and 1.7 (Massen, 2013) indicating that a 1% decrease in TCO can result in increased UVR at the surface between 0.79% and 1.7%.

Since the early 2000s, there has been evidence that stratospheric ozone has started to recover mainly due to the decrease in ODS. However, the recovery of stratospheric ozone is not only dependent on the level of ODS in the atmosphere but the release of greenhouse gases will further influence ozone recovery (Bais et al., 2011). As discussed in Section 1.3.4, the recovery of stratospheric ozone extends beyond the stratosphere and impacts atmospheric processes such as the midlatitude jet in the troposphere. The midlatitude jet plays an important role in the formation of weather systems in the troposphere (Barnes et al., 2021).

Surface UVR depends on tropospheric factors such as cloud cover and aerosol loading, simulations of erythemal surface UVR have been produced from 1960 to 2100. Using projections from the chemistry-climate model, the simulations project that surface UVR will reach the 1980s level around midway through the 21st century in the Southern Hemisphere. Globally, surface UVR is expected to decrease throughout the 21st century as atmospheric ozone recovers (Bais et al., 2011).

2.2.2 Antarctic ozone hole

An important consequence of the formation of the Antarctic ozone hole is the dilution of ozone-depleted air masses into the midlatitudes of the Southern Hemisphere during the austral summer (Ajtić et al., 2004). The reduction in stratospheric ozone due to the dilution of the Antarctic ozone hole and increased UVB radiation has been most notable over South America (Abarca et al., 2002a; Abarca et al., 2002b; Kirchhoff et al., 1997; Pérez et al., 2000) but has also been observed over Australia (Gies et al., 2013). Dynamical transport models such as the Modèle Isentrope du transport Méso-échelle de l'Ozone Stratosphérique par Advection (MIMOSA) provide dynamical

components that can be used to trace the origin of ozone-poor air masses. PV can be used as a quasi-passive tracer of ozone when diabatic and frictional terms are small and PV is conserved on isentropic levels (Holton et al., 2012).

Some of the largest decreases in TCO due to the Antarctic ozone hole has been observed over South America. Cities such as Punta Arenas (53°S), Chile, Ushuaia (55°S), Argentina and Rio Gallegos (51.5°S), Argentina have all experienced increased surface UVR due to the dilution of the Antarctic polar vortex during the austral spring and summer. Between 1987 and 2000, decreases in TCO by as much as 56% (145 DU) were observed over both Punta Arenas and Ushuaia (Abarca et al., 2002a). Similar low-ozone events have been observed over Rio Gallegos. During one particular event, Rio Gallegos was contained within the Antarctic polar vortex for three consecutive weeks in November 2009 (Akiyoshi et al., 2018). This resulted in TCO levels near 200 DU (Wolfram et al., 2012). Using dynamical transport models such as MIMOSA, the rapid changes in atmospheric ozone over Rio Gallegos have been attributed to the passage of the polar vortex at isentropic levels between 475 K and 675 K (Orte et al., 2019).

Across South America, low-ozone events such as these have resulted in increased levels of surface UVR. Increases in surface UVR at 300 nm (Abarca et al., 2002b), daily maximum UVI levels of 13 (Wolfram et al., 2012) and increases in the number of sunburn cases reported at hospitals have all be associated with the dilution of the Antarctic polar vortex.

Over southern Australia during August 2011, surface UVB radiation increased by approximately 40% due to a reduction in TCO. The reduction in TCO was due to the transport of ozone-poor air masses from the tropics in the lower stratosphere (395 K) as well as a filament of ozone-poor air from the edge of the Antarctic ozone hole in the high stratosphere (600 K) (Gies et al., 2013).

Over Irene, South Africa, a low ozone event occurred in May 2002 when TCO reached 226 DU, approximately 23 DU below the monthly average (Semane

et al., 2006). The analysis of the dynamical situation attributed the low ozone levels to the transport of ozone-poor air from Antarctica in the middle stratosphere (625 K) as well as the transport of ozone-poor air from the tropics in the lower stratosphere (400 K) (Semane et al., 2006). Furthermore, investigating the STE over Irene indicated that dynamics from the polar vortex affected STE over Irene at approximately 350 K (Mkololo et al., 2020).

The examples described here demonstrate that the Antarctic ozone hole can impact stratospheric ozone levels and surface solar UVR in the midlatitudes of the Southern Hemisphere. The Antarctic ozone hole usually affects ozone in the high stratosphere at approximately 600K. Furthermore, ozone in the lower stratosphere can be affected by ozone-poor air from the tropics. Dilution of the Antarctica ozone hole has been shown to impact surface UVR on other continents but not yet for Africa. In this thesis, the decreases in stratospheric ozone over South Africa due to the dilution of the Antarctic ozone hole and the possible impact on surface UVR were investigated. In Chapter 3, the results and discussion of the investigation into the impact of the Antarctic ozone hole on Cape Point as well as the relationship between UVR and ozone are presented.

In the following subsections (2.3.1 and 2.3.2), the radiative effect and transport of aerosols from volcanic eruptions and biomass burning are discussed.

2.3 Aerosols: UVR absorption and transport

Atmospheric aerosols from natural and anthropogenic sources play an important role in the radiation balance of the Earth. The radiative effect of aerosols is largely dependent on their optical properties. Volcanic eruptions and biomass burning events are responsible for some of the largest increases in aerosol loading. Aerosols from these events can be transported vast distances. To improve radiative transfer models, it is important to understand how aerosols with different optical properties impact surface UVR (Dubovik et al., 2002).

2.3.1 Aerosol anomalies and the effect on UVR

2.3.1.1 Volcanic aerosols and UVR

The optical properties of aerosols released by volcanic eruptions and biomass burning determine the impact on solar UVR (Diaz et al., 2014). Following the eruption of the Puyehue-Cordon Caulle Volcanic Complex (PCCVC) on 4 June 2011, the resulting volcanic plume affected the aerosol loading in nearby towns (Bonadonna et al., 2015; Diaz et al., 2014) and the Southern Hemisphere (Klüser et al., 2013). Across Southern Chile, increases in AOD and decreases in AE were accompanied by increases in aerosol variability in comparison with previous years. The resulting volcanic plume decreased solar UVR at several stations across southern Chile. At 305 nm and 320 nm, the average decrease in UVR following the eruption was approximately 20% and 10 %, respectively. At 380 nm, the decrease in UVR was not statistically significant, although large decreases were observed on days when the aerosol loading was higher (Diaz et al., 2014).

The radiative effect of volcanic aerosols has been observed following other volcanic eruptions as well. During the eruption of Mount Etan on 3 December 2015, surface UVR decreased over south-eastern Italy by approximately 60% as the volcanic plume passed over the region (Romano et al., 2018). Changes in AOD, temperature and relative humidity were also observed (Romano et al., 2018).

2.3.1.2 Biomass burning and UVR

Biomass burning is one of the major sources of carbonaceous aerosols in the Southern Hemisphere (Haywood et al., 2000) and can be present in both the troposphere and stratosphere. These aerosols can remain in the troposphere for several weeks and can potentially impact solar UVR (Haywood et al., 2000).

Between April and May 2006, biomass burning occurred in several Baltic countries. The particles released in the atmosphere by these fires were then transported over northern Europe. As a result, the Observatory of Jokioinen

(60.81 N, 23.50 E) in Finland observed large increases in AOD which resulted in decreased noon-time surface UVR at 340 nm of approximately 35% (Arola et al., 2007). The changes in AOD were most notable over a two-week period and were observed with both satellite and ground-based instruments.

Further anomalous AOD observations resulting from biomass burning have been identified using satellite observations from the Tropospheric Monitoring Instrument (TROPOMI). Some of the most notable events include the 2019 Amazon Basin fires and the 2019/2020 Australian Bush fires (Torres et al., 2020). As the aerosol plume from the Amazon Basin fires in 2019 was transported southeast, it reached major cities like São Paulo which were plunged into darkness (Hughes, 2019).

Over the north and eastern parts of Southern Africa, the annual biomass burning season occurs between July and November (Hobbs et al., 2003) when AOD and tropospheric ozone reach a maximum in the austral spring (Clain et al., 2009; Diab et al., 2004; Thompson et al., 2001). Using data from satellites, data from the Southern African Regional Science Initiative (SAFARI 2000) field campaign and the Edwards-Slingo radiative transfer code it was demonstrated how smoke from biomass burning has a negative radiative effect on surface UVR (Abel et al., 2005; Hobbs et al., 2003). Furthermore, the radiative effect of the smoke was sensitive to the vertical distribution and optical properties of aerosols (Abel et al., 2005).

2.3.1.3 Tropospheric ozone and UVR

Tropospheric ozone is a common chemical species found in urban smog and is a secondary pollutant formed due to the emissions from biomass burning and industrial activities (Madronich et al., 2011; Thompson et al., 2001). Previous studies found that there is an inverse relationship between surface UVR and tropospheric ozone (Brühl et al., 1989; Madronich et al., 2011). Using two control scenarios with differing tropospheric ozone levels over the United States of America, the study found that tropospheric ozone can result in small changes (<1%) in surface UVR (Madronich et al., 2011).

At the Irene weather station of the South African Weather Service (SAWS), the annual peak (in September) in tropospheric ozone is attributed to the transport of emissions from the biomass burning region due to the dominant subtropical anticyclone. Over the summer months, tropospheric ozone levels decrease due to the advection of air masses from the Indian Ocean by easterly winds and convective activity (Diab et al., 2004).

2.3.2 Volcanic aerosol transport

During volcanic eruptions, wildfires and biomass burning events, the transport of the particles or plumes released into the atmosphere is dependent on the injection height, the type of particles and the prevailing meteorological conditions at the time of the event (Bonadonna et al., 2015). To study the transport of aerosol plumes, satellites provide a global view of AOD, ash, carbon monoxide, sulphur dioxide and ash parameters which are all affected by emissions from volcanic eruptions, wildfires and biomass burning. Computational models such as the Flexible Particle (FLEXPART) dispersion model and the Hybrid Single-Particle Lagrangian Integrated Trajectory (HYSPLIT) model can simulate the trajectories of particles in forward or backward directions (Romano et al., 2018).

Volcanic ash, sulphur dioxide and chlorine dioxide are some of the chemical species that have been observed from satellite observations of volcanic eruptions. Satellites such as the Infrared Atmospheric Sounding Interferometer (IASI), the Global Ozone Monitoring Experiment (GOME) and the Ozone Monitoring Instrument (OMI) provide information on volcanic emissions which help mitigate the danger posed to the aviation industry (Athanassiadou, 2016).

The eruption of the PCCVC in June 2011 resulted in a volcanic plume that circled the Southern Hemisphere and affected air traffic on three continents (Klüser et al., 2013). Satellite observations of sulphur dioxide (Figure 2-1) (Clarisse et al., 2012) and volcanic ash from the IASI instrument clearly show

the south-easterly dispersion of the plume across South America as well the dispersion across the rest of the Southern Hemisphere (Clarisse et al., 2012;

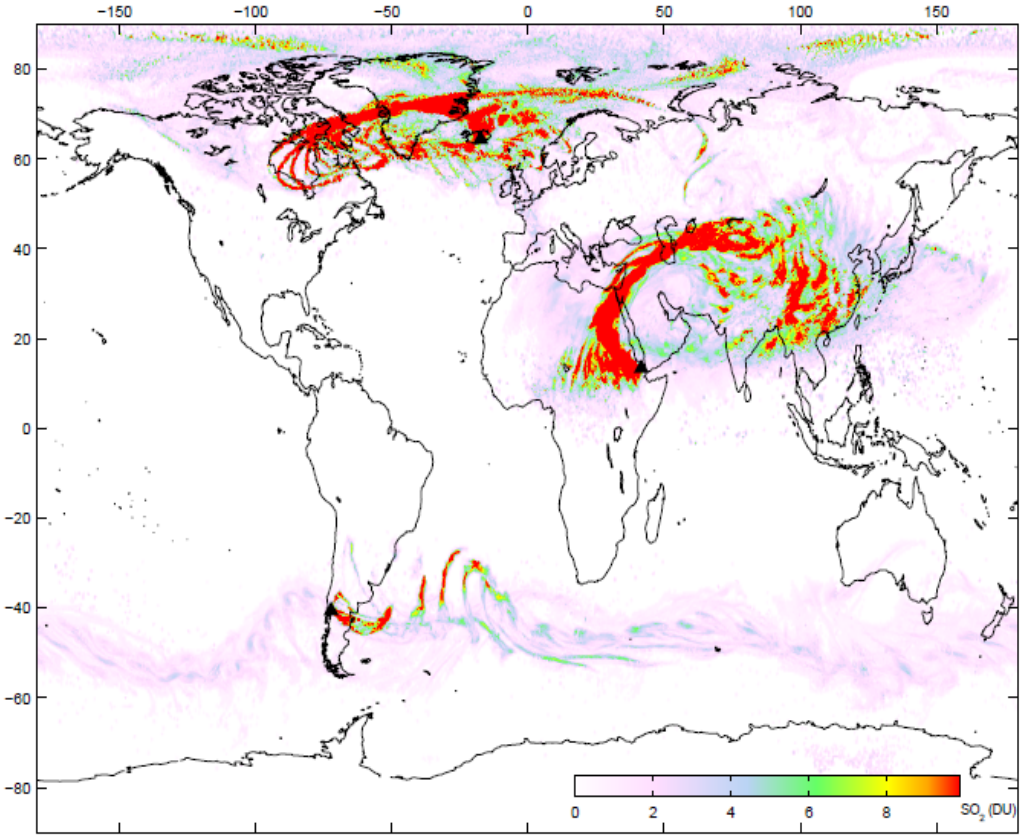

Figure 2-1. Composite image of Sulphur dioxide observed between 20 May to 30 June 2011 from IASI observations. (Retrieved Clarisse et. al., 2012 "Retrieval of sulphur dioxide from the Infrared Atmospheric Sounding Interferometer (IASI)."

Klüser et al., 2013; Theys et al., 2013). The plume circled the Southern Hemisphere within 10-days and was observed near the south-eastern parts of Australia at altitudes between 8 km and 12 km using aerosol profiles from the Cloud-Aerosol Lidar and Infrared Pathfinder Satellite Observations (CALIPSO) instrument (Vernier et al., 2013). Using the particle dispersion model FLEXPART, the dispersion of the plume across South America was investigated and found to be similar to the satellite observations (Klüser et al., 2013; Theys et al., 2013).

The long-range transport of volcanic aerosols has been demonstrated with satellite observations as well as dispersion models following previous volcanic eruptions such as the Mount Pinatubo eruption in June 1991, Jebel al-Tair

eruption in 2007 and the Calbuco eruption in 2015. The plume from the Mount Pinatubo eruption reached a height of 30 km, injecting particulate matter and sulphur dioxide into the stratosphere (McCormick et al., 1995). The resulting plume was dispersed westwards around the globe and was dispersed across the equator to 10°S (McCormick et al., 1995).

The Jebel al-Tair volcano in Yemen resulted in a volcanic plume that was dispersed over many countries on the Asian continent and reached as far as China (Clarisse et al., 2008). Using satellite observations and dispersion models, the dispersion of the Calbuco plume from South America across the Atlantic Ocean towards Southern Africa was demonstrated (Bègue et al., 2020; Shikwambana et al., 2018). The dispersion of the Calbuco plume resulted in AOD anomalies over Southern Africa (Bègue et al., 2020).

In the above-mentioned studies, the radiative effect of aerosols from volcanic eruptions and biomass burning as well as the transport of volcanic plumes demonstrate the impact on secondary sites at varying distance from the source regions. However, these studies do not investigate the impact on the aerosol loading of the volcanic eruption nor the radiative effect of biomass burning aerosols over South Africa. In this thesis, the effects of aerosols from a volcanic eruption and aerosols from biomass burning on surface UVR were investigated. The results and discussion are presented in Chapter 4 and Chapter 5, respectively

.

2.4 UV-induced skin cancer risks

The South African population consists of individuals of varying skin phototype (Wilkes et al., 2015). The relatively high incidence rate of skin cancer has resulted in substantial healthcare costs for treatments (Gordon et al., 2016). Since skin cancer is a preventable disease, the risks of skin cancer can be reduced if at-risk population groups avoid excessive sun exposure.

2.4.1 Risk factors

The risk of keratinocyte cancer is associated with several risk factors as given in Section 1.5. In subsections, 2.4.1.1 - 2.4.1.3, the roles of these risk factors relating to keratinocyte cancer are discussed.

2.4.1.1 Skin phototypes

Melanin in the basal layer of the epidermis is not only responsible for skin colouring but absorbs UVR, protecting humans from UVR (Brenner et al., 2008). The amount of melanin within the skin can be measured using a skin colourimeter which provided useful information for epidemiological studies (Wilkes et al., 2015). Due to the role that melanin plays in protecting humans from UVR, it is important to consider the skin phototype of an individual in keratinocyte risk assessments (Apalla et al., 2017; Madan et al., 2010).

Generally, the Fitzpatrick skin phototype (FST) (Fitzpatrick, 1988) classification (Table 2-1.) is used to determine the phototype of an individual by assessing the ability to tan and the tendency to burn. Although there is a strong link between FST and skin cancer, the FST classification method was not developed for this purpose and the interdependency between the ability to tan and the tendency to burn in the FST classification were based on data collected from questionnaires. This questionnaire resulted in a limited number of possible answers. As a result, Holm-Schou et. al. (2019) proposed a new skin cancer phototype (SCP) which is directly related to skin cancer risk (Holm-Schou et al., 2019). Using validated skin cancer data and skin attributes of individuals, the SCP showed a linear relation with skin cancer risk and therefore was suggested as a good predictor of skin cancer.

2.4.1.2 Age, occupation and activities

The incidence of keratinocyte cancer increases with age, with a larger percentage of new cases reported in people older than 60-years (Madan et al., 2010). Age furthermore plays an important role in the occupational and recreational activities of individuals. A 14-year sun exposure follow-up study (Thieden et al., 2019) showed that when individuals moved from high school

to indoor occupations there was a 30% decrease in the estimated annual dose as well as a decrease in exposure at peak UVR periods.

The sun exposure a working adult received during occupational activities is largely dependent on the type of occupation. For instance, sun exposure studies have shown that outdoor workers receive between two and nine times (Godar, 2005; Milon et al., 2014) the annual solar UVR exposure dose compared to indoor workers. Studies have shown that there is a strong relationship between occupational sun exposure and the incidence of both BCC and SCC (Bauer et al., 2011; Fartasch et al., 2012; Filon et al., 2019). Due to the higher annual doses received by outdoor workers, their risk of keratinocyte cancer and sunburn are higher (Guy et al., 2002; Vishvakarman et al., 2003; Wright et al., 2013).

Table 2-1 Fitzpatrick skin phototype classification. Standard Erythemal Dose (SED), where 1 SED is equal to 100 Jm^{-2}.

FST	Characteristics	Minimum dose for erythema (SED)
I	Extremely sensitive, white skin, light eyes, freckles	2 - 3
II	Overly sensitive, white skin, blonde hair, hazel/brown eyes	2.5 - 3.5
III	Moderately sensitive, light brown skin, brown hair, brown eyes	3 - 5
IV	Dark hair, light brown skin, dark eyes	4.5 - 6
V	Variable sensitivity, brown skin, brown eyes, dark brown or black hair	6 - 10
VI	Brown eyes, black skin, dark brown or black hair	10 - 20

Sun exposure studies have shown that certain activities and environments result in higher UVR exposure than others (Diffey, 2018). The exposure and risk related to activities such as golf were linked to the time that golfer started their round. Golfers starting in the mid to late morning were at greater risk (Downs et al., 2011). In comparison to hiking and skiing, triathletes receive higher UVR doses due to the long periods these individuals spend outdoors and the limited use of sun protection (Downs et al., 2020).

2.4.1.3 Risk management

For individuals to enjoy outdoor activities and the positive health benefits associated with sun exposure, sun-safe strategies can be used to limit the risks by managing the time and place when UVR exposure occurs. As explained described in Section 1.2.1.1, UVR is at a daily maximum near solar noon. Avoiding exposure during the time before noon and early afternoon is one way to limit the risk posed to an individual (Diffey, 2018).

Using physical and chemical barriers against UVR can further mitigate the risks posed to an individual. Physical barriers such as shading, clothing and hats provide protection from the sun. Hats do not only protect the scalp which is a site for keratinocyte cancer development but provide protection for the face and neck as well (Diffey, 2017). Lastly, chemical barriers such as sunscreen absorb UVR. The level of protection provided by a sunscreen is dependent on the Sun Protection Factor (SPF) and describes the period for which the sunscreen will provide protection (Diffey, 2017).

2.4.2 Risk assessment models

To estimate keratinocyte cancer risk, models have taken different approaches. One risk assessment model was based on epidemiology and experiments on hairless mice to determine keratinocyte cancer risk at a particular age (Slaper et al., 1987). This model incorporated the annual sun exposure of an individual (Diffey, 1992; Milon et al., 2014; Vishvakarman et al., 2003). Whiteman et al.2016 (Whiteman et al., 2016) proposed a logistic regression model to estimate keratinocyte cancer risk based on surgically

excised carcinomas from a large population cohort. The regression model was improved using different predictors (e.g., age, sex, ethnicity, freckling etc.). Using the predictor, namely >20 prior skin cancer excised, improved the reliability of the model.

The keratinocyte cancer risk assessment model has been used to quantify the increased risk of keratinocyte cancer due to stratospheric ozone depletion (Diffey, 1992), potential benefits of sun exposure downs (Downs et al., 2009) and the risk for indoor and outdoor workers in Australia and South Africa (Guy et al., 2002; Vishvakarman et al., 2003). These studies have shown that outdoor workers have more than twice the risk compared to indoors workers and that the risk increases for individuals over the age of 40 years.

Present studies consider the impact of occupation on sun exposure but do not account for individuals with different phototypes. In this thesis, a novel approach was used to estimate the keratinocyte cancer risk for individuals of different FSTs and the results are presented and discussed in Chapter 6. Risk assessments that provide detailed information about at-risk groups are key to developing skin cancer prevention and sun protection campaigns for high-risk group populations groups.

2.5 References

Abarca, J. F., & Casiccia, C. C. (2002a). Skin cancer and ultraviolet-B radiation under the Antarctic ozone hole: southern Chile, 1987–2000. *Photodermatology, photoimmunology & photomedicine, 18*(6), 294-302. doi:10.1034/j.1600-0781.2002.02782.x

Abarca, J. F., Casiccia, C. C., & Zamorano, F. D. (2002b). Increase in sunburns and photosensitivity disorders at the edge of the Antarctic ozone hole, Southern Chile, 1986-2000. *Journal of the American Academy of Dermatology, 46*(2), 193-199. doi:10.1067/mjd.2002.118556

Abel, S. J., Highwood, E. J., Haywood, J. M., & Stringer, M. A. (2005). The direct radiative effect of biomass burning aerosols over southern Africa. *Atmospheric Chemistry and Physics, 5*(7), 1999-2018. doi:10.5194/acp-5-1999-2005

Ajtić, J., Connor, B. J., Lawrence, B. N., Bodeker, G. E., Hoppel, K. W., Rosenfield, J. E., & Heuff, D. N. (2004). Dilution of the Antarctic ozone hole into southern midlatitudes, 1998–2000. *Journal of Geophysical Research: Atmospheres, 109*(D17). doi:10.1029/2003jd004500

Akiyoshi, H., Kadowaki, M., Nakamura, H., Sugita, T., Hirooka, T., Harada, Y., & Mizuno, A. (2018). Analysis of the Ozone Reduction Event Over the Southern Tip of South

America in November 2009. *Journal of Geophysical Research: Atmospheres, 123*(22), 12,523-512,542. doi:10.1029/2017JD028096

Apalla, Z., Lallas, A., Sotiriou, E., Lazaridou, E., & Ioannides, D. (2017). Epidemiological trends in skin cancer. *Dermatology practical & conceptual, 7*(2), 1. doi:10.5826/dpc.0702a01

Arola, A., Lindfors, A., Natunen, A., & Lehtinen, K. E. J. (2007). A case study on biomass burning aerosols: effects on aerosol optical properties and surface radiation levels. *Atmospheric Chemistry and Physics, 7*(16), 4257-4266. doi:10.5194/acp-7-4257-2007

Athanassiadou, M. (2016). The Mt Etna SO2 eruption in December 2015 – the view from space. *Weather, 71*(11), 273-279. doi:10.1002/wea.2794

Bais, A. F., Tourpali, K., Kazantzidis, A., Akiyoshi, H., Bekki, S., Braesicke, P., Chipperfield, M. P., Dameris, M., Eyring, V., Garny, H., Iachetti, D., Jöckel, P., Kubin, A., Langematz, U., Mancini, E., Michou, M., Morgenstern, O., Nakamura, T., Newman, P. A., Pitari, G., Plummer, D. A., Rozanov, E., Shepherd, T. G., Shibata, K., Tian, W., & Yamashita, Y. (2011). Projections of UV radiation changes in the 21st century: impact of ozone recovery and cloud effects. *Atmospheric Chemistry and Physics, 11*(15), 7533-7545. doi:10.5194/acp-11-7533-2011

Barnes, M. A., Turner, K., Ndarana, T., & Landman, W. A. (2021). Cape storm: A dynamical study of a cut-off low and its impact on South Africa. *Atmospheric Research, 249*, 105290. doi:10.1016/j.atmosres.2020.105290

Basher, R. E., Zheng, X., & Nichol, S. (1994). Ozone-related trends in solar UV-B series. *Geophysical Research Letters, 21*(24), 2713-2716. doi:10.1029/94GL02586

Bauer, A., Diepgen, T. L., & Schmitt, J. (2011). Is occupational solar ultraviolet irradiation a relevant risk factor for basal cell carcinoma? A systematic review and meta-analysis of the epidemiological literature. *British Journal of Dermatology, 165*(3), 612-625. doi:10.1111/j.1365-2133.2011.10425.x

Bègue, N., Shikwambana, L., Bencherif, H., Pallotta, J., Du Preez, J., Ranaivombola, M., Piketh, S., & Formenti, P. (2019). Statistical analysis of the long-range transport of the 2015 Calbuco volcanic eruption from ground-based and space-borne observations. *Annales Geophysicae Discussions*, 1-58. doi:10.5194/angeo-2019-138

Bègue, N., Shikwambana, L., Bencherif, H., Pallotta, J., Sivakumar, V., Wolfram, E., Mbatha, N., Orte, F., Du Preez, D. J., Ranaivombola, M., Piketh, S., & Formenti, P. (2020). Statistical analysis of the long-range transport of the 2015 Calbuco volcanic plume from ground-based and space-borne observations. *Annales Geophysicae, 38*(2), 395-420. doi:10.5194/angeo-38-395-2020

Bodeker, G. E., & McKenzie, R. L. (1996). An algorithm for inferring surface UV irradiance including cloud effects. *Journal of Applied Meteorology, 35*, 1860-1877.

Bodhaine, B. A., Dutton, E. G., Hofmann, D. J., McKenzie, R. L., & Johnston, P. V. (1997). UV measurements at Mauna Loa: July 1995 to July 1996. *Journal of Geophysical Research: Atmospheres, 102*(D15), 19265-19273. doi:10.1029/97JD01391

Bonadonna, C., Pistolesi, M., Cioni, R., Degruyter, W., Elissondo, M., & Baumann, V. (2015). Dynamics of wind-affected volcanic plumes: The example of the 2011 Cordón Caulle eruption, Chile. *Journal of Geophysical Research: Solid Earth, 120*(4), 2242-2261. doi:10.1002/2014jb011478

Booth, C. R., & Madronich, S. (1994). Radiation Amplification Factors: Improved formulation accounts for large increases in ultraviolet radiation associated with Antarctic ozone depletion. *Ultraviolet Radiation in Antarctica: Measurements and Biological effects. Antarctic Research Series, 62*, 39-42.

Brenner, M., & Hearing, V. J. (2008). The Protective Role of Melanin Against UV Damage in Human Skin. *Photochemistry and Photobiology, 84*(3), 539-549. doi:10.1111/j.1751-1097.2007.00226.x

Brühl, C., & Crutzen, P. J. (1989). On the disproportionate role of tropospheric ozone as a filter against solar UV-B radiation. *Geophysical Research Letters, 16*(7), 703-706. doi:10.1029/GL016i007p00703

Cadet, J.-M., Portafaix, T., Bencherif, H., Lamy, K., Brogniez, C., Auriol, F., Metzger, J.-M., Boudreault, L.-E., & Wright, C. Y. (2020). Inter-Comparison Campaign of Solar UVR Instruments under Clear Sky Conditions at Reunion Island (21° S, 55° E). *International Journal of Environmental Research and Public Health, 17*(8), 2867. doi:10.3390/ijerph17082867

Clain, G., Baray, J.-L., Delmas, R., Diab, R., de Bellevue, J. L., Keckhut, P., Posny, F., Metzger, J.-M., & Cammas, J.-P. (2009). Tropospheric ozone climatology at two Southern Hemisphere tropical/subtropical sites,(Reunion Island and Irene, South Africa) from ozonesondes, LIDAR, and in situ aircraft measurements. *Atmospheric Chemistry and Physics*.

Clarisse, L., Coheur, P. F., Prata, A. J., Hurtmans, D., Razavi, A., Phulpin, T., Hadji-Lazaro, J., & Clerbaux, C. (2008). Tracking and quantifying volcanic SO₂ with IASI, the September 2007 eruption at Jebel at Tair. *Atmospheric Chemistry and Physics, 8*(24), 7723-7734. doi:10.5194/acp-8-7723-2008

Clarisse, L., Coheur, P. F., Theys, N., Hurtmans, D., & Clerbaux, C. (2014). The 2011 Nabro eruption, a SO2 plume height analysis using IASI measurements. *Atmospheric Chemistry and Physics, 14*(6), 3095-3111. doi:10.5194/acp-14-3095-2014

Clarisse, L., Hurtmans, D., Clerbaux, C., Hadji-Lazaro, J., Ngadi, Y., & Coheur, P. F. (2012). Retrieval of sulphur dioxide from the Infrared Atmospheric Sounding Interferometer (IASI). *Atmospheric Measurement Techniques, 5*(3), 581-594. doi:10.5194/amt-5-581-2012

Diab, R., Barsby, J., Bodeker, G., Scourfleld, M., & Salter, L. (1992). Satellite observations of total ozone above South Africa. *South African Geographical Journal, 74*(1), 13-18.

Diab, R. D., Thompson, A. M., Mari, K., Ramsay, L., & Coetzee, G. J. R. (2004). Tropospheric ozone climatology over Irene, South Africa, from 1990 to 1994 and 1998 to 2002. *Journal of Geophysical Research, 109*(D20301). doi:10.1029/2004JD004793

Diaz, S. B., Paladini, A. A., Braile, H. G., Dieguez, M. C., Deferrari, G. A., Vernet, M., & Vrsalovic, J. (2014). Global and direct UV irradiance variation in the Nahuel Huapi National Park (Patagonia, Argentina) after the eruption of Puyehue-Cordon Caulle (Chile). *Journal of Atmospheric and Solar-Terrestrial Physics, 112*, 47-56. doi:10.1016/j.jastp.2014.02.006

Diffey, B. L. (1992). Stratospheric ozone depletion and the risk of non-melanoma skin cancer in a British population. *Physics in medicine & biology, 37*(12), 2267.

Diffey, B. L. (2017). *Sun Protection: A risk management approach*. Bristol, UK: IOP Publishing.

Diffey, B. L. (2018). Time and Place as Modifiers of Personal UV Exposure. *International Journal of Environmental Research and Public Health, 15*(6). doi:10.3390/ijerph15061112

Downs, N., Parisi, A., & Schouten, P. (2011). Basal and squamous cell carcinoma risks for golfers: An assessment of the influence of tee time for latitudes in the Northern and Southern hemispheres. *Journal of photochemistry and photobiology B: Biology, 105*(1), 98-105. doi:10.1016/j.jphotobiol.2011.07.007

Downs, N. J., Axelsen, T., Parisi, A. V., Schouten, P. W., & Dexter, B. R. (2020). Measured UV Exposures of Ironman, Sprint and Olympic-Distance Triathlon Competitors. *Atmosphere, 11*(5), 440. doi:10.3390/atmos11050440

Downs, N. J., Schouten, P. W., Parisi, A. V., & Turner, J. (2009). Measurements of the upper body ultraviolet exposure to golfers: non-melanoma skin cancer risk, and the potential benefits of exposure to sunlight. *Photodermatology, photoimmunology & photomedicine, 25*(6), 317-324.

Dubovik, O., Holben, B., Eck, T. F., Smirnov, A., Kaufman, Y. J., King, M. D., Tanré, D., & Slutsker, I. (2002). Variability of Absorption and Optical Properties of Key Aerosol Types Observed in Worldwide Locations. *Journal of the Atmospheric Sciences, 59*(3), 590-608. doi:10.1175/1520-0469(2002)059<0590:Voaaop>2.0.Co;2

Fartasch, M., Diepgen, T. L., Schmitt, J., & Drexler, H. (2012). The relationship between occupational sun exposure and non-melanoma skin cancer: Clinical Basics, Epidemiology, Occupational Disease Evaluation, and Prevention. *Deutsches Ärzteblatt International, 109*(43), 715-720. doi:10.3238/arztebl.2012.0715

Filon, F. L., Buric, M., & Fluehler, C. (2019). UV exposure, preventive habits, risk perception, and occupation in NMSC patients: A case-control study in Trieste (NE Italy). *Photodermatology, photoimmunology & photomedicine, 35*(1), 24-30. doi:10.1111/phpp.12417

Fioletov, V., Kerr, J. B., & Fergusson, A. (2010). The UV Index: Definition, Distribution and Factors Affecting it. *Canadian journal of public health, 101*(4), I5-I9. doi:10.1007/BF03405303

Fitzpatrick, T. B. (1988). The Validity and Practicality of Sun-Reactive Skin Types I Through VI. *Archives of dermatology, 124*(6), 869-871. doi:10.1001/archderm.1988.01670060015008

Gies, P., Klekociuk, A., Tully, M., Henderson, S., Javorniczky, J., King, K., Lemus-Deschamps, L., & Makin, J. (2013). Low Ozone Over Southern Australia in August 2011 and its Impact on Solar Ultraviolet Radiation Levels. *Photochemistry and Photobiology, 89*(4), 984-994. doi:10.1111/php.12076

Godar, D. E. (2005). UV doses worldwide. *Photochemistry and Photobiology, 81*(4), 736-749.

Gordon, L. G., Elliott, T. M., Wright, C. Y., Deghaye, N., & Visser, W. (2016). Modelling the healthcare costs of skin cancer in South Africa. *BMC health services research, 16*(1), 113. doi:10.1186/s12913-016-1364-z

Guarnieri, R. A., Padilha, L. F., Guarnieri, F. L., Echer, E., Makita, K., Pinheiro, D. K., Schuch, A. M. P., Boeira, L. S., & Schuch, N. J. (2004). A study of the anticorrelations between ozone and UV-B radiation using linear and exponential fits in southern Brazil. *Advances in Space Research, 34*, 764-768. doi:10.1016/j.asr.2003.06.040

Guy, C., & Diab, R. (2002). A health risk assessment of ultraviolet radiation in Durban. *South African Geographical Journal, 84*(2), 208-213.

Haywood, J., & Boucher, O. (2000). Estimates of the direct and indirect radiative forcing due to tropospheric aerosols: A review. *Reviews of Geophysics, 38*(4), 513-543. doi:10.1029/1999RG000078

Herman, J., McKenzie, R., Diaz, S., Kerr, J., Madronich, S., & Seckmeyer, G. (1998). Ultraviolet radiation at the Earth's surface, Chapter 9 In: Scientific Assessment of Ozone Depletion: 1998. *World Meteorological Organization, Global Ozone Research and Monitoring Project-Report N0, 44*.

Hobbs, P. V., Sinha, P., Yokelson, R. J., Christian, T. J., Blake, D. R., Gao, S., Kirchstetter, T. W., Novakov, T., & Pilewskie, P. (2003). Evolution of gases and particles from a savanna fire in South Africa. *Journal of Geophysical Research: Atmospheres, 108*(D13). doi:10.1029/2002JD002352

Holm-Schou, A.-S. S., Philipsen, P. A., & Wulf, H. C. (2019). Skin cancer phototype: A new classification directly related to skin cancer and based on responses from 2869 individuals. *Photodermatology, photoimmunology & photomedicine, 35*(2), 116-123. doi:10.1111/phpp.12432

Holton, J., & Hakim, G. (2012). An Introduction to Dynamic Meteorology 5th edition. In (pp. 110-115). USA: Academic Press.

Hughes, R. (2019). Amazon fires: What's the latest in Brazil? Retrieved from https://www.bbc.com/news/world-latin-america-49971563

Kirchhoff, V. W. J. H., Sahai, Y., Casiccia, C. A. R. S., Zamorano, B. F., & Valderrama, V. V. (1997). Observations of the 1995 ozone hole over Punta Arenas, Chile. *Journal of Geophysical Research: Atmospheres, 102*(D13), 16109-16120. doi:10.1029/97JD00276

Klüser, L., Erbertseder, T., & Meyer-Arnek, J. (2013). Observation of volcanic ash from Puyehue-Cordón Caulle with IASI. *Atmospheric Measurement Techniques, 6*(1), 35. doi:10.5194/amt-6-35-2013

Lucas, R. M., Norval, M., & Wright, C. Y. (2016). Solar ultraviolet radiation in Africa: a systematic review and critical evaluation of the health risks and use of photoprotection. *Photochemical & Photobiological Sciences, 15*(1), 10-23. doi:10.1039/c5pp00419e

Madan, V., Lear, J. T., & Szeimies, R.-M. (2010). Non-melanoma skin cancer. *The Lancet, 375*(9715), 673-685.

Madronich, S. (2007). Analytic Formula for the Clear-sky UV Index. *Photochemistry and Photobiology, 83*(6), 1537-1538. doi:10.1111/j.1751-1097.2007.00200.x

Madronich, S., Wagner, M., & Groth, P. (2011). Influence of Tropospheric Ozone Control on Exposure to Ultraviolet Radiation at the Surface. *Environmental Science & Technology, 45*(16), 6919-6923. doi:10.1021/es200701q

Massen, F. (2013). Computing the Radiation Amplification Factor RAF using a sudden dip in Total Ozone Column measured at Diekirch, Luxembourg (Eds.). available at: http://meteo.lcd.lu/papers/MASSEN/RAF_from_sudden_TOC_dip.pdf

McCormick, M. P., Thomason, L. W., & Trepte, C. R. (1995). Atmospheric effects of the Mt Pinatubo eruption. *Nature, 373*(6513), 399-404. doi:10.1038/373399a0

McKenzie, R. L., Matthews, W. A., & Johnston, P. V. (1991). The relationship between erythemal UV and ozone, derived from spectral irradiance measurements. *Geophysical Research Letters, 18*(12), 2269-2272. doi:10.1029/91GL02786

Milon, A., Bulliard, J. L., Vuilleumier, L., Danuser, B., & Vernez, D. (2014). Estimating the contribution of occupational solar ultraviolet exposure to skin cancer. *British Journal of Dermatology, 170*(1), 157-164. doi:10.1111/bjd.12604

Mkololo, T., Mbatha, N., Sivakumar, V., Bègue, N., Coetzee, G., & Labuschagne, C. (2020). Stratosphere–Troposphere Exchange and O3 Variability in the Lower Stratosphere and Upper Troposphere over the Irene SHADOZ Site, South Africa. *Atmosphere, 11*(6), 586. doi:10.3390/atmos11060586

Norval, M., Kellett, P., & Wright, C. Y. (2014). The incidence and body site of skin cancers in the population groups of South Africa. *Photodermatology, photoimmunology & photomedicine, 30*(5), 262-265. doi:10.1111/phpp.12106262

Orte, P. F., Wolfram, E., Salvador, J., Mizuno, A., Bègue, N., Bencherif, H., Bali, J. L., D'Elia, R., Pazmiño, A., Godin-Beekmann, S., Ohyama, H., & Quiroga, J. (2019). Analysis of a southern sub-polar short-term ozone variation event using a millimetre-wave radiometer. *Annales Geophysicae, 37*(4), 613-629. doi:10.5194/angeo-37-613-2019

Pérez, A., Crino, E., Aguirre de Cárcer, I., & Jaque, F. (2000). Low-ozone events and three-dimensional transport at midlatitudes of South America during springs of 1996 and 1997. *Journal of Geophysical Research: Atmospheres, 105*(D4), 4553-4561. doi:10.1029/1999JD901040

Prause, A. R., & Scourfield, M. W. J. (2002). Surface erythemal irradiance and total column ozone above Durban, South Africa, for the period 1996-1998 : research letter. *South African Journal of Science, 98*(3), 186-188. Retrieved from https://www.ingentaconnect.com/content/sabinet/sajsci/2002/00000098/00000003/art00020

Prause, A. R., Scourfield, M. W. J., Bodeker, G. E., & Diab, R. D. (1999). Surface UV-B irradiance and total column ozone above SANAE, Antarctica. *South African Journal of Science, 95*(1), 26-30. doi:10.10520/AJA00382353_7823

Romano, S., Burlizzi, P., Kinne, S., De Tomasi, F., Hamann, U., & Perrone, M. R. (2018). Radiative impact of Etna volcanic aerosols over south eastern Italy on 3 December 2015. *Atmospheric Environment, 182*, 155-170. doi:10.1016/j.atmosenv.2018.03.038

Saturno, J., Ditas, F., Penning de Vries, M., Holanda, B. A., Pöhlker, M. L., Carbone, S., Walter, D., Bobrowski, N., Brito, J., Chi, X., Gutmann, A., Hrabe de Angelis, I., Machado, L. A. T., Moran-Zuloaga, D., Rüdiger, J., Schneider, J., Schulz, C., Wang, Q., Wendisch, M., Artaxo, P., Wagner, T., Pöschl, U., Andreae, M. O., & Pöhlker, C.

(2018). African volcanic emissions influencing atmospheric aerosols over the Amazon rain forest. *Atmospheric Chemistry and Physics, 18*(14), 10391-10405. doi:10.5194/acp-18-10391-2018

Semane, N., Bencherif, H., Morel, B., Hauchecorne, A., & Diab, R. D. (2006). An unusual stratospheric ozone decrease in the Southern Hemisphere subtropics linked to isentropic air-mass transport as observed over Irene (25.5°; S, 28.1°; E) in mid-May 2002. *Atmospheric Chemistry and Physics, 6*(7), 1927-1936. doi:10.5194/acp-6-1927-2006

Shikwambana, L., & Sivakumar, V. (2018). Long-range transport of volcanic aerosols over South Africa: a case study of the Calbuco volcanic eruption in Chile during April 2015. *South African Geographical Journal, 100*(3), 349-363. doi:10.1080/03736245.2018.1498383

Slaper, H., & Van der Leun, J. C. (1987). Human exposure to ultraviolet radiation: quantitative modelling of skin cancer incidence. *Human Exposure to Ultraviolet Radiation*, 155-171.

Tesfaye, M., Sivakumar, V., Botai, J., & Mengistu Tsidu, G. (2011). Aerosol climatology over South Africa based on 10 years of Multiangle Imaging Spectroradiometer (MISR) data. *Journal of Geophysical Research: Atmospheres, 116*(D20). doi:10.1029/2011jd016023

Theys, N., Campion, R., Clarisse, L., Brenot, H., van Gent, J., Dils, B., Corradini, S., Merucci, L., Coheur, P. F., Van Roozendael, M., Hurtmans, D., Clerbaux, C., Tait, S., & Ferrucci, F. (2013). Volcanic SO₂ fluxes derived from satellite data: a survey using OMI, GOME-2, IASI and MODIS. *Atmospheric Chemistry and Physics, 13*(12), 5945-5968. doi:10.5194/acp-13-5945-2013

Thieden, E., Holm-Schou, A.-S. S., Philipsen, P. A., Heydenreich, J., & Wulf, H. C. (2019). Adult UVR exposure changes with life stage – a 14-year follow-up study using personal electronic UVR dosimeters. *Photochemical & Photobiological Sciences, 18*(2), 467-476. doi:10.1039/C8PP00365C

Thompson, A. M., Witte, J. C., Hudson, R. D., Guo, H., Herman, J. R., & Fujiwara, M. (2001). Tropical tropospheric ozone and biomass burning. *Science, 291*(5511), 2128-2132.

Torres, O., Jethva, H., Ahn, C., Jaross, G., & Loyola, D. G. (2020). TROPOMI aerosol products: evaluation and observations of synoptic-scale carbonaceous aerosol plumes during 2018–2020. *Atmospheric Measurement Techniques, 13*(12), 6789-6806. doi:10.5194/amt-13-6789-2020

Vernier, J.-P., Fairlie, T. D., Murray, J. J., Tupper, A., Trepte, C., Winker, D., Pelon, J., Garnier, A., Jumelet, J., Pavolonis, M., Omar, A. H., & Powell, K. A. (2013). An Advanced System to Monitor the 3D Structure of Diffuse Volcanic Ash Clouds. *Journal of Applied Meteorology and Climatology, 52*(9), 2125-2138. doi:10.1175/jamc-d-12-0279.1

Vishvakarman, D., & Wong, J. (2003). Description of the use of a risk estimation model to assess the increased risk of non-melanoma skin cancer among outdoor workers in Central Queensland, Australia. *Photodermatology, photoimmunology & photomedicine, 19*(2), 81-88. doi:10.1034/j.1600-0781.2003.00012.x

Whiteman, D. C., Thompson, B. S., Thrift, A. P., Hughes, M.-C., Muranushi, C., Neale, R. E., Green, A. C., Olsen, C. M., Whiteman, D. C., Green, A. C., Olsen, C. M., Neale, R. E., Webb, P. M., Jackman, L. M., Ranieri, B. A., Thompson, B. S., & Cicero, R. A. (2016). A Model to Predict the Risk of Keratinocyte Carcinomas. *Journal of Investigative Dermatology, 136*(6), 1247-1254. doi:10.1016/j.jid.2016.02.008

Wilkes, M., Wright, C. Y., du Plessis, J. L., & Reeder, A. (2015). Fitzpatrick skin type, individual typology angle, and melanin index in an African population: Steps toward universally applicable skin photosensitivity assessments. *JAMA dermatology, 151*(8), 902-903. doi:10.1001/jamadermatol.2015.0351

Wolfram, E. A., Salvador, J., Orte, F., D'Elia, R., Godin-Beekmann, S., Kuttippurath, J., Pazmiño, A., Goutail, F., Casiccia, C., Zamorano, F., Paes Leme, N., & Quel, E. J. (2012). The unusual persistence of an ozone hole over a southern mid-latitude

station during the Antarctic spring 2009: a multi-instrument study. *Annales Geophysicae, 30*(10), 1435-1449. doi:10.5194/angeo-30-1435-2012

Wright, C. Y., Brogniez, C., Ncongwane, K. P., Sivakumar, V., Coetzee, G., Metzger, J.-M., Auriol, F., Deroo, C., & Sauvage, B. (2013). Sunburn Risk Among Children and Outdoor Workers in South Africa and Reunion Island Coastal Sites. *Photochemistry and Photobiology, 89*(5), 1226-1233. doi:10.1111/php.12123

Wright, C. Y., du Preez, D. J., Millar, D. A., & Norval, M. (2020). The Epidemiology of Skin Cancer and Public Health Strategies for Its Prevention in Southern Africa. *International Journal of Environmental Research and Public Health, 17*(3), 1017. doi:10.3390/ijerph17031017

Chapter 3 Results: The relationship between ozone and ultraviolet radiation

3.1 Paper overview

As solar UVR passes through the atmosphere it is scattered, absorbed and reflected by gases and particles in the atmosphere. Apart from atmospheric parameters, surface UVR is dependent on site-specific factors such as altitude, latitude and surface albedo (Fioletov et al., 2010) as described in Section 1.2.

Stratospheric ozone can significantly reduce incoming UVB (UVR between 280 - 320 nm) radiation (Bais et al., 2019). The release of ODS and the formation of the Antarctic ozone hole during the austral spring have resulted in decreased stratospheric ozone concentrations in the Southern Hemisphere during the summer months (Bais et al., 2015). The decline in stratospheric ozone and the break-up of the polar vortex during the austral spring and summer have led to increases in surface UVR particularly when ozone-poor air masses from the ozone hole are transported over areas such as South America, Australia, and New Zealand (Abarca et al., 2002a; Abarca et al., 2002b; Gies et al., 2013; McKenzie et al., 1999). These elevated levels of solar UVR at the surface can have negative impacts on public health (Young et al., 2017).

This manuscript investigated the relationship between ozone, both total column and stratospheric, and solar UVR. A dynamical transport model was used to model the isentropic transport ozone-poor air masses to determine their origin. Using ground-based solar UVB radiation data and satellite data for ozone, results showed that UVB radiation is at maximum between December and February while TCO and stratospheric ozone decline from a maximum in spring months towards the summer months.

A clear-sky determination method was used to remove the effects of clouds when investigating the relationship between ozone and UVR. The RAF indicated that a 1%

decrease in TCO would result in a 0.59% increase in UVR at the surface. The strongest correlation (R^2=0.53) between ozone and UVR was found at SZA 25°.

Low-ozone events were identified and on clear-sky days, it was found that decreases in TCO and stratospheric ozone can result in increased UVB radiation at the surface between 6% and 45%. The Mesoscale Isentropic Transport Model of Stratospheric Ozone by Advection and Chemistry (Modèle Isentropique du transport Méso-échelle de l'ozone stratosphérique par advection avec CHIMIE or MIMOSA-CHIM) was used to trace the source of ozone-poor air over Cape Point during spring and summer months. Using PV as a dynamic tracer, it was found that the Antarctic ozone hole has a limited effect on ozone concentrations over Cape Point. Instead, Cape Point is influenced by air masses from sub-tropical regions.

The results also showed that an inverse relationship exists between ozone and solar UVB radiation and that decreases in TCO and stratospheric ozone can result in increased UVB radiation at the surface. Furthermore, the dynamical transport model showed that Cape Point is largely unaffected by the break-up of the ozone hole.

3.1.1 Limitations of study

The RAF values presented in Table 1 of the published article are lower than those presented in previous research which suggest that RAF values should range between 1±0.2 (Micheletti et al., 2003). Since the RAF, compares solar UVR and TCO from one day with another, the presence of clouds and aerosols would have influenced the RAF calculations. Although only clear-sky days were used in the analysis it is possible that some clouds were not removed in the process. Furthermore, the effect of aerosols was not considered during the RAF calculations. As aerosols and clouds can decrease surface solar UVR, decreased UVR levels could have been observed and resulted in lower RAF values.

The increases in UVI were determined in comparison to the UVI climatology. As with the RAF calculations, aerosols and clouds would have impacted the observed UVI. The negative 'increases' imply that UVI actually decreased

instead of increasing as expected. The effect of aerosols on surface UVI was not included in this study, it is possible that an increase in aerosol loading could have decreased surface UVI.

In the published manuscript, the RAF values were not calculated using the climatological values of UVI or ozone. The RAF value for a specific day was compared to a randomly selected clear-sky day. This is stated in Section 2.2.4 of the published article. Taking the average RAF values irrespective of season or SZA would have resulted in errors in the derived RAF values.

Based on these limitations, suggestions for future research have been included in Chapter 7.

3.2 Thesis contribution

This manuscript contributes to the thesis by addressing Objective 1 which was to investigate the relationship between solar UVB radiation and stratospheric ozone on clear-sky days and to identify solar UVB radiation anomalies resulting from changes in stratospheric ozone.

The findings of this manuscript contribute towards the understanding of the relationship between surface UVB radiation and atmospheric ozone at an unpolluted site in South Africa. Furthermore, the manuscript demonstrates the limited effect of the Antarctic ozone hole on stratospheric ozone over South Africa and that increases in surface UVB radiation can be attributed to decreases in TCO and stratospheric ozone.

3.3 Contribution of candidate

D. Jean du Preez was responsible for the data collection and analysis, interpretation and discussion of results and writing the manuscript. The co-authors contributed towards the interpretation and discussion of the results as well as the final manuscript preparation.

3.4 Publication status

du Preez, D. J., Ajtić, J. V., Bencherif, H., Bègue, N., Cadet, J. M., & Wright, C. Y. (2019). Spring and summer time ozone and solar ultraviolet radiation variations over Cape Point, South Africa. Annales Geophysicae, 37(2), 129-141. https://doi.org/10.5194/angeo-37-129-2019

3.5 References

Abarca, J. F., & Casiccia, C. C. (2002a). Skin cancer and ultraviolet-B radiation under the Antarctic ozone hole: southern Chile, 1987–2000. *Photodermatology, photoimmunology & photomedicine, 18*(6), 294-302. doi:10.1034/j.1600-0781.2002.02782.x

Abarca, J. F., Casiccia, C. C., & Zamorano, F. D. (2002b). Increase in sunburns and photosensitivity disorders at the edge of the Antarctic ozone hole, Southern Chile, 1986-2000. *Journal of the American Academy of Dermatology, 46*(2), 193-199. doi:10.1067/mjd.2002.118556

Bais, A. F., Bernhard, G., McKenzie, R. L., Aucamp, P., Young, P. J., Ilyas, M., Jöckel, P., & Deushi, M. (2019). Ozone–climate interactions and effects on solar ultraviolet radiation. *Photochemical & Photobiological Sciences, 18*(3), 602-640. doi:10.1039/C8PP90059K

Bais, A. F., McKenzie, R. L., Bernhard, G., Aucamp, P. J., Ilyas, M., Madronich, S., & Tourpali, K. (2015). Ozone depletion and climate change: impacts on UV radiation. *Photochemical & Photobiological Sciences, 14*(1), 19-52. doi:10.1039/c4pp90032d

Fioletov, V., Kerr, J. B., & Fergusson, A. (2010). The UV Index: Definition, Distribution and Factors Affecting it. *Canadian journal of public health, 101*(4), I5-I9. doi:10.1007/BF03405303

Gies, P., Klekociuk, A., Tully, M., Henderson, S., Javorniczky, J., King, K., Lemus-Deschamps, L., & Makin, J. (2013). Low Ozone Over Southern Australia in August 2011 and its Impact on Solar Ultraviolet Radiation Levels. *Photochemistry and Photobiology, 89*(4), 984-994. doi:10.1111/php.12076

McKenzie, R., Connor, B., & Bodeker, G. (1999). Increased Summertime UV Radiation in New Zealand in Response to Ozone Loss. *Science, 285*(5434), 1709-1711. doi:10.1126/science.285.5434.1709

Micheletti, M. I., Piacentini, R. D., & Madronich, S. (2003). Sensitivity of Biologically Active UV Radiation to Stratospheric Ozone Changes: Effects of Action Spectrum Shape and Wavelength Range¶. *Photochemistry and Photobiology, 78*(5), 456-461. doi:10.1562/0031-8655(2003)0780456SOBAUR2.0.CO2

Young, A. R., Claveau, J., & Rossi, A. B. (2017). Ultraviolet radiation and the skin: Photobiology and sunscreen photoprotection. *Journal of the American Academy of Dermatology, 76*(3, Supplement 1), S100-S109. doi:10.1016/j.jaad.2016.09.038

3.6 Manuscript 1

Ann. Geophys., 37, 129–141, 2019
https://doi.org/10.5194/angeo-37-129-2019

Annales Geophysicae Open Access EGU

Spring and summer time ozone and solar ultraviolet radiation variations over Cape Point, South Africa

David J. du Preez[1,2], Jelena V. Ajtić[3], Hassan Bencherif[4,5], Nelson Bègue[4], Jean-Maurice Cadet[4], and Caradee Y. Wright[1,6]

[1]Department Geography, Geoinformatics and Meteorology, University of Pretoria, Pretoria, 0002, South Africa
[2]South African Weather Service, Pretoria, 0181, South Africa
[3]Faculty of Veterinary Medicine, University of Belgrade, Bulevar oslobodjenja 18, 11000 Belgrade, Serbia
[4]Université de La Réunion, Laboratoire de l'Atmosphère et des Cyclones, UMR 8105, 15 Avenue René Cassin, CS 92003, Saint-Denis, Cedex, Réunion, France
[5]School of Chemistry and Physics, University of KwaZulu-Natal, Westville, Durban, South Africa
[6]Environment and Health Research Unit, South African Medical Research Council, Pretoria, 0001, South Africa

Correspondence: David J. du Preez (dupreez.jd@gmail.com)

Received: 30 May 2018 – Discussion started: 7 June 2018
Revised: 17 January 2019 – Accepted: 21 February 2019 – Published: 6 March 2019

Abstract. The correlation between solar ultraviolet radiation (UV) and atmospheric ozone is well understood. Decreased stratospheric ozone levels which led to increased solar UV radiation levels at the surface have been recorded. These increased levels of solar UV radiation have potential negative impacts on public health. This study was done to determine whether the break-up of the Antarctic ozone hole has an impact on stratospheric columnar ozone (SCO) and resulting ambient solar UV-B radiation levels at Cape Point, South Africa, over 2007–2016. We investigated the correlations between UV index, calculated from ground-based solar UV-B radiation measurements and satellite-retrieved column ozone data. The strongest anti-correlation on clear-sky days was found at solar zenith angle 25° with exponential fit R^2 values of 0.45 and 0.53 for total ozone column and SCO, respectively. An average radiation amplification factor of 0.59 across all SZAs was calculated for clear-sky days. The MIMOSA-CHIM model showed that the polar vortex had a limited effect on ozone levels. Tropical air masses more frequently affect the study site, and this requires further investigation.

1 Introduction

Solar ultraviolet (UV) radiation is a part of the electromagnetic spectrum of energy emitted by the Sun (Diffey, 2002). Solar UV radiation comprises a wavelength band of 100–400 nm; however, not all wavelengths reach the Earth. Solar UV radiation is divided into UV-A, UV-B and UV-C bands depending on the wavelength. The UV-C and UV-A bands cover the shortest and longest wavelengths, respectively. The UV-B part of the spectrum spans a wavelength range between 280 and 315 nm (WHO, 2017). The reason behind this sub-division of UV radiation is a large variation in biological effects related to the different wavelengths (Diffey, 2002). Moreover, an interaction of different UV bands with the atmospheric constituents results in an altered UV radiation reaching the surface: all UV-C and ∼ 90 % of UV-B radiation is absorbed, while the UV-A band is mostly unaffected (WHO, 2017). The amount of solar UV-B radiation at the surface of the Earth is largely impacted by the amount of atmospheric ozone (Lucas and Ponsonby, 2002), but also several other factors, such as altitude, solar zenith angle (SZA), latitude and pollution (WHO, 2017). The SZA has a significant impact on the amount of surface solar UV-B radiation (McKenzie et al., 1996). Under clear-sky conditions and low pollution levels, atmospheric ozone (of which approximately 90 % is found in the stratosphere) absorbs solar UV-B radiation (Fahey and Hegglin, 2011). A study in the

south of Brazil found a strong anti-correlation between ozone and solar UV-B radiation on clear-sky days using fixed SZAs (Guarnieri et al., 2004).

Anthropogenic and natural factors can cause changes in the amount of atmospheric ozone. Unlike natural ozone variability which is mostly of a seasonal nature and therefore has a reversible character, human activities, such as the release of ozone-depleting substances, have led to a long-term ozone decline in a greater part of the atmosphere (Bais et al., 2015), and, in turn, to higher levels of solar UV-B radiation at the Earth's surface (Fahey and Hegglin, 2011). An outstanding example of ozone depletion is the formation of the Antarctic ozone hole, a phenomenon discovered in the 1980s (Farman et al., 1985). Each austral spring, a severe ozone depletion occurs under the unique conditions in the Antarctic polar vortex, decreasing total ozone column (TOC) below 220 Dobson units (DU), a threshold defining the ozone hole.

The Antarctic ozone hole has been extensively studied (WMO, 2011). Apart from its direct influence on the ozone amounts in the Southern Hemisphere (Ajtić et al., 2004; de Laat et al., 2010) the Antarctic ozone hole affects a wide range of atmospheric phenomena as well as the climate of the Southern Hemisphere. For example, ozone depletion over Antarctica has altered atmospheric circulation, temperature and precipitation patterns in the Southern Hemisphere during the austral spring and summer (Brönnimann et al., 2017; Bandoro et al., 2014). Another notable consequence of decreased atmospheric ozone is an increase in solar UV radiation at the surface of the Earth, which has been supported by experimental evidence (Herman and McKenzie, 1998). This anti-correlation and association with the Antarctic ozone hole has been confirmed at Lauder, New Zealand (McKenzie et al., 1999).

Our analysis investigated the anti-correlation between the content of ozone in the atmosphere and solar UV-B radiation over the Western Cape Province, South Africa. The objectives in our study were (1) to determine the climatology of solar UV-B radiation and the climatology of TOC and stratospheric column ozone (SCO) for Cape Point, South Africa; (2) to determine clear-sky days for Cape Point and use them to analyse the anti-correlation between solar UV-B radiation and TOC, on the one hand, and solar UV-B radiation and SCO, on the other hand; (3) to identify low TOC and SCO events at Cape Point during spring and summer months; (4) to use a transport model to determine the origin of ozone-poor air observed during the identified low-ozone events; and (5) to explore whether the Antarctic ozone hole influenced the identified low-ozone events at Cape Point. To the best of our knowledge these objectives, in a South African context, and in relation to increased solar UV-B radiation over South Africa directly related to the Antarctic ozone depletion, have not been studied before.

2 Data and methods

2.1 UV data

The study site was Cape Point (34.35° S, 18.50° E, 230 m a.s.l.), a weather station in the Western Cape, South Africa (Fig. 1). The station is one of the World Meteorological Organization (WMO) Global Atmosphere Watch (GAW) baseline monitoring sites. It is located around 60 km south of Cape Town and although it is considered free of air pollution (Slemr et al., 2008), it may still be affected by maritime aerosols. Since aerosols can have a pronounced effect on the amount of UV radiation reaching the surface (Bais et al., 2015), our choice of Cape Point offers a setting in which a modification of the UV-B radiation by anthropogenic aerosols can be overlooked.

Solar UV-B radiation data, with the original hourly recording interval, were obtained from the South Africa Weather Service (SAWS) for Cape Point station for the period 2007–2016. The solar UV-B radiation measurements were made with the Solar Light Model Biometer 501 Radiometer. The biometer measures solar UV radiation with a wavelength of 280–320 nm. The measured solar UV radiation is proportional to the analogue voltage output from the biometer with a controlled internal temperature (Solarlight, 2014). Two different instruments were used at Cape Point between 2007 and 2016: Instrument 3719 (January 2007–March 2016) and Instrument 1103 (April–December 2016). Both instruments were calibrated at Solar Light in June 2006 according to the "Calibration of the UV radiometer – Procedure and error analysis". During the period of operation three inter-comparisons were conducted using recently calibrated standard reference instruments. The inter-comparisons aimed to verify that the instruments in operation were recording accurate measurements and the inter-comparisons did not include homogenisation of the data or the application of different calibration factors.

Measurements are given in minimal erythemal dose (MED) units where 1 MED is defined by SAWS as $210\,\mathrm{J\,m^{-2}}$ and any incorrect or missing values were indicated in the dataset. During October 2016, the measured MED values exceeded the expected values and were corrected with a correction factor as recommended by the SAWS. Despite periods of missing data during the study years, there were 3129 days of useable solar UV-B data for Cape Point. To convert from instrument-weighted UV radiation to erythemally weighted UV radiation, a correction factor was applied as the instrument does not measure the full spectral range of the UV index (Seckmeyer et al., 2005; Cadet et al., 2017). Solar UV-B radiation values in MED were converted to UV index (UVI) using

$$\mathrm{UVI} = \mathrm{MED}[\mathrm{h}^{-1}]\frac{210\left[\mathrm{J\,m^{-2}}\right] \times 40\,[\mathrm{m^2\,W^{-1}}]}{3600[\mathrm{s}]}. \quad (1)$$

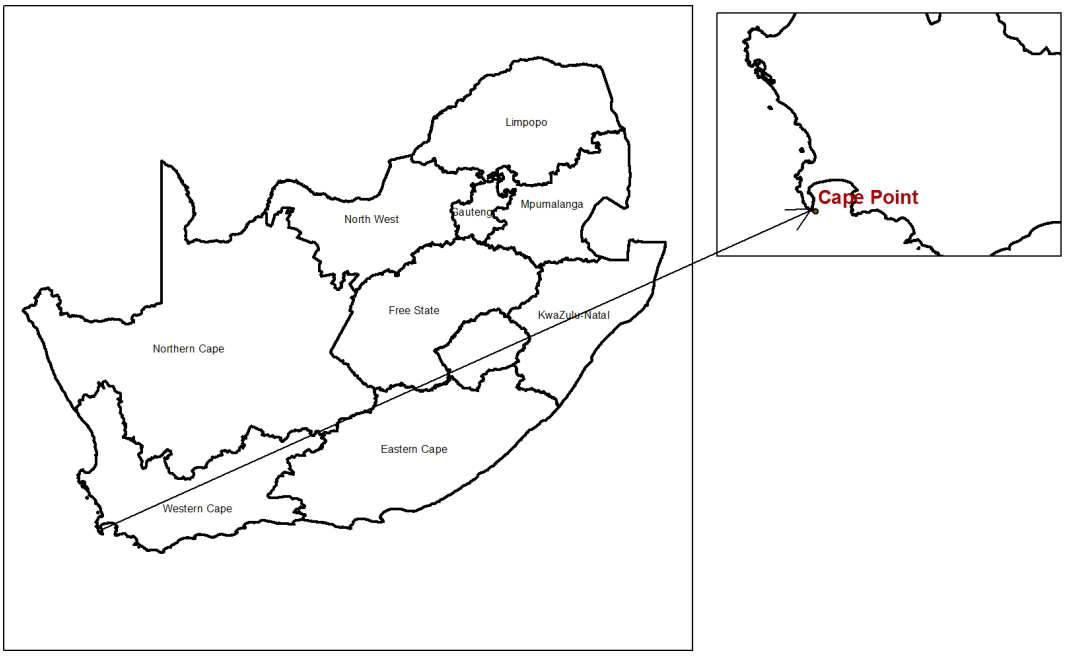

Figure 1. The map of South Africa and the location of the SAWS Cape Point Weather station in the Western Cape.

Since the correlation between solar UV-B radiation and ozone can be better observed when controlling SZA (Booth and Madronich, 1994), we also calculated SZA. First, we computed 10 min SZAs using an online tool, the Measurement and Instrument Data Centre's Solar Position Calculator (MIDC SPA) (https://midcdmz.nrel.gov/solpos/spa.html, last access: February 2017), which utilises the date, time and location of the site of interest and has an accuracy of ±0.0003° (Reda and Andreas, 2008). Second, from the 10 min SZAs we calculated hourly averages.

2.2 Column ozone data

TOC and SCO data were obtained for 2007–2016 (inclusive) for the grid area which was bound by the following coordinates – west: 16.5° E, south: 36.35° S, east: 20.6° E, north: 31.98° S. This grid area limited the TOC and SCO data to the area directly above Cape Point. The daily TOC data were measured with the Ozone Monitoring Instrument – Total Ozone Mapping Spectrometer (OMI – TOMS) on NASA's Aura satellite. OMI has a spatial resolution of 0.25°, which results in a ground resolution at nadir with a range of 13 km × 24 km to 13 km × 48 km (Levelt et al., 2006). Relative to other ozone observations, OMI has a bias of 1.5 % (McPeters et al., 2015). In the Southern Hemisphere, OMI-TOMS data have a lower seasonal dependence compared to the Northern Hemisphere. Overall, observations are within 3 % of Dobson and Brewer spectrophotometer observations (Balis et al., 2007).

The daily SCO data were measured with the Microwave Limb Sounder (MLS) instrument on NASA's Aura satellite. The MLS ozone data consisted of ozone profiles at 55 pressure levels and SCO values up to the thermal tropopause. The thermal tropopause is determined by the temperature data taken by the MLS instrument. The ozone profiles were used between 261 and 0.02 hPa (Livesey et al., 2017). The daily SCO values were extracted from the MLS data files. SCO observations from the MLS overestimate ozone in the stratosphere over 30° S but this overestimation is lower than compared to the Northern Hemisphere (Jiang et al., 2007). MLS SCO observations have a high correlation coefficient, 0.96–0.99, with OMI SCO observations (Huang et al., 2017).

2.3 Transport model

The Mesoscale Isentropic Transport Model of Stratospheric Ozone by Advection and Chemistry (Modèle Isentropique du transport Méso-échelle de l'ozone stratosphérique par advection avec CHIMIE or MIMOSA-CHIM) was used to identify the source of ozone-poor air above Cape Point. MIMOSA-CHIM results from the off-line coupling of the MIMOSA dynamical model (Hauchecorne et al., 2002) from the Reactive Processes Ruling the Ozone Budget in the Stratosphere (REPROBUS) chemistry model (Lefèvre et al., 1994). The ability of MIMOSA-CHIM to simulate and analyse the transport of stratospheric air masses has been highlighted in several previous studies over the polar regions (Kuttippurath et al., 2013, 2015; Tripathi et al., 2007; Semane et al., 2006; Marchand et al., 2003). The dynamical component of the model is forced by meteorological data such as wind, temperature and pressure fields from the European Centre for Medium-Range Weather Forecasts (EMCWF) daily analy-

ses. The dynamical component of potential vorticity (PV) was used to trace the origin of ozone-poor air masses. PV can be used as a quasi-passive tracer when diabatic and frictional terms are small. Therefore, over short periods of time, PV is conserved on isentropic surfaces following the motion (Holton and Hakim, 2013). A spatial area from 10° N to 90° S was used for the model with a $1° \times 1°$ resolution. The model has stratospheric isentropic levels ranging from 350 to 950 K. The MIMOSA-CHIM model created an output file for every 6 h. Simulations for each low-ozone event were initialised to run for at least 14 days prior to the low-ozone event to account for the model spin-up period. The PV maps were analysed at isentropic levels that correspond to 18, 20 and 24 km above ground level, thus covering the lower part of the ozone layer (Sivakumar and Ogunniyi, 2017).

2.4 Method

The climatologies of UVI, TOC and SCO were determined using the available days with data. These would provide a reliable baseline to which observations from specific days could be compared. Next, clear-sky days were determined from the solar UV-B radiation data based on a method that looks at the diurnal pattern of UV-B radiation. Once the clear-sky days had been determined, the correlation analysis between ozone and UVI was calculated using two methods. Only using clear-sky days removed the effect of clouds on UV-B radiation. Lastly, we determined low-ozone events and used the MIMOSA-CHIM model to identify the origin of ozone-poor air masses.

2.4.1 Climatologies

The hourly UVI value was averaged for each day in a specific month across the 10-year period and was used to determine the UVI climatology at Cape Point. All days were used to determine the climatology. The TOC and SCO climatologies were calculated using monthly averages.

2.4.2 Determination of clear-sky days

Cloud cover has a range of impacts on surface UV radiation, and therefore calculating cloud-free conditions is important to understand cloud impacts on UV radiation. Partly cloudy skies can reduce or increase UV radiation depending on the position of the Sun and clouds, while overcast skies decrease radiation (Bodeker and McKenzie, 1996; Bais et al., 2015). Due to the different spectral properties of clouds, the ability to detect clouds through solar radiation measurements is dependent on the wavelength of the spectrum that is measured (Zempila et al., 2017). Several studies (Bodeker and McKenzie, 1996; Zempila et al., 2017) have attended to determine cloud-free conditions and have all shown the challenges, in particular, for thin cloud conditions. Thus, determining cloud-free days is a step towards removing a contribution of all factors except amount of atmospheric ozone. As shown by McKenzie et al. (1991) a stronger correlation between ozone and solar UV-B radiation may be obtained if the days with clouds are removed.

The SAWS Cape Point site has no cloud cover data available. For that reason, we used a clear-sky determination method by Bodeker and McKenzie (1996) to find cloudy days and consequently remove them from our further analysis. First, days with solar UV-B measurements, TOC and SCO data were divided into seasons: summer – December, January, February (DJF), autumn – March, April, May (MAM), winter – June, July, August (JJA), and spring – September, October, November (SON). Then, clear-sky days were determined using three different tests.

The first test only considered the daily linear correlation between the UVI values measured before solar noon and the values after solar noon. Solar noon was determined as the hour interval with the lowest SZA value. Days with a linear correlation below 0.8 in the DJF, MAM and SON seasons were removed and were considered to be cloudy days. The first test was not performed on the winter season, when the UVI values, as well as the correlation values, were low.

The second test looked for a monotonic increase before solar noon and a monotonic decrease after solar noon for each day. On clear-sky days, UVI values before and after solar noon should monotonically increase and decrease, respectively. If monotonicity did not hold for the UVI values on a specific day, it was assumed that there was some cloud present on that day. The monotonicity test was performed for all seasons. It is interesting to note that at Cape Point, the second test of the clear-sky determination method identified more clear-sky afternoons than clear-sky mornings.

The third test removed days when the UVI values did not reach a threshold maximum value. This test was applied to all seasons. The threshold was determined as a value of 1.5 standard deviations (1.5 SD) below the UVI monthly average. The monthly average and standard deviations were determined from the solar UV-B radiation climatology for Cape Point.

Prior to applying the clear-sky determination method to the Cape Point UV-B radiation data, we tested the methodology against measurements from the Cape Town weather station where cloud cover data are available. In the test, we used the daily 06:00 and 12:00 UTC cloud cover observations, and randomly selected two years for the validation. The results showed that when the observations indicated more than four-eighths of cloud present, our methodology also identified these days as cloudy. Furthermore, we examined the diurnal radiometric curves from another year and found that the determined clear-sky days' radiometric curves closely followed the expected diurnal radiometric curve. This validation implied that the clear-sky tests removed approximately 87 % of cloudy days. Overall, approximately 500 days were determined to be clear-sky days that had UV-B, TOC and SCO data and they were used in our further analyses. For the DJF,

MAM, JJA and SON seasons there were 150, 104, 137 and 102 clear-sky days respectively.

2.4.3 Correlations

In addition to removing anthropogenic aerosols by choosing an air-pollution-free site and alleviating cloud effects by looking only at the clear-sky days, the correlation between solar UV-B radiation and ozone can be better observed when controlling SZA (Booth and Madronich, 1994). The correlation calculations were performed at fixed SZAs. The strength of the correlation between the amount of ozone (TOC and SCO data) and UVI was determined using the first-order exponential fit (Guarnieri et al., 2004):

$$y = ae^{bx}, \quad (2)$$

where $y =$ UVI and $x =$ ozone values (TOC or SCO).

The significance of the goodness of fit was determined for a 95 % confidence interval. The log-UVI (y axis) values were taken to test whether the goodness-of-fit R^2 values of the exponential fits were statistically significant (Hazarika, 2013).

2.4.4 Radiation amplification factor

The radiation amplification factor (RAF) describes a relationship between ozone values and solar UV-B radiation (Booth and Madronich, 1994). The RAF was introduced as a quantification of the effect that decreased ozone concentrations have on solar UV-B radiation levels. The RAF is a unitless coefficient of sensitivity and here we used its definition given by Booth and Madronich (1994) in Eq. (3). The RAF value at fixed SZAs was calculated using a specific clear-sky day compared to another random clear-sky day from a different year (Booth and Madronich, 1994).

$$\mathrm{RAF} = \ln\left(\frac{\mathrm{O_3}}{\mathrm{O_3'}}\right) / \ln\left(\frac{\mathrm{UVI'}}{\mathrm{UVI}}\right), \quad (3)$$

where $\mathrm{O_3}$ and $\mathrm{O_3'}$ are the first and second ozone values and UVI and UVI′ are the first and second UV measurements, respectively.

2.4.5 Low-ozone days

Days of low TOC and SCO values were determined from the set of clear-sky days, but only during spring and summer seasons, when solar UV radiation levels are highest. Days of low TOC values might not have had low SCO values and vice versa. Low TOC and SCO days were determined as days when the respective values were below 1.5 SD from the mean as determined in the climatology analyses (Schuch et al., 2015).

We then used the MIMOSA-CHIM model to identify whether the origin of ozone-poor air masses was from the polar region. In other words, on low-ozone days we looked into the maps of advected PV from MIMOSA-CHIM to identify the source of ozone-poor air parcels over the study area.

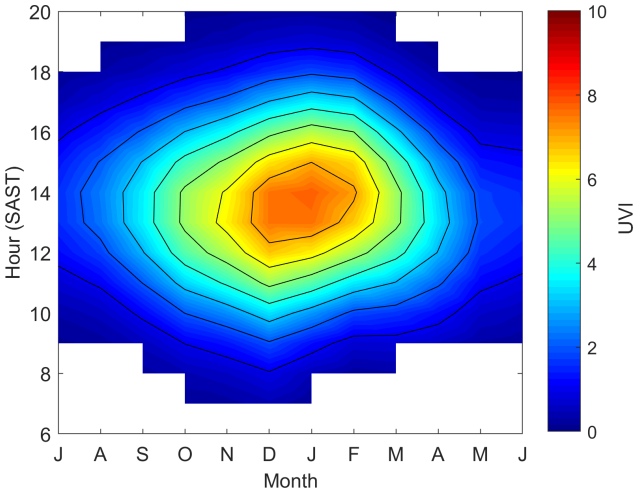

Figure 2. The UVI climatology for all sky conditions at Cape Point. The x axis starts with the month of July and ends with June.

3 Results and discussion

3.1 Climatologies and trends

3.1.1 UVI climatology

The monthly means of UVI for Cape Point during 2007–2016 were calculated as a function of time of the day and month of the year (Fig. 2). This climatology provides a reliable baseline against which observations can be compared and reveals the general patterns of the UVI signal recorded at the surface over the investigated 10-year period.

At Cape Point, the UVI maximum value of approximately 8 UVI occurs between 13:00 and 15:00 South African Standard Time (SAST), which corresponds to between 11:00 and 13:00 UTC (Fig. 2). The maximum UVI values are not centred on the local noon, implying that more UV radiation reaches this site in the afternoon. Indeed, as previously mentioned, our clear-sky determination method identified more clear-sky afternoons than clear-sky mornings (Sect. 2.4.2), which, under the assumption that cloud cover at Cape Point generally attenuates UV radiation reaching the surface, could explain the observed shift in the UVI maximum to about 14:00 SAST.

The seasons of maximum (DJF) and minimum (JJA) solar UV-B radiation at Cape Point are as expected for a site in the Southern Hemisphere and are similar to those found in studies at other South African sites, namely Pretoria, Durban, De Aar, and Port Elizabeth and Cape Town (Wright et al., 2011; Cadet et al., 2017). The maximum UVI values found in this study occur at similar times to Cadet et al. (2017) and Wright et al. (2011).

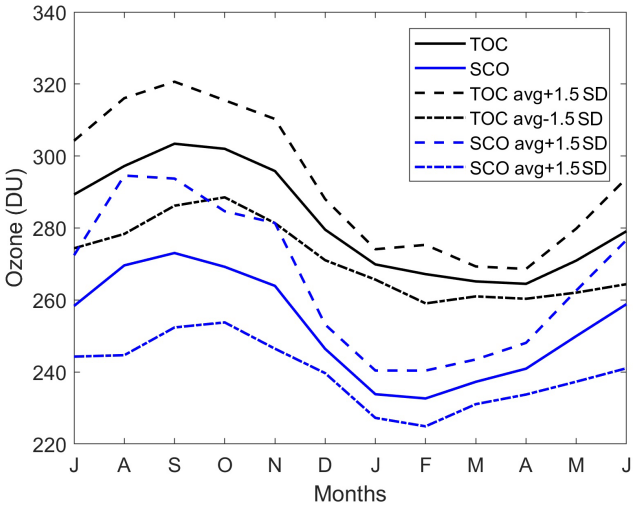

Figure 3. Monthly means ±1.5 SD for total ozone column and stratospheric column ozone starting in July and ending in June.

3.1.2 Ozone climatologies

At Cape Point, TOC (with the maximum of 303.4 DU) and SCO (with the maximum of 273.1 DU) values peaked during September and decreased to a minimum in February for SCO (232.65 DU) and April for TOC (254.49 DU) (Fig. 3). The variations in TOC and SCO are largest at the maximum values and smallest at the minimum values. Over Irene in Pretoria the greatest variation in SCO was seen during spring (Paul et al., 1998), which is in agreement with our results. It is suggested that this variability in TOC is due to the movement of mid-latitude weather systems which move further north during the Southern Hemisphere winter (Diab et al., 1992). The climatology of TOC over South Africa is mainly affected by atmospheric dynamics rather than by the effects of atmospheric chemistry (Bodeker and Scourfield, 1998).

The increase in TOC values during the winter months and the maximum during spring months are due to an ozone-rich mid-latitude ridge that forms on the equator side of the polar vortex. The ridge is a result of a distorted meridional flow caused by the Antarctic polar vortex that forms in late autumn. The vortex prevents poleward transport of the air and thus allows for a build-up of ozone-rich air in mid-latitudes. The lower TOC values over summer could be due to the dilution effect of ozone-poor air from the Antarctic ozone hole. The dilution effect occurs when the vortex breaks up (Bodeker and Scourfield, 1998; Ajtić et al., 2004).

3.2 Correlation between the amount of ozone and UVI

The first-order exponential goodness-of-fit R^2 values at fixed SZAs (Table 1) describe the anti-correlation between the amount of ozone in the atmosphere and UVI. The strongest anti-correlation was found at a fixed SZA 25° for both TOC and SCO. In this study the first-order exponential fit was used to describe the anti-correlation between ozone and solar UV radiation as in some instances this is best described with a non-linear fit (Guarnieri et al., 2004). A study on the anti-correlation between solar UV-B irradiance and TOC in southern Brazil found that the percentage of the R^2 values for exponential fits (66.0 %–85.0 %) explained the variations in solar UV-B irradiance due to TOC variations on clear-sky days at the same fixed SZA categories used in our study (Guarnieri et al., 2004).

Table 1. The correlation statistics for amount of ozone and UVI at Cape Point on clear-sky days.

SZA (°)	TOC: R^2 expo. fit	SCO: R^2 expo. fit	RAF
15	0.25*	0.18*	1.60
20	0.26*	0.23*	0.19
25	0.45*	0.53*	0.26
30	0.28*	0.20*	0.82
35	0.21*	0.11*	0.15
40	0.30*	0.30*	0.42
45	0.26*	0.29*	0.69
Average			0.59

* Indicates R^2 values were statistically significant at a 95 % confidence interval.

The exponential R^2 values of TOC found at Cape Point at a fixed SZA were much lower than those for southern Brazil (Guarnieri, et al., 2004). In our study and in other studies the R^2 value is smaller at the largest SZAs (Guarnieri et al., 2004; Wolfram et al., 2012). The correlation at smaller SZAs may be weaker than expected due to the limited number of data points at smaller SZAs. An improvement can be made on the correlations between SZA by discriminating between morning and afternoon SZAs.

At Cape Point, the RAF value for clear-sky days range between 0.15 and 1.60 with an average RAF value of 0.59. This can be interpreted as follows: for every 1 % decrease in TOC, UV-B radiation at the surface will increase by 0.59 %. RAF values specific to ozone and solar UV studies found in the literature range between 0.79 and 1.7 (Massen, 2013). RAF values have been used to describe the effect of other meteorological factors such as clouds and aerosols on surface UV radiation (Serrano et al., 2008; Massen, 2013). The differences to the RAF values found here and those found in the literature can be attributed to changes in time and location (Massen, 2013).

Salt build-up on the biometer at Cape Point may also have contributed to the accuracy of measurements taken by the biometer. Solar UV-B radiation data with a higher temporal resolution (e.g. 10 min) may have provided more data points for the analysis at fixed SZAs. Higher temporal resolution solar UV-B radiation data would have improved the determi-

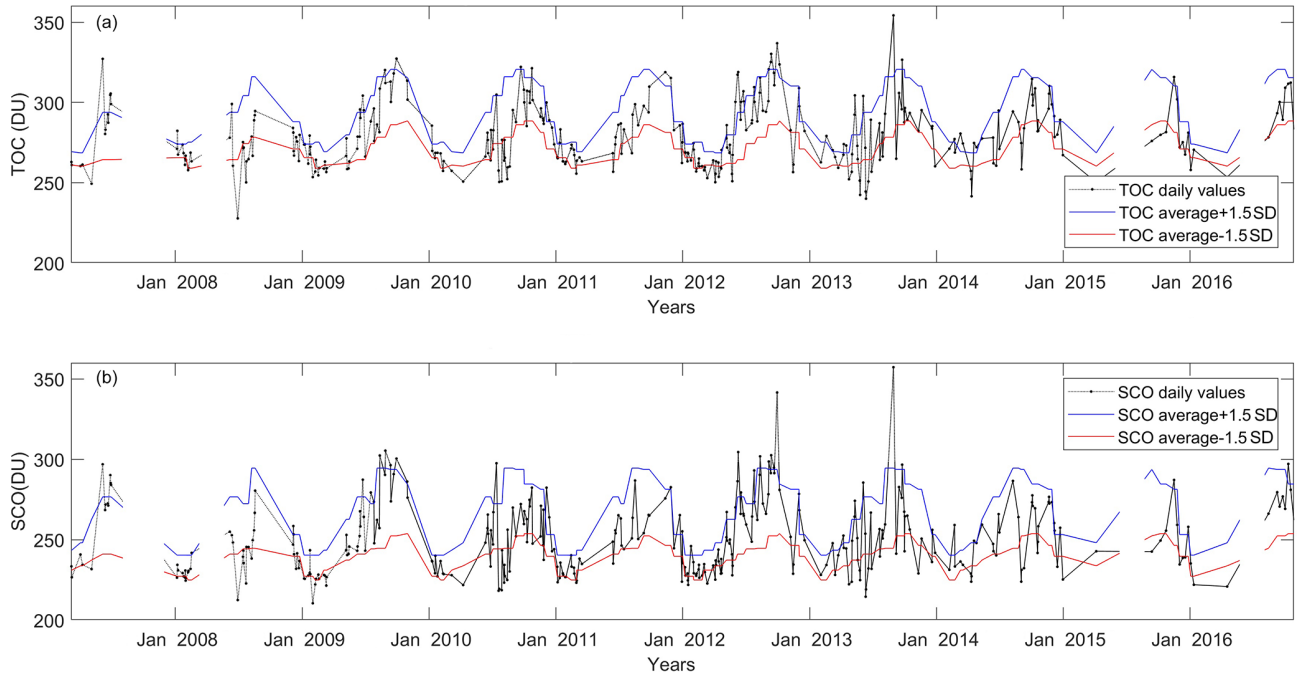

Figure 4. TOC **(a)** and SCO **(b)** values on clear-sky days over Cape Point and an indication of the average ±1.5 SD limits. Each dot corresponds to a TOC and SCO measurement on a clear-sky day from 2007 to 2016. Interrupted lines indicate missing data.

nation of clear-sky days. An improvement on the correlation and RAF values could be made by investigating the aerosol concentrations over the station.

3.3 Low-ozone events

Low-ozone events which occurred during the SON and DJF months were identified from the time series of TOC and SCO data on clear-sky days (Fig. 4). The highest frequency of low TOC and low SCO events occurred during January months and January and December months, respectively.

The low TOC and low SCO events along with the respective percentage decrease in TOC and SCO (Table 2) represent some of the largest decreases that occurred in DJF and SON seasons between 2007 and 2016 on clear-sky days. The DJF seasons of 2009–2010 and 2015–2016 are classified as El Niño years (Climate Prediction Center Internet Team, 2015). During these seasons higher TOC levels are expected over the mid-latitude regions (Kalicharran et al., 1993). From the identified low TOC events at Cape Point, none occurred during El Niño years.

This analysis aimed to discuss effects of stratospheric ozone and tropospheric ozone on surface UV-B radiation variations. When TOC and SCO reductions are similar, the effect of stratospheric ozone decrease is dominant. Conversely, when the reduction of TOC is high, and the reduction of SCO is low, the effect of tropospheric ozone is dominant.

All of the low-ozone events which occurred during January were due to decreased SCO. A decrease of 10.1 % in SCO was recorded on 30 January 2009 with a TOC decrease of 6.1 %. During February months we obtained the weakest reductions in TOC and SCO. Low-ozone events that occurred during September were mainly due to stratospheric ozone decreases, with the largest ozone reduction recorded on 1 September 2014 (18 % in SCO reduction) (Table 2).

We compared the UVI levels recorded during low-ozone events within the SON and DJF seasons to the UVI climatology to determine if the ozone reductions reflected on the UVI levels during low-ozone events. At Cape Point, the largest increases in the UVI levels were recorded for low-ozone events during November. The largest increase (46.5 %) in UVI occurred on 13 November 2012.

In the Southern Hemisphere, during the spring season (SON) low-ozone events are predominately due to the distortion and filamentation of the Antarctic ozone hole and to the dilution of the associated polar vortex. The dilution effect occurs later in the early summer season, when ozone-poor air masses from the polar region mix with air masses from the mid-latitudes and result in decreased ozone concentrations (Ajtić et al., 2004). There are no studies that refer to low-ozone events at Cape Point. In South Africa, a decrease in TOC was observed over Irene (25.9° S, 28.2° E) during May 2002 when TOC levels were 8 %–12 % below normal and at a minimum of 219.0 DU (Semane et al., 2006). The relative position of the surface high or low pressure can result in increases or decreases in TOC. The effect on TOC by weather systems is seasonally dependent (Barsby and Diab, 1995).

Table 2. Identified low-ozone events on clear-sky days at Cape Point during spring and summer months and the percentage decrease calculated from the relative climatological monthly mean.

Date	TOC (DU)	SCO (DU)	Decrease TOC (%)	Decrease SCO (%)	Increase UVI (%)
30 Jan 2009	253.5*	210.4*	6.1	10.1	30.4
6 Feb 2009	253.9*	222.2*	5.0	4.5	36.2
15 Feb 2009	254.6*	228.3	4.7	1.9	34.2
28 Feb 2011	255.7*	223.2*	4.3	4.1	6.8
16 Jan 2012	268.2	221.9*	0.6	5.1	21.2
8 Feb 2012	257.0*	227.5	3.8	2.2	31.7
13 Nov 2012	256.6*	228.8	13.3	13.3	46.5
14 Nov 2012	261.3*	234.6	11.7	11.1	42.1
6 Sep 2013	265.0*	241.3*	12.7	11.6	22.3
9 Nov 2013	282.3	229.0*	4.6	13.3	21.9
1 Sep 2014	274.7*	223.9*	9.5	18.0	−2.5
2 Sep 2014	258.4*	231.2*	14.9	15.3	−2.3
9 Sep 2014	284.0*	232.3*	6.4	14.9	−5.5
11 Jan 2016	270.6	221.9*	−0.3	5.1	−7.9

* Indicates whether the low-ozone event was due to low TOC and/or low SCO values.

The increased levels of solar UV-B radiation found in this study due to low SCO events are similar to those found at other Southern Hemisphere sites (Gies et al., 2013; McKenzie et al., 1999; Abarca et al., 2002). It is possible that low-ozone events that occurred over Cape Point during 2007–2016 have not been included. These events might have fallen outside the methods used in this study or were not considered due to the availability of solar UV-B radiation, TOC or SCO data. Moreover, it should be noted that the Cape Point site being located at 34° S, at the southern limit of the tropical stratospheric reservoir. Cape Point can be affected by dynamical and transport processes, and therefore air masses of different latitude origins can pass over it. Indeed, over our study period from September to February, the obtained low-ozone event could be of polar origin (i.e. in relation with the extension and distortion of the polar vortex) or of tropical origin (i.e. in relation with isentropic air masses transport across the subtropical barrier, as reported by Semane et al., 2006, and Bencherif et al., 2011, 2007). The following sub-section discusses low-ozone events with regard to the dynamical situations and origins of air masses above the study site.

3.4 Origin of ozone-poor air

In this section the model results from MIMOSA-CHIM are shown for a selection on low-ozone events. The latitude origin of air masses was classified according to the colour scale on the PV maps. Blue colours indicate air masses with relatively high PV values, implying their polar origins, while red colours indicate relatively low PV values of tropical origin.

The origin of the air masses for low-ozone events in January (Table 3) and February (Table 4) shows a consistent pattern: in the lower parts of the stratosphere, at 425 K, the air was of tropical origin; higher up, at 475 K, it was of mid-latitude origin; and at 600 K, air masses from the polar region were above Cape Point. This pattern is illustrated in the PV maps from MIMOSA-CHIM of the low-ozone event on 16 January 2012 (Fig. 5), which best demonstrates all January events. During this event, we identified low SCO (Table 2). Similarly, the PV maps from MIMOSA-CHIM for the low-ozone event on 6 February 2009 (Fig. 6) best demonstrate the situation for February months.

Table 3. Origin of ozone-poor air at isentropic levels for low-ozone events in January.

Date	Origin at 425 K	Origin at 475 K	Origin at 600 K
30 Jan 2009	Tropical	Mid-latitude	Polar
16 Jan 2012	Tropical	Mid-latitude	Polar
11 Jan 2016	Tropical	Mid-latitude	Polar

Our results imply that the low-ozone events during the months of January and February were not directly influenced by the Antarctic ozone hole as by that time, the polar vortex had already broken up. However, it is possible that these events are a consequence of the ensuing mixing of the polar ozone-poor air that reduces the mid-latitude ozone concentrations (Ajtić et al., 2004).

The origin of air masses for low-ozone events during September (Table 5) and the PV maps from MIMOSA-CHIM for the low-ozone event on 2 September 2014 (Fig. 7) show the transport of tropical air masses southward over the study site. During September months there was less mixing of air masses across latitudinal boundaries.

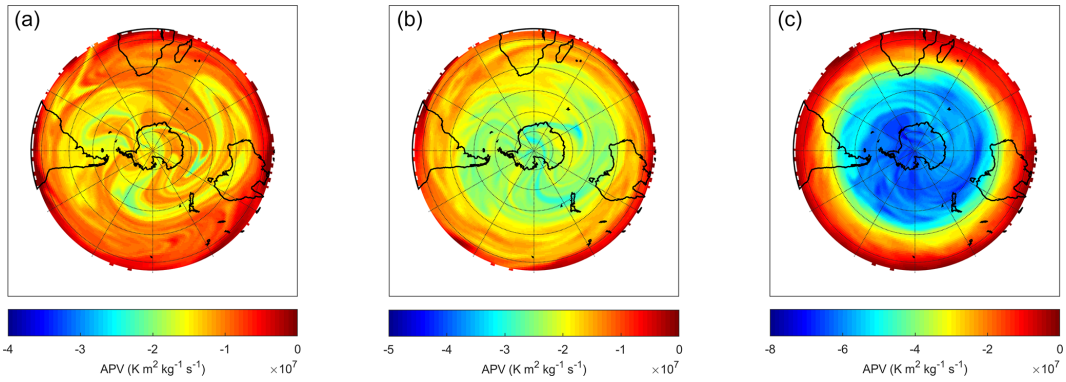

Figure 5. Advected potential vorticity (APV) maps from MIMOSA-CHIM at 425 K **(a)**, 475 K **(b)** and 600 K **(c)** on 16 January 2012.

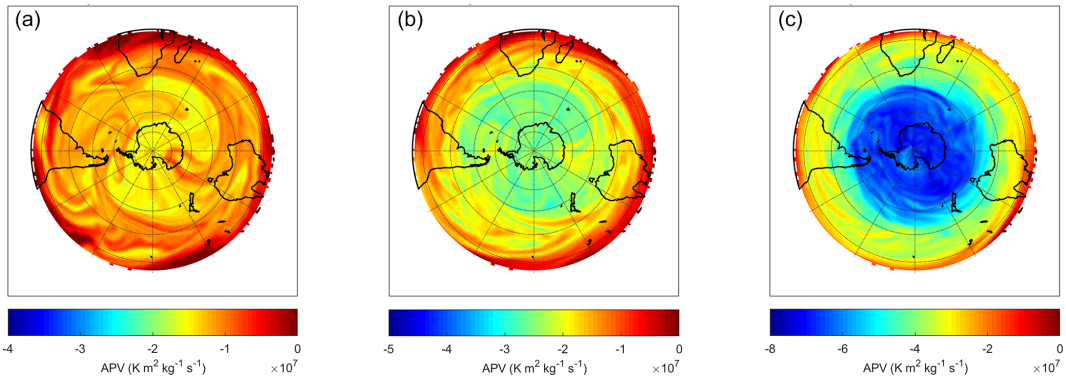

Figure 6. APV maps from MIMOSA-CHIM at 425 K **(a)**, 475 K **(b)** and 600 K **(c)** on 6 February 2009.

Table 4. Origin of ozone-poor air at isentropic levels for low-ozone events in February.

Date	Origin at 425 K	Origin at 475 K	Origin at 600 K
6 Feb 2009	Tropical	Mid-latitude	Polar
15 Feb 2009	Tropical	Mid-latitude	Polar
28 Feb 2011	Tropical	Mid-latitude	Polar
8 Feb 2012	Tropical	Mid-latitude	Polar

Table 5. Origin of ozone-poor air at isentropic levels for low-ozone events in September.

Date	Origin at 435 K	Origin at 485 K	Origin at 600 K
6 Sep 2013	Tropical	Mid-latitude	Mid-latitude–polar
1 Sep 2014	Tropical	Tropical	Mid-latitude–polar
2 Sep 2014	Tropical	Tropical	Mid-latitude–polar
9 Sep 2014	Tropical	Tropical	Mid-latitude–polar

The origin of air masses for low-ozone events in November (Table 6) shows that at 600 K polar air masses do affect the study site, but the ozone hole is no longer present over Antarctica. The PV maps from MIMOSA-CHIM for the low-ozone event on 14 November 2012 (Fig. 8) best demonstrate the situation for November months.

Table 6. Origin of ozone-poor air at isentropic levels for low-ozone events in November.

Date	Origin at 435 K	Origin at 480 K	Origin at 600 K
13 Nov 2012	Tropical	Mid-latitude	Polar
14 Nov 2012	Tropical	Mid-latitude	Polar
9 Nov 2013	Tropical	Mid-latitude	Polar

The PV maps from MIMOSA-CHIM suggest that the Antarctic polar vortex air masses with low-ozone levels have a limited effect on the ozone levels over Cape Point, South Africa. Instead, the study site is largely influenced by ozone-poor air masses from sub-tropical regions. The effect of these sub-tropical air masses on ozone concentrations is dependent on isentropic level and time of year. In fact, it is well known that Rossby planetary waves are generated due to the development of synoptic disturbances in the troposphere during winter and spring seasons. They propagate vertically through to the stratospheric layers when the zonal winds are west-

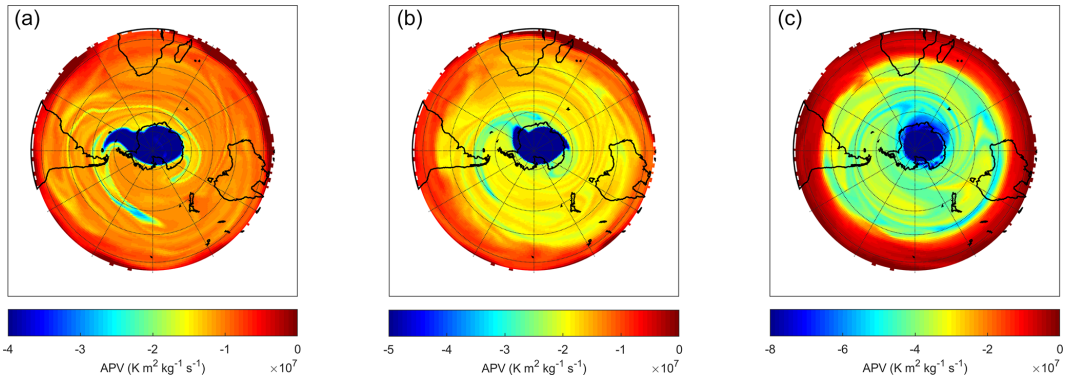

Figure 7. APV maps from MIMOSA-CHIM at 435 K **(a)**, 485 K **(b)** and 600 K **(c)** on 2 September 2014.

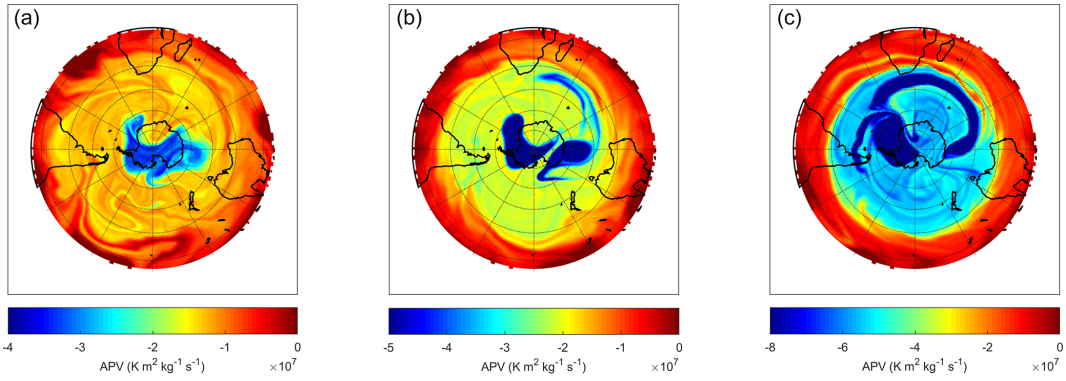

Figure 8. APV maps from MIMOSA-CHIM at 435 K **(a)**, 485 K **(b)** and 600 K **(c)** on 14 November 2012.

erly (Charney and Drazin, 1961; Leovy et al., 1985). Moreover, as reported by many authors, gravity and Rossby planetary waves are involved in isentropic transport across the subtropical barrier. Portafaix et al. (2003) studied the southern subtropical barrier by using MIMOSA-CHIM model advected PV maps, together with a numerical tool developed by LACy (Reunion University) named DyBaL (Dynamical Barrier Localisation) based on Nakamura formalism (Nakamura, 1996). They showed that the southern subtropical barrier is usually located around 25–30° S but has an increasing variability during winter and spring. Moreover, using MIMOSA-CHIM-adverted PV fields (Bencherif et al., 2007, 2003) showed that exchange processes between the stratospheric tropical reservoir and mid-latitudes are episodic and take place through the subtropical barrier due to planetary wave-breaking inducing increases or decreases in ozone at tropical and subtropical locations depending on the isentropic levels. It is known that atmospheric ozone over South Africa is mainly impacted by dynamical factors (Bodeker et al., 2002). Another dynamical factor that influences ozone over the study area is stratospheric–tropospheric exchanges, which mostly influence SCO levels. One or a combination of these dynamical factors likely result in low-ozone levels over Cape Point.

4 Conclusions

This study evaluated the anti-correlation between ground-based solar UV-B radiation and satellite ozone observations based on clear-sky days at Cape Point, South Africa. The study further investigated whether the break-up of the Antarctic ozone hole during spring–summer has an impact on the ozone concentrations over the study area and, as a result, affects solar UV-B radiation levels.

The solar UV-B climatology for Cape Point as well as the climatologies of TOC and SCO followed the expected annual cycle for the Southern Hemisphere. The determination of clear-sky days proved to be reliable in identifying cloudy days. The clear-sky tests removed approximately 87 % of days that were affected by cloud cover. At Cape Point, at SZA 25°, exponential goodness-of-fit R^2 values of 0.45 and 0.53 for TOC and SCO, respectively, were found. An average RAF value of 0.59 was found across all SZAs.

Our results from the MIMOSA-CHIM model imply that the break-up of the Antarctic polar vortex has a limited influence on the SCO concentrations over Cape Point. The study site was affected to some extent by Antarctic polar air masses during November months, predominately at 600 K. During September low-ozone events, there was less exchange of air masses between latitudes compared to other months and the

study site was mostly under the influence of mid-latitude air masses. The study site seems to be more frequently affected by air masses from the tropical regions, especially in the lower stratosphere. Further, the influence of tropical air masses on the study site is larger during January and February months. During low-SCO events in September and November, the recorded UVI levels were $\sim 20\,\%$ above the climatological monthly mean.

The relationship between atmospheric ozone and solar UV-B radiation is well understood around the world. The impact of the Antarctic ozone hole on atmospheric ozone concentrations over South Africa is less well understood. Our study showed instances when the Antarctic ozone hole seems to have a limited effect on ozone concentrations over Cape Point but also showed the effect of tropical air masses on ozone levels at Cape Point.

Data availability. The solar UV-B radiation data are available from the South African Weather Service on request. The total ozone column (https://aura.gsfc.nasa.gov/omi.html) and stratospheric column ozone (https://mls.jpl.nasa.gov/) data are available online from the sources as stated in the paper (Bhartia, 2012, Schwartz et al., 2017).

Author contributions. JDP and CYW conceived and designed the experiments, JDP performed the experiments, and JDP and CYW analysed the data. JMC assisted with data conversion. JVA, HB and NB contributed to data analysis and interpretation. JDP and CYW wrote the paper. All authors contributed towards the preparation of the paper.

Competing interests. The authors declare that they have no conflict of interest.

Acknowledgements. The authors would like to thank the South African Weather Service for providing solar UV-B radiation data and cloud cover data. The authors acknowledge the use of Total Ozone Column data from the Ozone Monitoring Instrument (OMI) and Stratospheric Column Ozone data from the Microwave Limb Sounder (MLS). The following persons are thanked for the various inputs into this project: Greg Bodeker of Bodeker Scientific, funded by the New Zealand Deep South National Science Challenge; Richard McKenzie, National Institute of Water and Atmospheric Research, New Zealand; and Liesl Dyson, University of Pretoria. The University of Reunion Island is thanked for the provision of the MIMOSA-CHIM model and the CCUR team for the use of the TITAN supercomputer. The SA–French ARSAIO (Atmospheric Research in Southern Africa and Indian Ocean) and PHC-Protea programmes are also thanked for support for research visits at the University of Reunion. This study was funded in part by the South African Medical Research Council as well as the National Research Foundation of South Africa to grant-holder Caradee Y. Wright.

Edited by: Petr Pisoft
Reviewed by: three anonymous referees

References

Abarca, J. F., Casiccia, C. C., and Zamorano, F. D.: Increase in sunburns and photosensitivity disorders at the edge of the Antarctic ozone hole, Southern Chile 1986–2000, J. Am. Acad. Dermatol., 46, 193–199, https://doi.org/10.1067/mjd.2002.118556, 2002.

Ajtić, J., Connor, B. J., Lawrence, B. N., Bodeker, G. E., Hoppel, K. W., Rosenfield, J. E., and Heuff, D. N.: Dilution of the Antarctic ozone hole into the southern midlatitudes, J. Geophys. Res., 109, D17107, https://doi.org/10.1029/2003JD004500, 2004.

Bais, A. F., Mckenzie, R. L., Bernhard, G., Aucamp, P. J., llysa, M., Madronich, S., and Tourpali, K.: Ozone depletion and climate change: Impacts on UV radiation, Photochem. Photobiol. Sci., 14, 19–52, https://doi.org/10.1039/c4pp90032d, 2015.

Balis, D., Kroon, M., Koukouli, M. E., Brinksma, E. J., Labow, G., Veefkind, J. P., and McPeters, R. D.: Validation of Ozone Monitoring Instrument total ozone column measurements using Brewer and Dobson spectrophotometer ground-based observations, J. Geophys. Res., 112, D24S46, https://doi.org/10.1029/2007JD008796, 2007.

Bandoro, J., Solomon, S., Donohoe, A., Thompson, D. W., and Santer, B. D.: Influences of the Antarctic Ozone Hole on Southern Hemispheric Summer Climate Change, J. Clim., 27, 6245–6264, https://doi.org/10.1175/JCLI-D-13-00698.1, 2014.

Barsby, J. and Diab, R. D.: Total ozone and synoptic weather relationships over southern Africa and surrounding oceans, J. Geophys. Res., 100, 3023–3032, https://doi.org/10.1029/94JD01987, 1995.

Bencherif, H., Portafaix, T., Baray, J. L., Morel, B., Baldy, S., Leveau, J., Hauchecorne, A., Keckhut, K., Moorgawa, A., Michaelis, M. M., and Diab, R.: LIDAR observations of lower stratospheric aerosols over South Africa linked to large scale transport across the southern subtropical barrier, J. Atmos. Sol.-Terr. Phy., 65, 707–715, 2003.

Bencherif, H., Amraoui, L. E., Semane, N., Massart, S., Vidyaranya Charyulu, D., Hauchecorne, A., and Peuch, V.: Examination of the 2002 major warming in the southen hemisphere using ground-based and Odin/SMR assimilated data: Stratospheric ozone distributions and tropic/mid-latitude exchange, Can. J. Phys., 85, 1287–1300, https://doi.org/10.1139/P07-143, 2007.

Bencherif, H., El Amraoui, L., Kirgis, G., Leclair De Bellevue, J., Hauchecorne, A., Mzé, N., Portafaix, T., Pazmino, A., and Goutail, F.: Analysis of a rapid increase of stratospheric ozone during late austral summer 2008 over Kerguelen (49.4° S, 70.3° E), Atmos. Chem. Phys., 11, 363–373, https://doi.org/10.5194/acp-11-363-2011, 2011.

Bhartia, P. K.: OMI/Aura Ozone (O_3) Total Column Daily L2 Global Gridded $0.25° \times 0.25°$ V3, , Goddard Earth Sciences Data and Information Services Center (GES DISC), https://doi.org/10.5067/Aura/OMI/DATA2025 (last access: 15 April 2017), 2012.

Bodeker, G.E. and McKenzie, R. L.: An algorithm for inferring surface UV irradiance including cloud effects, J. Appl. Meteor., 35, 1860–1877, 1996.

Bodeker, G. E. and Scourfield, M. W.: Estimated past and future variability in UV radiation in South Africa based on trends in total ozone, S. Afr. J. Sci., 94, 24–32, 1998.

Bodeker, G. E., Struthers, H., and Connor, B. J.: Dynamical containment of Antarctic ozone depletion, Geophys. Res. Lett., 29, 7 pp., https://doi.org/10.1029/2001GL014206, 2002.

Booth, C. R. and Madronich, S.: Radiation Amplification Factors: Improved formulation accounts for large increases in ultraviolet radiation associated with Antarctic ozone depletion, in: Ultraviolet Radiation in Antarctica: Measurements and Biological Effects, 62, Washington, D. C., American Geophysical Union, https://doi.org/10.1029/AR062p0039, 1994.

Brönnimann, S., Jacques-Coper, M., Rozanov, E., Fischer, A. M., Morgenstern, O., Zeng, G., Akiyoshi, H., and Yamashita, Y.: Tropical circulation and precipitation response to ozone depletion and recovery, Environ. Res. Lett., 12, 064011, https://doi.org/10.1088/1748-9326/aa7416, 2017.

Cadet, J.-M., Benchrif, H., Portafaix, T., Lamy, K., Ncongwane, K., Coetzee, G. J., and Wright, C. Y.: Comparison of Ground-Based and Satellite-Derived Solar UV Index Levels at Six South African Sites, Int. J. Env. Res. Pub. He., 14, 1384, https://doi.org/10.3390/ijerph14111384, 2017.

Charney, J. G. and Drazin, P. G.: Propagation of planetary-scale distrubances from the lower into the upper atmosphere, J. Geophys Res., 66, 83–109, 1961.

Climate Prediction Center Internet Team: Cold and warm episodes by season, http://www.cpc.ncep.noaa.gov/products/analysis_monitoring/ensostuff/ensoyears.shtml, last access: 30 August 2017.

de Laat, A., van der A, R. J., Allaart, M. F., van Weele, M., Benitez, G. C., Casiccia, C., Paes Leme, N. M., Quel, E., Salvador, J., and Wolfram, E.: Extreme sunbathing: Three weeks of small total O3 columns and high UV radiation over the southern tip of South America during the 2009 Antartci O3 hole season, Geophys. Res. Lett., 37, L14805, https://doi.org/10.1029/2010GL043699, 2010.

Diab, R., Barsby, J., Bodeker, G., Scourfield, M., and Salter, L.: Satellite observations of total ozone above South Africa, S. Afr. Geogr. J., 74, 13–18, 1992.

Diffey, B. L.: Sources and measurement of ultraviolet radiation, Methods, 28, 4–13, 2002.

Fahey, D. W. and Hegglin, M. L.: Twenty Questions and Answers About the Ozone Layer: 2010 Update, in: Scientific Assesment of Ozone depletion: 2010, Geneva: World Meteorological Organisation, 2011.

Farman, J. C., Gardinier, B. G., and Shanklin, J. D.: Large losses of total ozone in Antarctica reveal seasonal CIO/NO interaction, Nature, 315 207–209, 1985.

Gies, P., Klekociuk, A., Tully, M., Henderson, S., Javorniczky, J., King, K., Lemus-Deschamps, L., and Makin, J.: Low ozone over southern Australia in August 2011 and its imapct on solar ultraviolet radiation levels, Photochem. Photobiol., 89, 984–994, 2013.

Guarnieri, R. A., Padilha, L. F., Guarnieri, F. L., Echer, E., Makita, K., Pinheiro, D. K., Schuch, A. M. P., Boeira, L. S., and Schuch, N. J.: A study of the anticorrelations between ozone and UV-B radiation using linear and exponential fits in southern Brazil, Adv. Space Res., 34, 764–768, 2004.

Hauchecorne, A., Godin, S., Marchand, M., Hesse, B., and Souprayen, C.: Quantification of the transport of chemical constituents from the polar vortex to midlatitudes in the lower stratosphere using the high-resolution advection model MIMOSA and effective diffusivity, J. Geophys. Res., 107, D208289, https://doi.org/10.1029/2001JD000491, 2002.

Hazarika, N.: Correlation and Data Transformations, availibe at: https://blog.majestic.com/case-studies/correlation-data-transformations/ (last access: 30 August 2018), 2013.

Herman, J. R. and McKenzie, R. L.: Ultraviolet radiation at the Earth's surface, in: Scientific Assesment of ozone depletion: 1998, World Meteorological Organisation, 1998.

Holton, J. R. and Hakim, G. J. (Fith Eds.): Circulation, Vorticity and potential vorticity, in: An Introduction to dynamic meteorology Oxford, Academic Press, 2013.

Huang, G., Liu, X., Chance, K., Yang, K., and Cai, Z.: Validation of 10-year SAO OMI ozone profile (PROFOZ) product using Aura MLS measurements, Atmos. Meas. Tech., 11, 17–32, https://doi.org/10.5194/amt-11-17-2018, 2018.

Jiang, Y. B., Froidevaux, L., Lambert, A., Livesey, N. J., Read, W. G., Waters, J. W., Bojkov, B., Leblanc, T., McDermid, I. S., Godin-Beekmann, S., Filipiak, M. J., Harwood, R. S., Fuller, R. A., Daffer, W. H., Drouin, B. J., Cofield, R. E., Cuddy, D. T., Jarnot, R. F., Knosp, B. W., Perun, V. S., Schwartz, M. J., Snyder, W. V., Stek, P. C., Thurstans, R. P., Wagner, P. A., Allaart, M., Andersen, S. B., Bodeker, G., Calpini, B., Claude, H., Coetzee, G.,Davies, J., De Backer, H., Dier, H., Fujiwara, M., Johnson, B., Kelder, H., Leme, N. P., König-Langlo, G., Kyro, E., Laneve, G., Fook, L. S., Merrill, J., Morris, G., Newchurch, M., Oltmans, S., Parrondos, M. C., Posny, F., Schmidlin, F., Skrivankova, P., Stubi, R., Tarasick, D., Thompson, A., Thouret, V., Viatte, P., Vömel, H., von Der Gathen, P., Yela, M., and Zablocki, G.: Validation of Aura Microwave Limb Sounder Ozone by ozonesonde and lidar measurements, J. Geophys. Res., 112, D24S34, https://doi.org/10.1029/2007JD008776, 2007.

Kalicharran, S., Diab, R. D., and Sokolic, F.: Trends in total ozone over southern African stations between 1979 and 1991, Geophys. Res. Lett., 20, 2877–2880, https://doi.org/10.1029/93GL03427, 1993.

Kuttippurath, J., Lefèvre, F., Pommereau, J.-P., Roscoe, H. K., Goutail, F., Pazmiño, A., and Shanklin, J. D.: Antarctic ozone loss in 1979–2010: first sign of ozone recovery, Atmos. Chem. Phys., 13, 1625–1635, https://doi.org/10.5194/acp-13-1625-2013, 2013.

Kuttippurath, J., Godin-Beekmann, S., Lefèvre, F., Santee, M. L., Froidevaux, L., and Hauchecorne, A.: Variability in Antarctic ozone loss in the last decade (2004–2013): high-resolution simulations compared to Aura MLS observations, Atmos. Chem. Phys., 15, 10385–10397, https://doi.org/10.5194/acp-15-10385-2015, 2015.

Lefèvre, F., Brasseur, G. P., Folkins, I., Smith, A. K., and Simon, P: Chemistry of the 199–1992 stratospheric winter: three-dimensional model simulations, J. Geophys. Res., 99, 8183–8195, 1994.

Leovy, C. B., Sun, C. R., Hitchman, M. H., Remsberg, E. E., Russel, J. M., Gordley, L. L., and Lyiak, L. V.: Transport of ozone in the middle stratosphere: evidence for planetary wave breaking, J. Atmos. Sci., 42, 230–244, 1985.

Levelt, P. F., Hilsenrath, E., Leppelmeier, G. W., van den Oord, G. H., Bhartia, P. K., Tamminen, J., and Veefkind, J. P.: Science Objectives of the ozone monitoring in-

strument, IEEE T. Geosci. Remote Sens., 44, 1199–1208, https://doi.org/10.1109/TGRS.2006.872336, 2006.

Livesey, N. J., Read, W. G., Wagner, P. A., Froidevaux, L., Lambert, A., Manney, G. L., Millan, L. F., Pumphrey, H. C., Santee, M. L., Schwartz, M. J., Wang, S., Fuller, R. A., Jarnot, R. F., Knosp, B. W., and Martinez, E.: The earth observing system (EOS) Aura microwave limb sounder (MLS) Version 4.2xlevel 2 data quality and description document, available at: https://mls.jpl.nasa.gov/data/v4-2_data_quality_document.pdf, last access: 8 May 2017.

Lucas, R. M. and Ponsonby, A.-L.: Ultraviolet radiation and health: friend and foe, Med. J. Australia, 11, 594–598, 2002.

Marchand, M. S., Godin, A., Hauchecorne, A., Lefèvre, F., Bekki, S., and Chipperfield, M.: Influence of polar ozone loss on northern midlatitude regions estimated by a high-resolution chemistry transport model during winter 1999/2000, J. Geophys. Res., 108, https://doi.org/10.1029/2001JD000906, 2003.

Massen, F.: Computing the Radiation Amplification Factor RAF using a sudden dip in Total Ozone Column measured at Diekirch, Luxembourg, https://doi.org/10.13140/RG.2.1.2911.0644, 2013.

McKenzie, R., Connor, B., and Bodeker, G.: Increased summertime UV radiation in New Zealand in response to ozone loss, Science, 285, 1709–1711, 1999.

McKenzie, R. L., Matthews, W. A., and Johnston, P. V.: The relationship between Erythemal UV and ozone derived from spectral irradiance measurements, Geophys. Res. Lett., 18, 2269–2272, https://doi.org/10.1029/91GL02786, 1991.

McKenzie, R. L., Bodeker, G. E., Keep, D. J., and Kotkamp, M.: UV Radiation in New Zealand: North-to-South differences between two sites, and relationship to other latitudes, Weath. Clim., 16, 17–26, 1996.

McPeters, R. D., Frith, S., and Labow, G. J.: OMI total column ozone: extending the long-term data record, Atmos. Meas. Tech., 8, 4845–4850, https://doi.org/10.5194/amt-8-4845-2015, 2015.

Paul, J., Fortuin, F., and Kelder, H.: An ozone climatology based on ozonesonde and satellite measurements, J. Geophys. Res., 103, 709–734, https://doi.org/10.1029/1998JD200008, 1998.

Portafaix, T., Morel, B., Bencherif, H., and Baldy, S.: Fine-scale study of a thick stratospheric ozone lamina at the edge of the southern subtropical barrier, J. Geophys. Res., 108, D64196, https://doi.org/10.1029/2002JD002741, 2003.

Reda, I. and Andreas, A.: NREL's Solar Position Algorithm (SPA), availible at: https://www.nrel.gov/midc/spa/ (last access: 15 August 2017), 2008.

Schuch, A. P., dos Santos, M. B., Lipinski, V. M., Vaz Peres, L., dos Santos, C. P., Cechin, S. Z., Schuch, N. J., Pinheiro, D. K., and da Silva Loreto, E. L.: Identification o finfluential eventsconcerning the Antarctic ozone hole over southern Brazil and the biological effects induced by UVB and UVA radiation in an endemic treefrog species, Ecotox. Environ. Safety, 118, 190–198, https://doi.org/10.1016/j.ecoenv.2015.04.029, 2015.

Schwartz, M., Froidevaux, L., Livesey, N., and Read, W.: MLS/Aura Level 2 Ozone (O3) Mixing Ratio V004, Greenbelt, MD, USA, Goddard Earth Sciences Data and Information Services Center (GES DISC), https://doi.org/10.5067/Aura/MLS/DATA2017 (last access: 8 May 2017), 2015.

Seckmeyer, G., Bais, A., Bernhard, G., Blumthaler, M., Booth, C. R., Lantz, K., and Webb, A.: A *Instruments to MeasureSolar Ultraviolet Radiation. Part 2: Broadband Instruments Measuring Erythemally Weighted Solar Irradiance*, Geneva, Switzerland, World Meteorological Organization (WMO), 2005.

Semane, N., Bencherif, H., Morel, B., Hauchecorne, A., and Diab, R. D.: An unusual stratospheric ozone decrease in the Southern Hemisphere subtropics linked to isentropic air-mass transport as observed over Irene (25.5° S, 28.1° E) in mid-May 2002, Atmos. Chem. Phys., 6, 1927–1936, https://doi.org/10.5194/acp-6-1927-2006, 2006.

Serrano, A., Antón, M., Cancillo, M. L., and García, J. A.: Proposal of a new erythemal UV radiation amplification factor, Atmos. Chem. Phys. Discuss., 8, 1089–1111, https://doi.org/10.5194/acpd-8-1089-2008, 2008.

Sivakumar, V. and Ogunniyi, J.: Ozone climatology and variablity over Irene, South Africa detrermined by ground based and satellite observations. Part 1: Vertical variations in the troposphere and stratopshere, Atmosfera, 30, 337–353, 2017.

Slemr, F., Brunke, E. G., Labuschagne, C., and Ebinghaus, R.: Total gaseous mercury concentrations at the Cape Point GAW station and their seasonality, Geophys. Res. Lett., 35, L11807, https://doi.org/10.1029/2008GL033741, 2008.

Solarlight: Model 501 UVB Radiometer, availible at: http://solarlight.com/wp-content/uploads/2015/01/Meters_Model-501-.pdf (last access: 3 September 2016), 2014.

Tripathi, O. P., Godin-Beekmann, S., Lefévre, F., Pazmiño, A., Hauchecorne, A., Chipperfield, M., Feng, W., Millard, G., Rex, M., Streibel, M., and Von der Gathen, P.: Comparison of polar ozone loss rates simulated by one-dimensional and three-dimensional models with match observations in recent Antarctic and Arctic winters, J. Geophys. Res., 112, D12307, https://doi.org/10.1029/2006JD008370, 2007.

WMO: Scientific Asessment of Ozone Depletion: 2010, Global Ozone Research and Monitoring Project- Report No52, Geneva, Switzerland, 2011.

WHO: Ultraviolet radiation and the INTERSUN Programme: http://www.who.int/uv/uv_and_health/en/, last access: 25 January 2017.

Wolfram, E. A., Salvador, J., Orte, F., D'Elia, R., Godin-Beekmann, S., Kuttippurath, J., Pazmiño, A., Goutail, F., Casiccia, C., Zamorano, F., Paes Leme, N., and Quel, E. J.: The unusual persistence of an ozone hole over a southern mid-latitude station during the Antarctic spring 2009: a multi-instrument study, Ann. Geophys., 30, 1435–1449, https://doi.org/10.5194/angeo-30-1435-2012, 2012.

Wright, C. Y., Coetzee, G., and Ncongwane, K.: Ambient solar UV radiation and seasonal trends in potential sunburn risk among schoolchilren in South Africa, S. Afr. J. Child Health, 5, 33–38, 2011.

Zempila, M.-M., van Geffen, J. H. G. M., Taylor, M., Fountoulakis, I., Koukouli, M.-E., van Weele, M., van der A, R. J., Bais, A., Meleti, C., and Balis, D.: TEMIS UV product validation using NILU-UV ground-based measurements in Thessaloniki, Greece, Atmos. Chem. Phys., 17, 7157–7174, https://doi.org/10.5194/acp-17-7157-2017, 2017.

Chapter 4 Results: The large-scale transport of a volcanic plume and the effect of atmospheric composition at a secondary site

4.1 Paper overview

Gases, aerosols and ash emitted from volcanic eruptions can be transported over vast distances and can attenuate solar UVR (Diaz et al., 2014). On 4 June 2011, the PCCVC erupted and the initial plume reached heights of between 9 and 12 km (Klüser et al., 2013). Within 10-days the plume had circled the Southern Hemisphere (Clarisse et al., 2012). The eruption continued at low levels for several months (Bonadonna et al., 2015). Near the eruption site, changes in surface UVR were observed (Diaz et al., 2014) due to the scatter and absorption caused by particles in the volcanic plume.

This manuscript investigated the effect of the volcanic plume from the PCCVC eruption on the aerosol loading at Cape Point, as well as the trajectory and dispersion of the plume using modelled and satellite data. The aerosol loading at Cape Point, South Africa, is considered relatively low due to the clean air masses that are transported from the South Atlantic Ocean by the prevailing winds. Therefore, anomalies in the aerosol loading over Cape Point due to the volcanic eruption would be easier to detect than at generally more polluted sites.

Daily satellite observations of surface UVR averaged over June 2011, showed that on average surface UVR between 20°S and 35°S was lower in June 2011 compared to previous years. AOD observations from the Precision-Filter Radiometer (PFR) at Cape Point showed that there was a noticeable increase in AOD between 9-12 June 2011 which was well above the background monthly average.

The FLEXPART model was used to investigate the dispersion on the volcanic plume, using sulphur dioxide as a proxy for volcanic ash. Along with the dispersion model, observations of sulphur dioxide and volcanic ash from the IASI were used to trace the dispersion on the plume. The model and observations indicated that the plume

passes near Cape Point between 11-20 June 2011. This coincided with the increase in AOD observed.

Changes in surface UVR at Cape Point (i.e., the secondary site) may not be evident due to cloud cover and stratospheric ozone levels. However, the dispersion model and observations indicated that the increase in AOD at the secondary site can be attributed to the volcanic plume. These results showed that the effect of a volcanic eruption can impact the aerosols loading at secondary sites and could have possible effects on surface UVR.

4.2 Thesis contribution

This paper contributes to the second objective of this thesis which was to investigate the impact of a volcanic plume on AOD and the impact on surface UVB radiation at a secondary site.

Using satellite and modelled data, this manuscript demonstrated how the long-range transport of volcanic aerosols can be responsible for changes in the aerosol loading at a secondary site as well as the influence on surface UVR over a large region.

4.3 Contribution of candidate

D. Jean du Preez was responsible for the data analysis, model simulations, interpretation of results and writing the manuscript. L. Clarisse provided the IASI data sets and all co-authors contributed to the discussion and final manuscript preparations.

4.4 Publication status

du Preez, D. J., Bencherif, H., Bègue, N., Clarisse, L., Hoffman, R. F., & Wright, C. Y. (2020). Investigating the Large-Scale Transport of a Volcanic Plume and the Impact on a Secondary Site. Atmosphere, 11(548). https://doi.org/10.3390/atmos11050548

4.5 References

Bonadonna, C., Pistolesi, M., Cioni, R., Degruyter, W., Elissondo, M., & Baumann, V. (2015). Dynamics of wind-affected volcanic plumes: The example of the 2011 Cordón Caulle eruption, Chile. *Journal of Geophysical Research: Solid Earth, 120*(4), 2242-2261. doi:10.1002/2014jb011478

Clarisse, L., Hurtmans, D., Clerbaux, C., Hadji-Lazaro, J., Ngadi, Y., & Coheur, P. F. (2012). Retrieval of sulphur dioxide from the Infrared Atmospheric Sounding Interferometer (IASI). *Atmospheric Measurement Techniques, 5*(3), 581-594. doi:10.5194/amt-5-581-2012

Diaz, S. B., Paladini, A. A., Braile, H. G., Dieguez, M. C., Deferrari, G. A., Vernet, M., & Vrsalovic, J. (2014). Global and direct UV irradiance variation in the Nahuel Huapi National Park (Patagonia, Argentina) after the eruption of Puyehue-Cordon Caulle (Chile). *Journal of Atmospheric and Solar-Terrestrial Physics, 112*, 47-56. doi:10.1016/j.jastp.2014.02.006

Klüser, L., Erbertseder, T., & Meyer-Arnek, J. (2013). Observation of volcanic ash from Puyehue-Cordón Caulle with IASI. *Atmospheric Measurement Techniques, 6*(1), 35. doi:10.5194/amt-6-35-2013

4.6 Manuscript 2

atmosphere

MDPI

Article

Investigating the Large-Scale Transport of a Volcanic Plume and the Impact on a Secondary Site

David Jean Du Preez [1,2,*], Hassan Bencherif [2,3], Nelson Bègue [2], Lieven Clarisse [4], Rebecca F. Hoffman [5] and Caradee Yael Wright [1,6]

1 Department of Geography, Geoinformatics and Meteorology, University of Pretoria, Pretoria 0002, South Africa; caradee.wright@mrc.ac.za
2 Laboratoire de l'Atmosphère et des Cyclones (UMR 8105 CNRS, Université de La Réunion, MétéoFrance), 97744 Saint-Denis de La Réunion, France; hassan.bencherif@univ-reunion.fr (H.B.); nelson.begue@univ-reunion.fr (N.B.)
3 School of Chemistry and Physics, University of KwaZulu-Natal, Durban 4041, South Africa
4 Spectroscopy, Quantum Chemistry and Atmospheric Remote Sensing (SQUARES), Université libre de Bruxelles (ULB), 1050 Bruxelles, Belgium; lclariss@ulb.ac.be
5 South African Weather Service, Private Bag X097, Pretoria 0001, South Africa; rebecca.hoffman@weathersa.co.za
6 Environmental and Health Research Unit, South African Medical Research Council, University of Pretoria, Pretoria 0001, South Africa
* Correspondence: dupreez.dj@tuks.co.za

Received: 21 April 2020; Accepted: 22 May 2020; Published: 25 May 2020

Abstract: Volcanic plumes can be transported across vast distances and can have an impact on solar ultraviolet radiation (UVR) reaching the surface due to the scattering and absorption caused by aerosols. The dispersion of the volcanic plume from the Puyehue-Cordón Caulle volcanic complex (PCCVC) eruption was investigated to determine the effect on aerosol loading at Cape Point, South Africa. The eruption occurred on 4 June 2011 and resulted in a plume reaching a height of between 9 and 12 km and was dispersed across the Southern Hemisphere. Satellite sulphur dioxide (SO_2) observations and a dispersion model showed low concentrations of SO_2 at the secondary site. However, satellite observations of volcanic ash and ground-based aerosol measurements did show increases between 10 and 20 June 2011 at the secondary site. Furthermore, there was good agreement with the dispersion model results and observations from satellites with most of the plume located between latitudes 40°–60° South.

Keywords: aerosols; sulphur dioxide; FLEXPART; plume transport; volcanic eruption

1. Introduction

Volcanic eruptions can eject a highly reactive mix of aerosols and gases into the atmosphere [1]. Some of the main gases associated with volcanic activity are water vapour (H_2O), carbon dioxide (CO_2), sulphur dioxide (SO_2), hydrogen sulphide (H_2S) and hydrochloric acid (HCl) [2]. Volcanic emissions are the largest natural sources of SO_2 in the atmosphere. Volcanic eruptions occur with various levels of intensity. Larger eruptions can inject volcanic aerosols into the stratosphere, while smaller, less intense eruptions only inject aerosols into the troposphere. SO_2 is suspended in the troposphere for only a short period of time, but SO_2 injected into the stratosphere through volcanic eruptions can remain there for up to three years as sulphuric acid aerosols [3,4]. The injection of ash and SO_2 from volcanic eruptions affects the climate, aviation and human health due to the deposition of ejected matter [5].

SO_2 injected into the stratosphere can be dispersed around the globe and can have an important climatic effect. Sulphur species react with hydroxide (OH) and water vapour (H_2O) to form sulfuric

acid (H_2SO_4). These H_2SO_4 aerosols have a radiative effect during eruptions [6]. Furthermore, solar ultraviolet radiation (UVR) passing through the atmosphere is affected by the aerosol loading. During volcanic eruptions the aerosol loading and size distribution are modified by injected ash particles [7]. UV-absorbing aerosols such as volcanic ash affect surface UVR flux which impact public health and some photochemical reactions. The effect of UV-absorbing aerosols on UVR is dependent on the altitude, particle size distribution and single scattering albedo of the ash particles [8].

The Puyehue-Cordón Caulle volcanic complex (PCCVC) is located in the Andes Mountains in southern Chile (40.58° S, 72.13° W) at 2 240 m above sea level [9]. After 41 years of inactivity, an eruption started on 4 June 2011 at approximately 18:30 UTC. The resulting plume reached the stratosphere with maximum heights between ~9–12 km [4,7] with a peak mean flow rate (MFR) in the order of 10^7 kg·s^{-1}. On 13 June 2011, the plume reached a height of ~7–9 km [10]. Due to the westerly winds in the mid-latitudes, widespread dispersion of aerosols and fine particles occurred across the Southern Hemisphere [11].

By 14 June 2011, the plume had circumnavigated the Southern Hemisphere and reached the original eruption site [4]. The plume was subjected to cross-wind and down-wind spreading, with most of the velocity as a result of the wind. The umbrella cloud and the rising plume were both affected by the prevailing westerly winds, showing the significant effect that the wind had on the dispersion of the aerosols and ash, although some of the spreading was due to physical processes in the plume such as density-driven mechanisms [10]. Following the initial eruption, the volcano continued to produce low-intensity plumes for several months [10].

In this study, SO_2 anomalies were identified at the eruption site as well as at a secondary site, Cape Point, South Africa was selected as the secondary site because air traffic was reportedly restricted on 18–19 June 2011 due to 'ash' from the eruption being visible at Cape Town International Airport. The secondary site was included to consider the extent of the impact of PCCVC 2011 eruption over a distance. Furthermore, the trajectory and dispersion of the plume was investigated using satellite observations and model output to determine whether the plume did reach the secondary site and whether or not SO_2 anomalies at the secondary site could be attributed to the volcanic eruption.

2. Data and Methods

2.1. Data

The eruption site, PCCVC (40.58° S; 72.11° W), and the secondary site, Cape Point (34.35° S; 18.50° E) (Figure 1) were selected to investigate the dispersion of the plume and the effect on a secondary site.

The Cape Point station is part of the Global Atmosphere Watch (GAW) network and equipment at the station is used to monitor trace gases. The station is situated 230 m above sea level and is mainly influenced by air masses from the South Atlantic Ocean due to the prevailing southeasterly winds throughout the year. During the austral winter the station may be influenced by anthropogenic emissions from local and regional biomass burning, transported by northerly winds as a result of changes in circulation patterns caused by frontal systems [12].

Daily noon ultraviolet index (UVI) data (2007–2016, inclusive) from the Ozone Monitoring Instrument (OMI) were used to determine if the volcanic plume had any impact on surface solar UVR. The OMI data has a 1° × 1° spatial resolution [13] and OMI has a spectral resolution of 0.45 nm [14]. The UVI is a scale used to represent erythemal radiation levels [15]. During the time that the plume was likely to impact surface solar UVR levels, ground-based observations of solar UVR levels at Cape Point were not available but there is known to be good agreement between the Cape Point ground-based observations and OMI data [16]. Previous studies have shown that OMI estimations of surface UVR are above the ground-based observations indicating a positive bias which is decreased under clear-sky conditions [14].

Aerosol optical depth (AOD) data (2011 to 2018, inclusive) from a precision filter radiometer (PFR) located at Cape Point were used to identify any anomalies in AOD as a result of the volcanic plume. The data for the PFR were obtained from the World Data Centre for Aerosols (WDCA) website (http://ebas.nilu.no/). The PFR sun photometer measures AOD at four wavelengths (λ = 368, 412, 500, 862 nm) and started operation in February 2008 but only data from 2011 were available. From calibration tests, the PFR located at Cape Point had an uncertainty of less than ± 1%. Hourly average AOD values were determined from 1-minute data using GAW-PFR algorithms [17,18] and cloud screening routines [19].

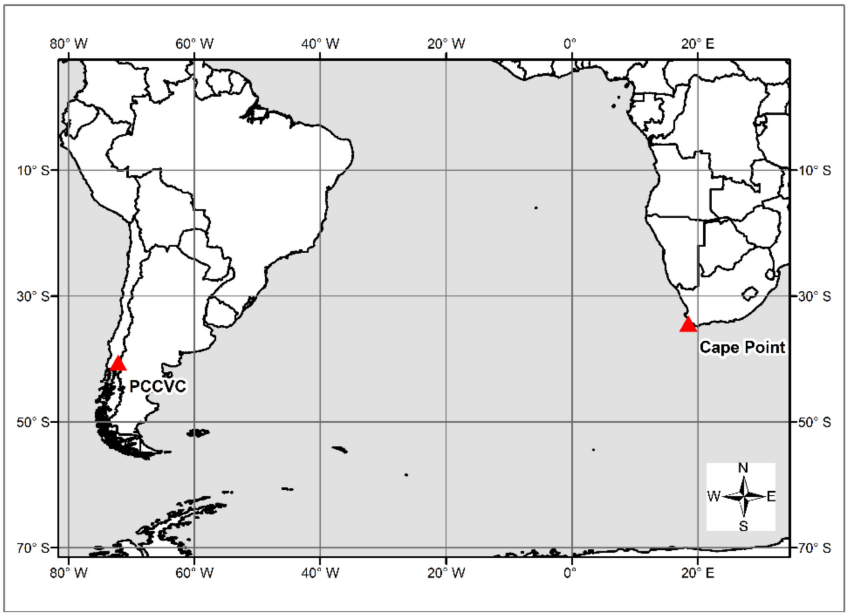

Figure 1. Map showing the location of the eruption site, Puyehue-Cordón Caulle volcanic complex in South America and the secondary site, Cape Point in South Africa [20].

Hourly reanalysis data from Modern-Era Retrospective Analysis for Research and Applications version 2 (MERRA-2) spatial resolution of 0.5° × 0.65° [21] was used to identify anomalies in SO_2 column mass density (kg·m^{-2}) (2007–2016). MERRA-2 uses observations from the Earth Observing System (EOS). The Goddard Global Ozone Chemistry Aerosol Radiation and Transport (GOCART) and Goddard Earth Observing System 5 (GEOS-5) models simulate atmospheric processes [22].

SO_2 vertical column density and volcanic ash observations were obtained from the Infrared Atmospheric Sounding Interferometer (IASI) instrument on board the MetOp-A satellite. The SO_2 is given in Dobson Units (DU) and computed using the algorithm outlined which calculates the total column SO_2 using the assumed height of the SO_2 layer and is dependent on factors from data retrieved from the instrument [23]. Volcanic ash absorbs and scatters radiation with wavelengths between 7 µm and 15 µm [24–26]. In [27] a volcanic ash identification algorithm was presented, that determines for each IASI spectral band whether a spectral signature is present that is compatible with the presence of ash. In the same study, the algorithm was illustrated on the observations of Puyehue to estimate the fraction of spectra with detectable quantities of ash. It is this dataset that is also used here.

2.2. Methods

The monthly mean UVI for June was calculated using nine-years (2007–2010, inclusive and 2012–2016, inclusive) and 2011 data were excluded to remove the possible influence of the volcanic eruption. To identify UVI anomalies during June 2011, the calculated mean UVI for June was subtracted from the mean UVI for June 2011.

Similarly, daily mean and standard deviation (SD) values were calculated for the MERRA-2 SO_2 column data at both sites. Using the PFR AOD data for 2011, the daily mean was calculated. The remaining seven years of data (2012–2018, inclusive) were used to calculate the monthly mean and SD values of the PFR AOD data at Cape Point. The mean and SD values of UVI, MERRA-2 and PFR data were compared to the 2011 observations to identify any outliers.

The flexible particle (FLEXPART) model is a Lagrangian particle dispersion model which was used to model the dispersion of the volcanic plume. The model simulates the transport, diffusion, wet and dry deposition and first order chemical reactions of tracer particles released from a point source or area source [28]. In this study, forecast meteorological data from the European Centre for Medium Range Forecasts (ECMWF) was used as input for the model. The meteorological data has a 3-hour temporal resolution, 1° × 1° spatial resolution and 138 vertical levels. In this study, no a priori information was used in the FLEXPART model simulation. Using SO_2 as a proxy for volcanic ash [29] has been done in several previous studies [4,30] and is dependent on environmental conditions [27]. A similar model setup was used as described by Klüser et al. (2013) [4], where a large number of particles of unit mass were released from 4–13 June 2011, between 2–14 km above the eruption site at 6-hour intervals [4]. The simulation was run from 1–30 June 2011 to observe the dispersion of the plume across the Southern Hemisphere. An output grid of 1° × 1° was produced every 12 h at 1 km intervals from 4–14 km and the SO_2 column given in ng·m^{-3} was converted to Dobson units.

3. Results and Discussion

3.1. Surface Ultraviolet Radiation (UVR)

The UVI anomalies for June 2011 (Figure 2) indicated changes of ± 0.5 UVI. The region between 20° S and 35° S was dominated by decreases in UVR. In the region between 40° S and 60° S, small increases and decreases in UVI were observed.

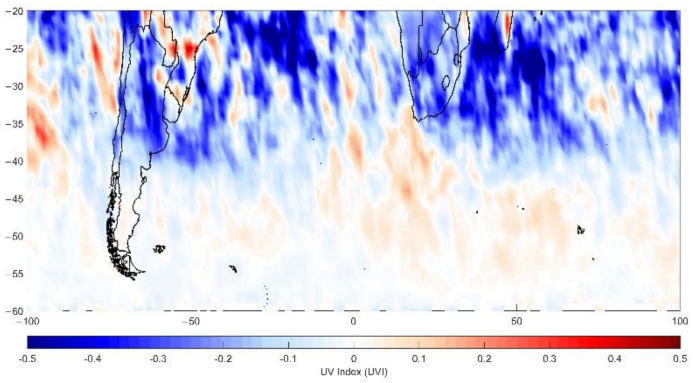

Figure 2. Ultraviolet index (UVI) anomalies for June 2011 where positive values indicate an increase in UVI and vice versa.

3.2. Aerosol Optical Depth (AOD) and SO_2 Anomalies

The monthly mean and ± 1 standard deviation (SD) of PFR AOD at 368 and 412 nm (Figure 3) showed that there was no clear seasonal cycle evident at these two wavelengths which can be due to the low aerosol concentrations present in air masses from the Southern Ocean [31]. The 500 and 862 nm wavelengths were excluded due to missing data in the data set. The largest daily variability occurred during the austral summer which could be due to biomass burning in the surrounding areas [32].

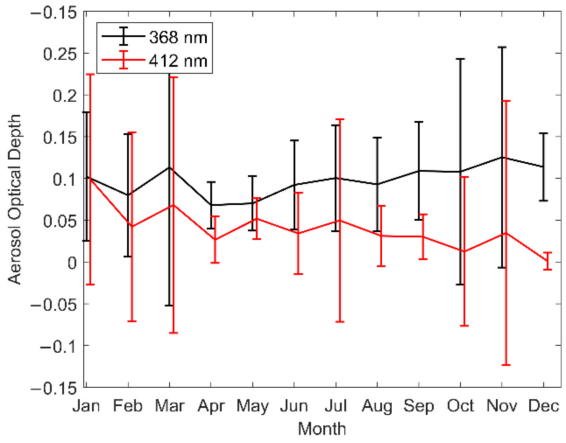

Figure 3. Monthly mean and ± 1 standard deviation (SD) error bars of aerosol optical depth (AOD) from precision filter radiometer (PFR) measurements for 368 and 412 nm at Cape Point.

The daily mean of PFR AOD at 368 and 412 nm (Figure 4) showed an increase in AOD between 9 June and 13 June 2011 as well as on 27 June 2011. These values were above their respective monthly mean.

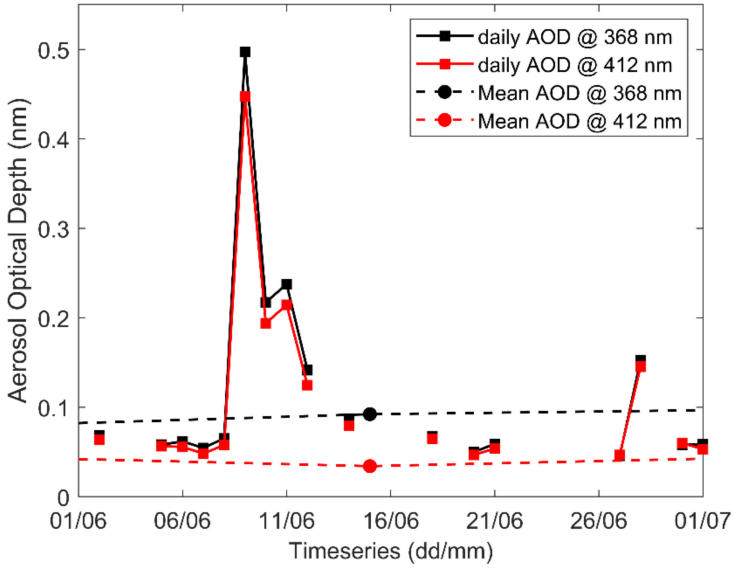

Figure 4. Daily mean and monthly mean of PFR measurements during May–July 2011 at 368 and 412 nm at Cape Point.

At the eruption site, the mean monthly and mean daily MERRA-2 SO_2 columns (Figure 5a) indicated a seasonal peak which occurred between February and April. During June and July 2011, the highest SO_2 level (3.7×10^{-5} kg·m^{-2}) was recorded on 5 June 2011 (Figure 5b), the day after the eruption started. The monthly mean for 2011 was above the climatological mean and there was increased variability during June and July 2011.

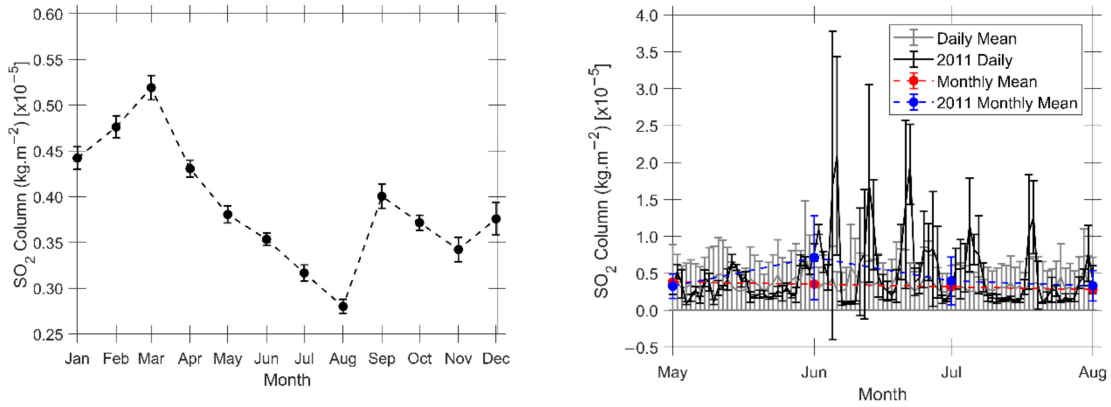

(a) (b)

Figure 5. Monthly mean and ± 1 SD for each month (2007–2016) (**a**) and daily mean and ± 1 SD error bars during May–July 2011 (**b**) for SO_2 column from Modern-Era Retrospective Analysis for Research and Applications version 2 (MERRA-2) at the Puyehue-Cordón Caulle volcanic complex (PCCVC).

At the secondary site, the SO_2 columns (Figure 6) were one order of magnitude smaller compared to the eruption site. The mean monthly and ± 1 SD error bars of SO_2 column (Figure 6a) showed a peak and increased variability during June to August. At Cape Point, SO_2 columns showed an increase from autumn months and reached a maximum during winter. The maximum was followed by a decrease during the spring months. In June and July 2011 (Figure 6b), the daily mean values were below the monthly mean values. However, between 10 and 20 June 2011 there was large variability in daily mean values. Between 12 June to 20 June 2011, the daily mean was above the climatological mean except for 15 June. During July 2011, there was a large increase in SO_2. The climatological seasonal variations of SO_2 were found to be as expected for a Southern Hemisphere site [33]. The increase during autumn, peaking in winter, and decreasing from spring into summer months may be due to the typical, prevailing synoptic circulation patterns [31].

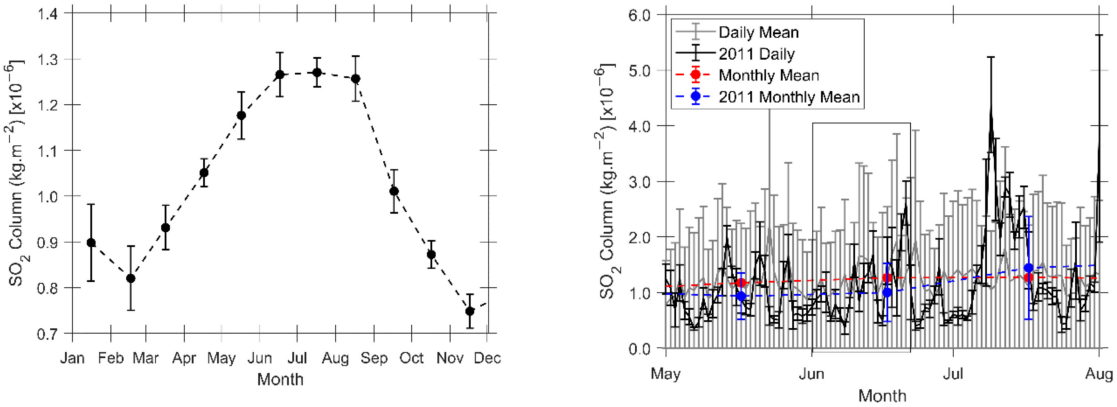

(a) (b)

Figure 6. Monthly mean and ± 1 SD for each month (2007–2016) (**a**) and daily mean and ± 1 SD error bars during May–July 2011, with 10–20 June 2011 indicated in the rectangle (**b**) for SO_2 column from MERRA-2 at Cape Point.

3.3. Infrared Atmospheric Sounding Interferometer (IASI) and Flexible Particle Model (FLEXPART)

The composite images of IASI SO_2 column (Figure 7), IASI ash (Figure 8) and FLEXPART SO_2 column (Figure 9) for 4–30 June 2011 shows the trajectory of the plume across the Southern Hemisphere.

The SO_2 column from IASI and FLEXPART indicated that the highest concentrations of SO_2 were found closest to the eruption site and decreased eastward. FLEXPART shows higher dispersion near the release point. The IASI ash observations showed a similar result compared to the SO_2 column observations but showed more longitudinal dispersion.

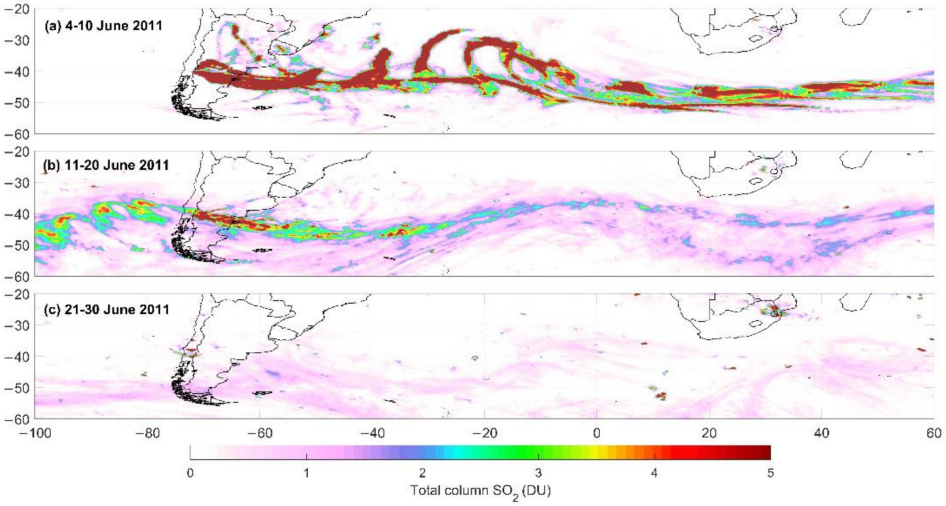

Figure 7. Composite image of Infrared Atmospheric Sounding Interferometer (IASI) SO_2 column for 4–10 June 2011 (**a**), 11–20 June 2011 (**b**) and 21-30 June 2011 (**c**).

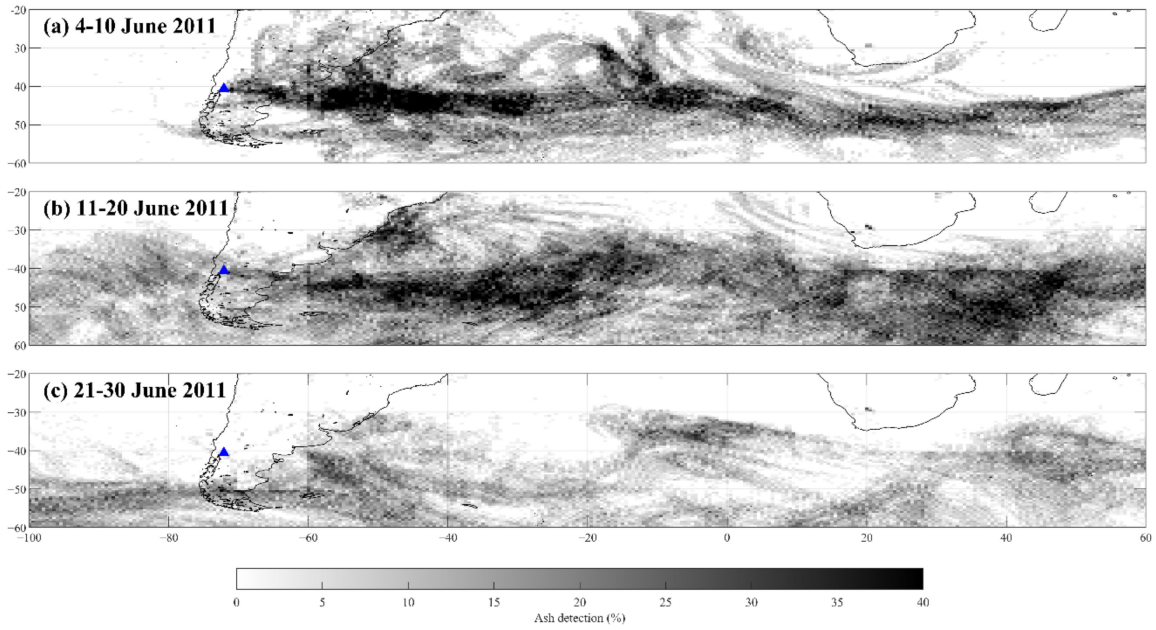

Figure 8. Composite image of IASI ash for 4–10 June 2011 (**a**), 11–20 June 2011 (**b**) and 21–30 June 2011 (**c**).

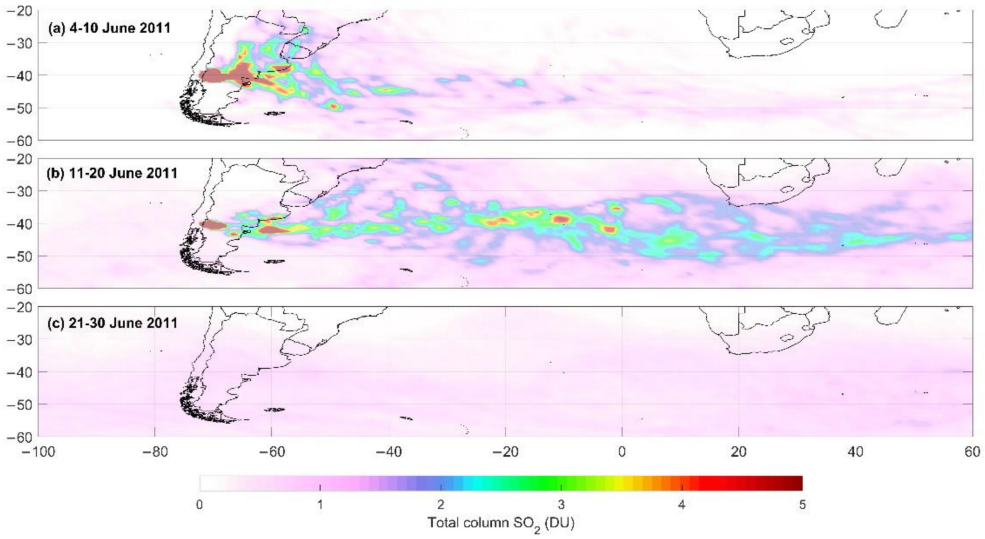

Figure 9. Composite image of flexible particle model (FLEXPART) SO_2 column for 4–10 June 2011 (**a**), 11–20 June 2011 (**b**) and 21–30 June 2011 (**c**).

The composite image of IASI SO_2 column (Figure 7a), IASI ash (Figure 8a) and FLEXPART SO_2 column (Figure 9a) for 4–10 June 2011 indicated that most of the plume was located between 20° S and 60° S. The SO_2 column from IASI and FLEXPART showed that the plume did not pass over Cape Point, but the IASI ash observations showed a low percentage ash near Cape Point. The composite image of the IASI SO_2 column (Figure 7b), IASI ash (Figure 8b) and FLEXPART SO_2 column (Figure 9b) for 11–20 June 2011 indicated that the plume had circumnavigated the Southern Hemisphere. During this period, the IASI and FLEXPART showed low levels of SO_2 and ash near Cape Point. This was more evident in the FLEXPART and IASI ash observations. The composite image of the IASI SO_2 column (Figure 7c), IASI ash (Figure 8c) and FLEXPART SO_2 column (Figure 9c) for 21–30 June 2011 each showed more dispersion and lower levels of SO_2 and ash compared to the period between 11–20 June 2011.

Comparing the plume from IASI observations and FLEXPART simulations showed similarities with this and other studies in the trajectory of the plume. A similar eastward transport was seen from the eruption site towards the Indian Ocean while most of the plume was distributed between 40°–60° S. From both IASI and FLEXPART a north-eastwards trajectory was seen on 4–10 June 2011 which resulted in the volcanic ash transport over Buenos Aires [9]. The dominant eastward trajectory and location of the plume south of Cape Point as indicated by the IASI and FLEXPART results agreed with results from other studies [23,26,27].

There were differences in dispersion results produced by IASI and FLEXPART, which were likely due to several factors. Lower volcanic emission after 10 June 2011 meant that IASI was not able to detect the eruption after this date [26]. In FLEXPART, the resolution of the meteorological data, number of particles released, mass, atmospheric lifetime of chemical species and changes in emissions would have had an impact on the FLEXPART simulation [4]. Furthermore, in high wind-shear environments ash and SO_2 follow different trajectories due to the deposition of ash [29].

The dispersion of the volcanic plume across the Southern Hemisphere did not have a large impact on surface UVR between 20° S and 60° S. This could be due to factors such as cloud cover and stratospheric ozone [34]. Furthermore, the eruption occurred during the austral winter when UVR are low. Although an increase in AOD was observed between 9–13 June 2011 at Cape Point. It is likely that the increase in AOD was due to the dispersion of volcanic ash (Figure 8) and not SO_2 as the dispersion of these particles vary depending on prevailing weather conditions. Furthermore, due to the danger that volcanic ash poses to aircraft, flights to and from Cape Town International Airport were affected between 9–19 June 2011 [35].

4. Conclusions

The dispersion of the volcanic plume from the PCCVC eruption on 4 June 2011 was investigated using satellite observations as well as a dispersion model. The observations and simulations were used to determine whether changes in surface solar UVR levels, AOD and SO_2 at the eruption site and a secondary, mid-latitude site could be attributed to the volcanic plume.

Over South America, the volcanic aerosols had an impact on surface solar UVR levels which was largely dependent on the wavelength. At the secondary site, Cape Point, increases in SO_2 column and AOD at 368 and 412 nm occurred between 10 June 2011 and 20 June 2011. The increase in AOD was likely due to the dispersion of volcanic ash. Satellite observations showed low levels of SO_2 near Cape Point, the secondary site. Future research should investigate the effect of volcanic aerosols using radiative transfer models.

Author Contributions: Conceptualization, D.J.D.P., H.B., N.B., R.F.H. and C.Y.W.; writing—original draft preparation, D.J.D.P., H.B., N.B., R.F.H. and C.Y.W.; UVI, PFR, MERRA-2 data analysis, D.J.D.P.; IASI data analysis, D.J.D.P., L.C.; FLEXPART modelling, D.J.D.P., N.B.; writing—review and editing, All authors. All authors have read and agreed to the published version of the manuscript.

Funding: D.J.D.P received a Doctoral scholarship from the University of Pretoria and a scholarship from the French Embassy in South Africa. C.W. receives research funding from the South African Medical Research Council, the National Research Foundation and the University of Pretoria. The APC was funded by LACy (Laboratoire de l'Atmosphère et des Cyclones).

Acknowledgments: The authors would like to acknowledge the initial work started by R.H and the Casper Labuschagne from the South African Weather Service for providing the PRF data from Cape Point. Authors acknowledge the French South-African PROTEA programme and the CNRS-NRF International Research Project ARSAIO (Atmospheric Research in Southern Africa and Indian Ocean), for supporting research activities.

Conflicts of Interest: The authors declare no conflict of interest.

References

1. Roberts, T.J.; Vignelles, D.; Liuzzo, M.; Giudice, G.; Aiuppa, A.; Coltelli, M.; Salerno, G.; Chartier, M.; Couté, B.; Berthet, G.; et al. The primary volcanic aerosol emission from Mt Etna: Size-resolved particles with SO2 and role in plume reactive halogen chemistry. *Geochim. Cosmochim. Acta* **2018**, *222*, 74–93. [CrossRef]
2. Daag, A.S.; Tubianosa, B.S.; Newhall, C.; Tungol, N.; Javier, D.; Dolan, M.; Delos Reyes, P.; Arboleda, R.; Martinez, M.; Regalado, T. Monitoring sulfur dioxide emission at Mount Pinatubo. In *Fire and Mud: Eruptions and lahars of Mount Pinatubo, Philippines*; University of Washington: Seattle, WA, USA, 1996; pp. 409–414.
3. Halmer, M.M.; Schmincke, H.U.; Graf, H.F. The annual volcanic gas input into the atmosphere, in particular into the stratosphere: A global data set for the past 100 years. *J. Volcanol. Geotherm. Res.* **2002**, *115*, 511–528. [CrossRef]
4. Klüser, L.; Erbertseder, T.; Meyer-Arnek, J. Observation of volcanic ash from Puyehue-Cordón Caulle with IASI. *Atmos. Meas. Tech.* **2013**, *6*, 35. [CrossRef]
5. Bignami, C.; Corradini, S.; Merucci, L.; de Michele, M.; Raucoules, D.; De Astis, G.; Stramondo, S.; Piedra, J. Multisensor Satellite Monitoring of the 2011 Puyehue-Cordon Caulle Eruption. *IEEE J. Sel. Topics Appl. Earth Observ. Remote Sens.* **2014**, *7*, 2786–2796. [CrossRef]
6. Robock, A. Volcanic eruptions and climate. *Rev. Geophys* **2000**, *38*, 191–219. [CrossRef]
7. Diaz, S.B.; Paladini, A.A.; Braile, H.G.; Dieguez, M.C.; Deferrari, G.A.; Vernet, M.; Vrsalovic, J. Global and direct UV irradiance variation in the Nahuel Huapi National Park (Patagonia, Argentina) after the eruption of Puyehue-Cordon Caulle (Chile). *J. Atmospheric Sol. Terr. Phys* **2014**, *112*, 47–56. [CrossRef]
8. Carn, S.A.; Krotkov, N.A. Chapter 12—Ultraviolet Satellite Measurements of Volcanic Ash. In *Volcanic Ash*; Mackie, S., Cashman, K., Ricketts, H., Rust, A., Watson, M., Eds.; Elsevier: Amsterdam, The Netherlands, 2016; pp. 217–231.
9. Raga, G.B.; Baumgardner, D.; Ulke, A.G.; Torres Brizuela, M.; Kucienska, B. The environmental impact of the Puyehue–Cordon Caulle 2011 volcanic eruption on Buenos Aires. *Nat. Hazards Earth Syst. Sci.* **2013**, *13*, 2319–2330. [CrossRef]

10. Bonadonna, C.; Pistolesi, M.; Cioni, R.; Degruyter, W.; Elissondo, M.; Baumann, V. Dynamics of wind-affected volcanic plumes: The example of the 2011 Cordón Caulle eruption, Chile. *J. Geophys. Res. Solid Earth* **2015**, *120*, 2242–2261. [CrossRef]
11. Silva Parejas, C.; Lara, L.; Bertin, D.; Amigo, A.; Orozco, G. The 2011-2012 eruption of Cordón Caulle volcano (Southern Andes): Evolution, crisis management and current hazards. Proceedings of EGU General Assembly Conference Abstracts, Vienna, Austria, 22–27 April 2012; p. 9382.
12. Brunke, E.-G.; Labuschagne, C.; Scheel, H.E. Trace gas variations at Cape Point, South Africa, during May 1997 following a regional biomass burning episode. *Atmos. Environ.* **2001**, *35*, 777–786. [CrossRef]
13. Hovila, J.; Arola, A.; Tamminen, J. *OMI/Aura Surface UVB Irradiance and Erythemal Dose Daily L3 Global Gridded 1.0 degree x 1.0 degree V3*; NASA Goddard Space Flight Center, Ed.; Goddard Earth Sciences Data and Information Services Center (GES DISC): Greenbelt, MD, USA, 2013. [CrossRef]
14. Brogniez, C.; Auriol, F.; Deroo, C.; Arola, A.; Kujanpää, J.; Sauvage, B.; Kalakoski, N.; Pitkänen, A.; Riku, M.; Catalfamo, M. Validation of satellite-based noontime UVI with NDACC ground-based instruments: Influence of topography, environment and satellite overpass time. *Atmos. Chem. Physics* **2016**, *16*. [CrossRef]
15. Fioletov, V.; Kerr, J.B.; Fergusson, A. The UV index: Definition, distribution and factors affecting it. *Can. J. Public Health* **2010**, *101*, I5–I9. [CrossRef] [PubMed]
16. Cadet, J.-M.; Bencherif, H.; Portafaix, T.; Lamy, K.; Ncongwane, K.; Coetzee, G.J.R.; Wright, C.Y. Comparison of Ground-Based and Satellite-Derived Solar UV Index Levels at Six South African Sites. *Int. J. Environ. Res. Public Health* **2017**, *14*, 1384. [CrossRef]
17. McArthur, L.J.B.; Halliwell, D.H.; Niebergall, O.J.; O'Neill, N.T.; Slusser, J.R.; Wehrli, C. Field comparison of network Sun photometers. *J. Geophys. Res. Atmos.* **2003**, *108*. [CrossRef]
18. Nyeki, S.; Halios, C.H.; Baum, W.; Eleftheriadis, K.; Flentje, H.; Gröbner, J.; Vuilleumier, L.; Wehrli, C. Ground-based aerosol optical depth trends at three high-altitude sites in Switzerland and southern Germany from 1995 to 2010. *J. Geophys. Res. Atmos.* **2012**, *117*, D18202. [CrossRef]
19. Smirnov, A.; Holben, B.; Eck, T.; Dubovik, O.; Slutsker, I. Cloud-screening and quality control algorithms for the AERONET database. *Remote Sens. Environ.* **2000**, *73*, 337–349. [CrossRef]
20. Greene, C.A.; Thirumalai, K.; Kearney, K.A.; Delgado, J.M.; Schwanghart, W.; Wolfenbarger, N.S.; Thyng, K.M.; Gwyther, D.E.; Gardner, A.S.; Blankenship, D.D. The climate data toolbox for MATLAB. *Geochem. Geophys. Geosystems* **2019**, *20*, 3774–3781. [CrossRef]
21. Global Modeling and Assimilation Office (GMAO). *MERRA-2 tavg1_2d_aer_Nx: 2d,1-Hourly, Time-averaged, Single-Level, Assimilation, Aerosol Diagnostics V5.12.4*; Goddard Earth Sciences Data and Information Services Center (GES DISC): Greenbelt, MD, USA, 2015. [CrossRef]
22. Ukhov, A.; Mostamandi, S.; Krotkov, N.; Flemming, J.; da Silva, A.; Li, C.; Fioletov, V.; McLinden, C.; Anisimov, A.; Alshehri, Y.M.; et al. Study of SO Pollution in the Middle East Using MERRA-2, CAMS Data Assimilation Products, and High-Resolution WRF-Chem Simulations. *J. Geophys. Res. Atmos.* **2020**, *125*, e2019JD031993. [CrossRef]
23. Clarisse, L.; Hurtmans, D.; Clerbaux, C.; Hadji-Lazaro, J.; Ngadi, Y.; Coheur, P.F. Retrieval of sulphur dioxide from the infrared atmospheric sounding interferometer (IASI). *Atmos. Meas. Tech.* **2012**, *5*, 581–594. [CrossRef]
24. Clarisse, L.; Prata, F. Infrared sounding of volcanic ash. In *Volcanic ash: Methods of observation and monitoring*; Mackie, S., Cashman, K., Ricketts, H., Rust, A., Watson, M., Eds.; Elsevier: Amsterdam, The Netherlands, 2015.
25. Moxnes, E.D.; Kristiansen, N.I.; Stohl, A.; Clarisse, L.; Durant, A.; Weber, K.; Vogel, A. Separation of ash and sulfur dioxide during the 2011 Grímsvötn eruption. *J. Geophys. Res. Atmos.* **2014**, *119*, 7477–7501. [CrossRef]
26. Theys, N.; Campion, R.; Clarisse, L.; Brenot, H.; van Gent, J.; Dils, B.; Corradini, S.; Merucci, L.; Coheur, P.F.; Van Roozendael, M.; et al. Volcanic SO_2 fluxes derived from satellite data: A survey using OMI, GOME-2, IASI and MODIS. *Atmos. Chem. Phys.* **2013**, *13*, 5945–5968. [CrossRef]
27. Carboni, E.; Grainger, R.G.; Mather, T.A.; Pyle, D.M.; Thomas, G.E.; Siddans, R.; Smith, A.J.A.; Dudhia, A.; Koukouli, M.E.; Balis, D. The vertical distribution of volcanic SO2 plumes measured by IASI. *Atmos. Chem. Phys.* **2016**, *16*, 4343–4367. [CrossRef]
28. Pisso, I.; Sollum, E.; Grythe, H.; Kristiansen, N.; Cassiani, M.; Eckhardt, S.; Arnold, D.; Morton, D.; Thompson, R.L.; Groot Zwaaftink, C.D.; et al. The Lagrangian particle dispersion model FLEXPART version 10.3. *Geosci. Model Dev.* **2019**, *2019*, 1–67. [CrossRef]

29. Walker, J.C.; Carboni, E.; Dudhia, A.; Grainger, R.G. Improved detection of sulphur dioxide in volcanic plumes using satellite-based hyperspectral infrared measurements: Application to the Eyjafjallajökull 2010 eruption. *J. Geophys. Res. Atmos.* **2012**, *117*. [CrossRef]
30. Eckhardt, S.; Prata, A.J.; Seibert, P.; Stebel, K.; Stohl, A. Estimation of the vertical profile of sulfur dioxide injection into the atmosphere by a volcanic eruption using satellite column measurements and inverse transport modeling. *Atmos. Chem. Phys.* **2008**, *8*, 3881–3897. [CrossRef]
31. Nyeki, S.; Wehrli, C.; Gröbner, J.; Kouremeti, N.; Wacker, S.; Labuschagne, C.; Mbatha, N.; Brunke, E.G. The GAW-PFR aerosol optical depth network: The 2008–2013 time series at Cape Point Station, South Africa. *J. Geophys. Res. Atmos.* **2015**, *120*, 5070–5084. [CrossRef]
32. Tesfaye, M.; Sivakumar, V.; Botai, J.; Mengistu Tsidu, G. Aerosol climatology over South Africa based on 10 years of Multiangle Imaging Spectroradiometer (MISR) data. *J. Geophys. Res. Atmos.* **2011**, *116*. [CrossRef]
33. Balashov, N.V.; Thompson, A.M.; Piketh, S.J.; Langerman, K.E. Surface ozone variability and trends over the South African Highveld from 1990 to 2007. *J. Geophys. Res. Atmos.* **2014**, *119*, 4323–4342. [CrossRef]
34. Kerr, J.B. Understanding the factors that affect surface ultraviolet radiation. *Optical Eng.* **2005**, *44*, 041002. [CrossRef]
35. Günther, T.; Schulze, M.; Friederici, A.; Theisel, H. Visualizing Volcanic Clouds in the Atmosphere and Their Impact on Air Traffic. *IEEE Comput. Graph. Appl.* **2016**, *36*, 36–47.

Chapter 5 Results: The radiative effect of aerosols and tropospheric ozone

5.1 Paper overview

Incoming solar UVR is influenced by ozone, clouds, sulphur dioxide and aerosols as it passes through the atmosphere (Bais et al., 1993). Over Southern Africa, emissions from biomass burning are the largest contributor to tropospheric aerosols (Bencherif et al., 2020). Previous studies have shown how emissions from biomass burning can result in decreases in surface UVR (Abel et al., 2005; Arola et al., 2007; Hobbs et al., 2003).

Tropospheric ozone is a secondary pollutant that forms through a photochemical reaction from ozone precursors (Vakkari et al., 2014) and can absorb UVR due to Rayleigh scattering in the lower, denser atmosphere (Brühl et al., 1989; Madronich et al., 2011). Therefore, changes in tropospheric ozone from biomass burning or industrial activities can affect not only surface UVR but have an impact on public health factors such as skin cancer and respiratory infections.

In Southern Africa, the biomass burning season occurs annually between July and November and significantly increases the aerosol loading over Southern Africa (Thompson et al., 2014). The release of aerosols and emissions from biomass burning contribute to the formation of tropospheric ozone which reaches a seasonal maximum, along with AOD, during the austral spring (Adesina et al., 2014; Diab et al., 2004).

The aim of this study was to investigate the radiative effect of aerosols and tropospheric ozone on surface UVR levels over Irene in Pretoria during the biomass burning season. The study used a radiative transfer model to assess the sensitivity of surface UVR to aerosols and tropospheric ozone during the biomass burning season.

Ground-based observations of aerosol properties and ozonesonde profiles from Pretoria indicated that AOD and tropospheric ozone reached an annual maximum between September and October. Although the biomass burning season is located far to the north and east of Pretoria, the synoptic circulation pattern transports air masses from the biomass burning region to Pretoria (Clain et al., 2009).

Using the Tropospheric Ultraviolet-Visible (TUV) radiative transfer model, scenarios were simulated to assess the sensitivity of surface UVR to aerosols and tropospheric ozone from the biomass burning season in comparison with background levels of aerosols and tropospheric ozone. The modelled UVR data was compared to observed UVR data and it was found that aerosols have a larger radiative effect than tropospheric ozone.

5.2 Thesis contribution

This paper contributed to the third objective of this thesis which was to investigate the impact of aerosols and tropospheric ozone on surface UVR during the biomass burning season. The results from this manuscript demonstrate the radiative effect of both aerosols and tropospheric ozone during the Southern Africa biomass burning season.

5.3 Contribution of candidate

D. Jean du Preez was responsible for the data analysis, model simulations and writing the manuscript. All the co-authors contributed to the discussion and final manuscript preparations.

5.4 Publication status

du Preez, D.J., Bencherif, H., Portafaix, T., Lamy, K., & Wright, C.Y. (2021). Solar Ultraviolet Radiation in Pretoria and Its Relations to Aerosols and Tropospheric Ozone during the Biomass Burning Season. Atmosphere, 12(2). https://doi.org/10.3390/atmos12020132.

5.5 References

Abel, S. J., Highwood, E. J., Haywood, J. M., & Stringer, M. A. (2005). The direct radiative effect of biomass burning aerosols over southern Africa. *Atmospheric Chemistry and Physics, 5*(7), 1999-2018. doi:10.5194/acp-5-1999-2005

Adesina, A. J., Kumar, K. R., Sivakumar, V., & Griffith, D. (2014). Direct radiative forcing of urban aerosols over Pretoria (25.75°S, 28.28°E) using AERONET Sunphotometer data: First scientific results and environmental impact. *Journal of Environmental Sciences, 26*(12), 2459-2474. doi:10.1016/j.jes.2014.04.006

Arola, A., Lindfors, A., Natunen, A., & Lehtinen, K. E. J. (2007). A case study on biomass burning aerosols: effects on aerosol optical properties and surface radiation levels. *Atmospheric Chemistry and Physics, 7*(16), 4257-4266. doi:10.5194/acp-7-4257-2007

Bais, A. F., Zerefos, C. S., Meleti, C., Ziomas, I. C., & Tourpali, K. (1993). Spectral measurements of solar UVB radiation and its relations to total ozone, SO2, and clouds. *Journal of Geophysical Research: Atmospheres, 98*(D3), 5199-5204. doi:10.1029/92jd02904

Bencherif, H., Bègue, N., Pinheiro, D. K., du Preez, D. J., Cadet, J. M., da Silva Lopez, F. J., Shikwambana, L., Landulfo, E., Vescovini, T., labuschagne, C., Silva, J. J., Anabor, V., Coheur, P. F., Mbatha, N., Hadji-Lazaro, J., Sivakumar, V., & Clerbaux, C. (2020). Investigating the Long-Range Transport of Aerosol Plumes Following the Amazon Fires (August 2019): A Multi-Instrumental Approach from Ground-Based and Satellite Observations. *Remote Sensing, 12*(3846). doi:10.3390/rs12223846

Brühl, C., & Crutzen, P. J. (1989). On the disproportionate role of tropospheric ozone as a filter against solar UV-B radiation. *Geophysical Research Letters, 16*(7), 703-706. doi:10.1029/GL016i007p00703

Clain, G., Baray, J.-L., Delmas, R., Diab, R., de Bellevue, J. L., Keckhut, P., Posny, F., Metzger, J.-M., & Cammas, J.-P. (2009). Tropospheric ozone climatology at two Southern Hemisphere tropical/subtropical sites,(Reunion Island and Irene, South Africa) from ozonesondes, LIDAR, and in situ aircraft measurements. *Atmospheric Chemistry and Physics*.

Diab, R. D., Thompson, A. M., Mari, K., Ramsay, L., & Coetzee, G. J. R. (2004). Tropospheric ozone climatology over Irene, South Africa, from 1990 to 1994 and 1998 to 2002. *Journal of Geophysical Research, 109*(D20301). doi:10.1029/2004JD004793

Hobbs, P. V., Sinha, P., Yokelson, R. J., Christian, T. J., Blake, D. R., Gao, S., Kirchstetter, T. W., Novakov, T., & Pilewskie, P. (2003). Evolution of gases and particles from a savanna fire in South Africa. *Journal of Geophysical Research: Atmospheres, 108*(D13). doi:10.1029/2002JD002352

Madronich, S., Wagner, M., & Groth, P. (2011). Influence of Tropospheric Ozone Control on Exposure to Ultraviolet Radiation at the Surface. *Environmental Science & Technology, 45*(16), 6919-6923. doi:10.1021/es200701q

Thompson, A. M., Balashov, N. V., Witte, J. C., Coetzee, J. G. R., Thouret, V., & Posny, F. (2014). Tropospheric ozone increases over the southern Africa region: bellwether for rapid growth in Southern Hemisphere pollution? *Atmospheric Chemistry and Physics, 14*(18), 9855-9869. doi:10.5194/acp-14-9855-2014

Vakkari, V., Kerminen, V.-M., Beukes, J. P., Tiitta, P., van Zyl, P. G., Josipovic, M., Venter, A. D., Jaars, K., Worsnop, D. R., Kulmala, M., & Laakso, L. (2014). Rapid changes in biomass burning aerosols by atmospheric oxidation. *Geophysical Research Letters, 41*(7), 2644-2651. doi:10.1002/2014gl059396

5.6 Manuscript 3

atmosphere

MDPI

Article

Solar Ultraviolet Radiation in Pretoria and Its Relations to Aerosols and Tropospheric Ozone during the Biomass Burning Season

D. Jean du Preez [1,2,*], Hassan Bencherif [2,3], Thierry Portafaix [2], Kévin Lamy [2] and Caradee Yael Wright [1,4]

1 Department of Geography, Geoinformatics and Meteorology, University of Pretoria, Pretoria 0002, South Africa; caradee.wright@mrc.ac.za
2 Laboratoire de l'Atmosphère et des Cyclones (UMR 8105 CNRS, Université de La Réunion, MétéoFrance), 97744 Saint-Denis de La Réunion, France; hassan.bencherif@univ-reunion.fr (H.B.); thierry.portafaix@univ-reunion.fr (T.P.); kevin.lamy@univ-reunion.fr (K.L.)
3 School of Chemistry and Physics, University of KwaZulu-Natal, Durban 4041, South Africa
4 Environmental and Health Research Unit, South African Medical Research Council, Pretoria 0001, South Africa
* Correspondence: dupreez.dj@tuks.co.za

Abstract: Biomass burning has an impact on atmospheric composition as well as human health and wellbeing. In South Africa, the biomass burning season extends from July to October and affects the aerosol loading and tropospheric ozone concentrations which in turn impact solar ultraviolet radiation (UVR) levels at the surface. Using ground-based observations of aerosols, tropospheric ozone and solar UVR (as well as modelled solar UVR) we investigated the impact of aerosols and tropospheric ozone on solar UVR in August, September, and October over Pretoria. Aerosol optical depth (AOD) and tropospheric ozone reached a peak between September and October each year. On clear-sky days, the average relative difference between the modelled and observed solar Ultraviolet Index (UVI) levels (a standard indicator of surface UVR) at solar noon was 7%. Using modelled UVR—which included and excluded the effects of aerosols and tropospheric ozone from biomass burning—aerosols had a larger radiative effect compared to tropospheric ozone on UVI levels during the biomass burning season. Excluding only aerosols resulted in a 10% difference between the modelled and observed UVI, while excluding only tropospheric ozone resulted in a difference of −2%. Further understanding of the radiative effect of aerosols and trace gases, particularly in regions that are affected by emissions from biomass burning, is considered important for future research.

Keywords: aerosol optical depth; Africa; air pollution; atmospheric science; environmental health; ozone; UV

Citation: du Preez, D.J.; Bencherif, H.; Portafaix, T.; Lamy, K.; Wright, C.Y. Solar Ultraviolet Radiation in Pretoria and Its Relations to Aerosols and Tropospheric Ozone during the Biomass Burning Season. *Atmosphere* **2021**, *12*, 132. https://doi.org/10.3390/atmos12020132

Academic Editor: Andrei Skorokhod
Received: 2 November 2020
Accepted: 15 January 2021
Published: 20 January 2021

1. Introduction

As solar ultraviolet radiation (UVR) passes through the atmosphere it interacts with gases and particles which absorb, reflect, or scatter the incoming solar UVR. Solar UVR is classified into three bands: UVA (315–400 nm), UVB (280–315 nm), and UVC (100–280 nm) where the absorption of solar UVR by stratospheric ozone increases within the UVB spectrum [1]. As a result, surface solar UVR is decreased significantly at shorter wavelengths [1]. In the troposphere, solar UVR is further attenuated by tropospheric ozone, sulfur dioxide, aerosols, and clouds [2]. Other factors such as altitude, solar zenith angle, and albedo effect solar UVR levels at the surface [1,3].

Atmospheric aerosols have direct and indirect effects on the Earth's radiation budget. The direct effect of aerosols on the radiation budget is due to the scattering and absorption of UVR by aerosols [4], while the indirect effect of aerosols is due to the formation of clouds as aerosols can act as cloud condensation nuclei [5]. The radiative effect of aerosols is determined by their size, distribution, and optical properties [6]. Atmospheric aerosols can

be from natural or anthropogenic sources. Natural sources include dust storms, volcanic eruptions, sea salt spray, and biomass burning. Biomass burning emissions can also be anthropogenic along with other human-made emissions such as those from vehicles and industries. [7].

Biomass burning is one of the largest contributors to tropospheric aerosol loading where these aerosols also have a significant radiative effect [8,9]. In Southern Africa, the main biomass burning region is located over the north and eastern parts of South Africa and Mozambique. The biomass burning season reaches an annual peak at the end of the dry season between August and September [10]. Emissions from biomass burning are transported westward to the Atlantic Ocean as well as eastward towards the Indian Ocean [11]. During spring, the semi-permanent Indian Ocean anticyclone and easterly winds transport aerosols over southern Africa [10,12,13]. As a result, the radiative effect of aerosols is not limited to the burnt area and the resulting plumes can have an impact thousands of kilometers away [14,15].

The emissions released during the biomass burning process (and other pollution-generating activities) include ozone precursors such as nitrogen oxides (NOx), carbon monoxide (CO), and volatile organic compounds (VOCs) [16]. These gases react with sunlight to form ozone in the troposphere [17]. The formation of tropospheric ozone is dependent on the concentration of ozone precursors as well as temperature and humidity [18]. Tropospheric ozone has a short lifetime and is a greenhouse gas. It also impacts human health, vegetation, and crop yields [19]. The emission of ozone precursors is not the only source of tropospheric ozone. Stratosphere-troposphere exchange (STE) can result in an increase in tropospheric ozone levels due to the higher levels of ozone present in the stratosphere [17].

Due to the synoptic-scale circulation pattern, aerosol loading and tropospheric ozone levels over Pretoria are affected by biomass burning emissions. This study aimed to investigate the effect of aerosols and tropospheric ozone on surface UVR levels over Pretoria during the biomass burning season. Furthermore, a comparison of observed and modelled UVR was made to determine the separate and combined influence of aerosols and tropospheric ozone from biomass burning emissions on solar UVR. These findings are useful to improve the understanding of the radiative effect of tropospheric ozone and aerosols on solar UVR levels at the surface. In the data and methods section, the study area, data, instrumentation, and methods are described. The results from the data analysis show the seasonal cycle of tropospheric aerosols, ozone, and UVR as well as a case study and model simulations to demonstrate the radiative effect of tropospheric aerosols and ozone.

2. Data and Methods

Pretoria is situated on the inland plateau of South Africa in the Gauteng province at approximately 1300 m above sea level (Figure 1). The city experiences cool, dry winters and long, hot summers with rainfall occurring during the summer months. Pretoria was selected as the study area due to the known high levels of tropospheric ozone related to industrial activities [12,20] and the impact of the biomass burning season on aerosol distribution [21]. Data were collected from three stations, namely the South African Weather Service (SAWS) Bolepi House, SAWS Irene, and the Council for Scientific and Industrial Research (CSIR) head office due to their relative proximity to one another. The three different stations were located between 1322 m and 1529 m above sea level. The CSIR and Irene stations are approximately 18 km apart, while Bolepi House is approximately 6 km from the CSIR.

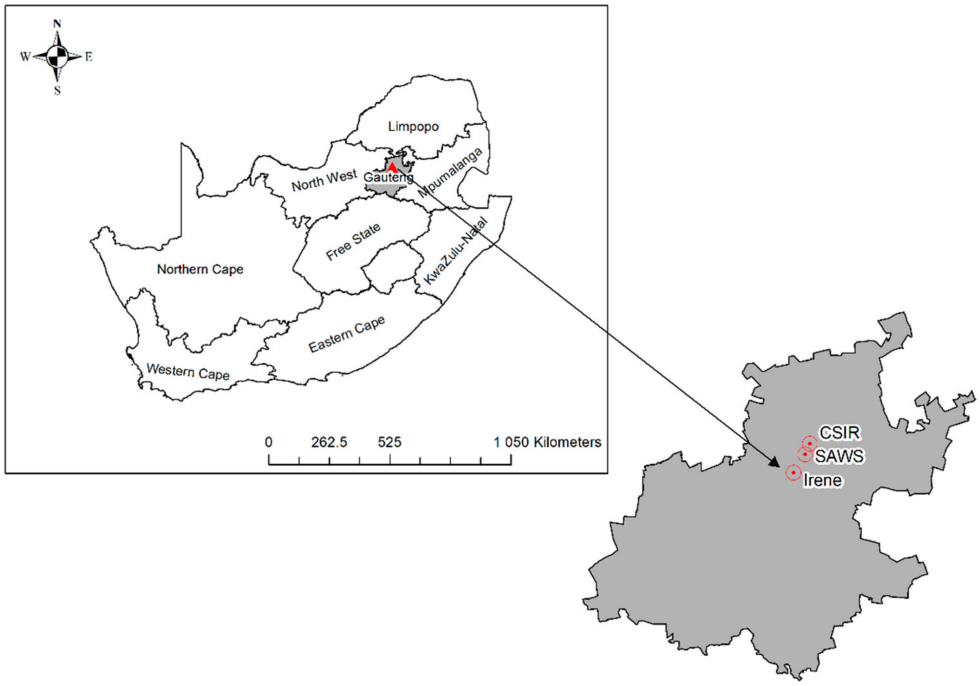

Figure 1. Map showing the location of Pretoria in South Africa and the three stations where data were collected from the Council for Scientific and Industrial Research (CSIR) head office, South African Weather Service (SAWS) Bolepi House and SAWS Irene weather stations, respectively.

2.1. Aerosol Data from the CSIR Station

A Cimel sun photometer is located at the CSIR head office in Pretoria (25.76° S, 28.28° E) at 1 449 m above sea level (Figure 1) and is part of the Aerosol Robotic Network (AERONET). The sun photometer has a spectral range of 340–1640 nm with eight spectral bands (340, 380, 440, 500, 675, 875, 1020, and 1640 nm) [22]. Details on the instrument, calibration and error estimation are published in Dubovik et al. [23]. Aerosol Optical Depth (AOD) is an indication of the distribution of aerosols in a column of air. Additional observations at 935 nm are used to estimate columnar water vapour [24]. The Ångström Exponent (AE) can be calculated using Equation (1) and can be used to estimate the size distribution of aerosols from spectral AOD observations [25]. AE values less than 1.0 indicated that coarse particles such as desert dust were dominant while AE values greater than 1.0 indicated the fine particles, such as smoke and sulfates, were dominant [25–28]. Equation (1) follows:

$$\alpha = -\frac{\log \frac{\tau_{\lambda 1}}{\tau_{\lambda 2}}}{\log \frac{\lambda_1}{\lambda_2}} \quad (1)$$

where α is the AE, τ_λ is the AOD at the first and second wavelengths (λ), respectively.

The AERONET inversion algorithm is used to provide aerosol optical properties such as single scattering albedo (SSA) which is derived from direct and diffuse radiation measurements from sun photometers [29]. The inversion algorithm assumes that the vertical distribution of the aerosols is similar to global models, particles are partitioned into spherical and non-spherical and it accounts for the gaseous absorption by ozone, nitrogen dioxide, and water vapor. Furthermore, the algorithm provides information on the quality of the output parameters produced [30]. SSA is an important factor related to the radiative effect of aerosols and represents the ratio between the scattering and extinction efficiencies of aerosols [31]. The level two daily average data of AOD (340 nm) and AE (340–440 nm) were obtained from the AERONET website (aeronet.gsfc.nasa.gov/) for the period from 1

July 2011 to 31 May 2018 (inclusive) and were used to calculate the monthly averages and standard deviations of AOD and AE.

2.2. Tropospheric Ozone Data from the Irene Station

Since 1998, ozone soundings have been conducted at the SAWS Irene weather station (25.9° S, 28.2° E) in Pretoria (Figure 1). The station is 1 529 m above sea level and operates within the Southern Hemisphere Additional Ozonesondes (SHADOZ) network [32–34]. The ozone soundings were conducted twice a month using an electrochemical cell comprising a cathode and anode cell. The solution of buffered potassium iodide (KI) and saturated solution of KI was used in the cathode and anode cell, respectively. An ion bridge connected the cells which allowed for electrons to flow between the two chambers and ozone was measured using the iodine/iodide electrode reactions. An interface board was connected to a radiosonde to transmit data regarding cell current, pump temperature, ambient temperature, pressure, and relative humidity [33].

The data for 1998–2018 were obtained from the SHADOZ website (tropo.gsfc.nasa.gov/shadoz/index.html). Between 1998 and 2018, 369 ozonesondes were launched, however, no ozonesondes were launched from 2008 to 2012. Within this dataset, there are gaps when launching ozonesondes was not possible due to various reasons. The raw data were obtained at two-second intervals and the ozone concentrations were averaged over 100 m intervals from the surface to the burst altitude (± 30 km) of the balloon. The tropospheric ozone column was calculated, in Dobson Units (DU), by integrating the vertical ozone profile from the surface to the lapse-rate tropopause (LRT). The LRT is defined as the lowest level at which the temperature lapse is less than 2 K km^{-1} for at least 2 km [35]. Each ozone sounding was used to determine the average tropospheric column and average ozone profile for the respective month.

2.3. Observed UVB Data for Pretoria

The SAWS had a surface UVB radiation monitoring station at their headquarters, Bolepi House, in Pretoria (25.81° S, 28.26° E) [36]. A Solar Light 501 UVB radiometer with a spectral wavelength of 280–315 nm was used to measure radiation at hourly intervals. The instrument provided an analogue voltage output proportional to the measured radiation [37] that was given in Minimal Erythemal Dose (MED) units. One MED was approximately 210 Jm^{-2}, where MED is a metric used to express the minimal erythemal dose required to induce erythema (also known as sunburn) [38]. The MED units were converted to UV Index (UVI), a standard indicator of UVR levels [1] using Equation (2) [39]:

$$\mathrm{UVI} = \frac{210\left[J.m^{-2}\right] \times 40\left[m^2.W^{-1}\right]}{3600[s/h]} \quad (2)$$

To correct the instrument-weighted UVB radiation to the erythemal weighted UVR spectrum (280–400 nm) a correction factor was applied [40]. The correction factor used satellite observed total column ozone to correct for the spectral and angular response of the instrument. A comparison between observed UVB and satellite-derived UVB showed that there was a moderately strong correlation between these variables at the Pretoria station [41]. The instrument was last calibrated in 2013 by the Deutscher Wetterdienst (DWD). The long period since calibration is noted as a limitation and may be a source of uncertainty in the UVB radiation data. Hourly data from 1 January 2009 to 30 April 2018 (inclusive) were obtained from this station for this study.

Clouds result in large spatial and temporal variability of surface UVR radiation levels. To remove the effect of clouds on observed UVR, clear-sky days were determined using a clear-sky determination method [42,43]. To do so, three steps were used. The first step calculated the correlation between UVR values before solar noon and after solar noon. The values after solar noon were reversed so that the UVR values with similar SZAs were correlated. When the correlation was below 0.8, the day was defined as cloudy. The second step tested for monotonic increases and decreases in UVR values before and after solar noon,

respectively. If the increases and decreases in UVR values were not monotonic, the days were defined as cloudy. Lastly, the data were used to determine the monthly hourly average values for all-sky conditions. If the UVR at solar noon was 1.5 standard deviations below the average, then the day was defined as cloudy. The clear-sky determination methods identified 1190 clear-sky days during the observation period (2009 to 2018).

From the hourly data, the monthly hourly averages, and standard deviations of UVR at solar noon were calculated only using days with a complete observation record. The observed clear-sky solar noon UVR values were compared to the modelled clear-sky UVR values to show that there was a consensus between the observed and modelled data (Section 2.4).

2.4. Modelled UVR over Pretoria

To investigate the radiative effect of aerosols and tropospheric ozone over Pretoria, the Tropospheric Ultraviolet-Visible (TUV) radiative transfer model version 5.3 [44] was used to model clear-sky UVI at Bolepi House. Using pseudo-spherical, eight-stream discrete ordinates to solve the radiative transfer algorithm [45] the model accounted for the scattering and absorption of UVR by gases and particles as it passed through the atmosphere [46]. The model calculated parameters including radiance, weight spectral integrals for specific wavelength bands and biologically-active irradiance, i.e., UVI. Input data for the model included total column ozone, total column nitrogen dioxide, climatological ozone, and temperature profiles, AOD (340 nm), AE (340–440 nm), SSA, and altitude.

In this study, daily total column ozone and nitrogen dioxide observations from the Ozone Monitoring Instrument (OMI) were used [47,48]. McPeters and Labouw [49] derived monthly averaged zonal ozone and temperature profile for different latitude regions between 0 and 60 km using data from ozonesondes for the troposphere, the Stratospheric Aerosol and Gas Experiment (SAGE II) [50] and Microwave Limb Sounder (MLS) instrument for the stratosphere [49]. The ozone and temperature climatological profiles for 25° S included data from the ozonesondes launched at Irene and the MLS instrument provided measurements down to the thermal tropopause. The input data for the aerosol optical properties included daily averages of AOD and AE which were obtained from the AERONET sun photometer at the CSIR and the aerosol distribution described by Elterman, 1968 [51]. Monthly SSA (550 nm) data were obtained from the Max-Planck Version 2 (MACv2) aerosol climatology [52] as the inversion algorithm did not provide sufficient data points. The MACv2 aerosol climatology used ground-based measurements and modelling to create global data fields.

Data on the aerosol optical properties (AOD and AE) were only available for 1 July 2011 to 31 May 2018. Therefore, the TUV model was used to calculate the clear-sky UVI levels for this period during which there were 1215 days which had complete input data required for the TUV simulations. The simulated UVI was compared to the observed clear-sky UVI by calculating the relative difference for each month using Equation (3):

$$\text{Relative difference} = 100 \times (\text{UVI}_{\text{TUV}} - \text{UVI}_{\text{obs}}) \div \text{UVI}_{\text{obs}} \quad (3)$$

where TUV represents the modelled UVI and Obs the observed UVI.

2.5. Effect of Aerosol and Ozone on UVR over Pretoria

Biomass burning affects atmospheric composition through the release of aerosols and ozone precursors. Approximately 31% of AOD observations were one standard deviation above the respective monthly averages from August to October (2011 to 2017). To investigate the radiative effect of aerosols, the observed clear-sky and model UVI values were compared to AOD observations during this period.

To assess the sensitivity of surface solar UVI to aerosols and tropospheric ozone during the biomass burning season (August to October) four TUV scenarios were simulated and compared to the ground-based UVI observations. The background level of aerosol optical properties (AOD, AE, and SSA) and tropospheric ozone were determined by averaging

the monthly values from November to July when AOD and tropospheric ozone were at their lowest. The aerosol optical properties and tropospheric ozone between August and October were determined to be the biomass burning component. The simulations were initialized with and without the biomass burning component using the background levels as the reference condition. The results from the simulations were then compared to ground-based observations. Studies investigating the contribution of stratospheric ozone to the tropospheric ozone budget have shown that, during the biomass burning season, the contribution of stratospheric ozone is insignificant in the lower troposphere over Irene [53,54].

3. Results and Discussion

In this section, the aerosol, tropospheric ozone and UVI patterns are presented. The relationship between aerosols/tropospheric ozone and UVI are presented to demonstrate the radiative effect of aerosols and tropospheric ozone.

3.1. Aerosol Climatology

Daily averages of AOD and AE from 2011 to 2018 were obtained for the AERONET station at the CSIR in Pretoria. The aerosol observations at the CSIR showed that AOD (Figure 2) reached an annual minimum in June (0.23) and increased to an annual maximum in September (0.46).

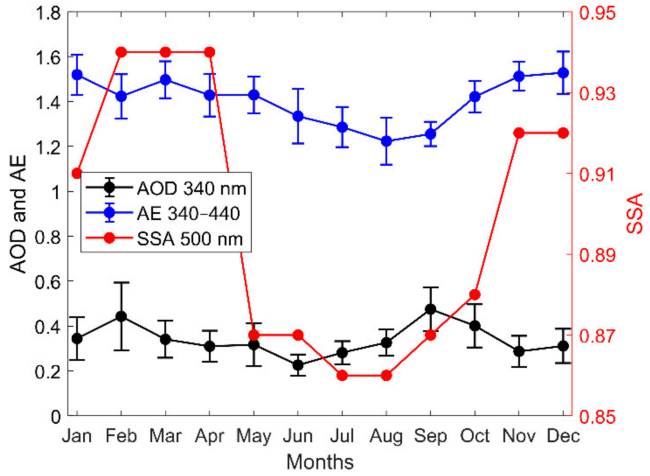

Figure 2. Monthly means and standard deviations of aerosol properties for 2011 to 2018 from sun photometer observations at the CSIR: Aerosol optical depth (AOD) at 340 nm (black) and Ångström Exponent (AE) (blue) in the 340–440 nm spectral band as well as monthly mean single scattering albedo (SSA) at 550 nm (red) from the MACv2 aerosol climatology.

The two annual AOD maxima (in February and September) coincided with summer (December, January, and February) and spring (September, October, and November), respectively. These peaks have also been identified in previous studies [21,55]. During spring, emissions from biomass burning could increase AOD, while in summer months, strong convection could result in the disturbance of surface particles thereby increasing AOD [56].

The AE parameter was inversely related to aerosol particle size. AE values (Figure 2) had a small range and were dominated by fine aerosols from anthropogenic emissions [21]. During the biomass burning season, AE values indicated that coarser particles were present which were typically associated with aerosols from biomass burning. AE increased from a minimum in August (~1.25) to a maximum in December (~1.55). Figure 2 also shows an inverse relationship between the seasonal variations of AOD and AE, which highlights the presence of biomass burning and urban/industrial aerosol types over Pretoria. The monthly SSA averages from the MACv2 aerosol climatology were lowest during the

austral winter and highest during summer. A similar seasonal cycle in SSA has been described in a previous study over Pretoria [21].

3.2. Tropospheric Ozone

Using the ozone sounding data from the Irene weather station, the tropospheric ozone profile and tropospheric ozone total column were derived for the periods 1998 to 2018 (369 ozonesondes) (Figure 3a,b) and 2012 to 2018 (113 ozonesondes) (Figure 4a,b). For the period 1998 to 2018, the tropospheric ozone total column (Figure 3a) reached an annual maximum (45 DU) around October each year. This was followed by a decrease over the summer months to an annual minimum in May, with the largest variability occurring during the spring and summer months. The vertical tropospheric ozone profile over Irene (Figure 3b) showed that the highest ozone mixing ratio took place during spring (from August to October) and extended down to 3.5 km. The vertical ozone profile was similar to that reported by Sivakumar et al. [20] with the increases in tropospheric ozone occurring during the biomass burning season.

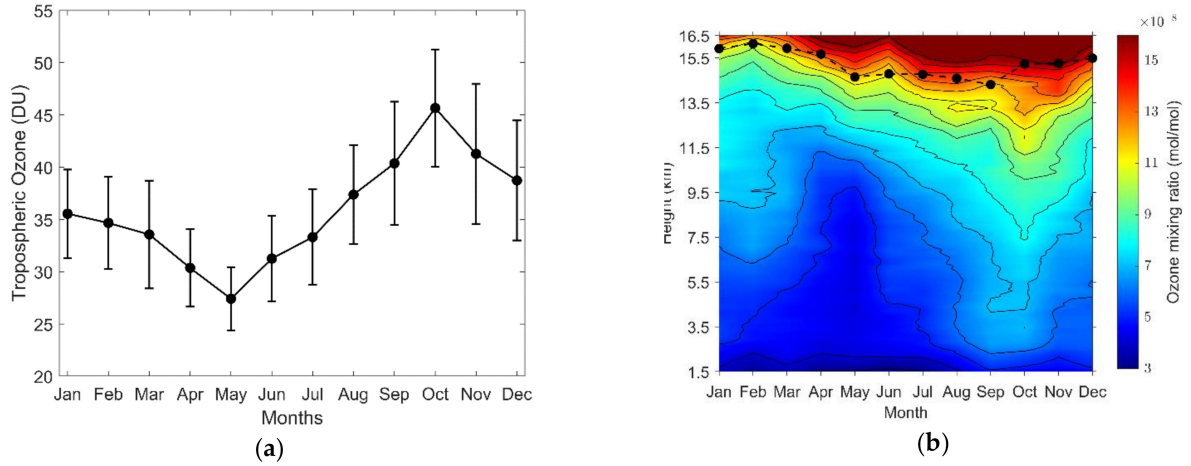

Figure 3. Tropospheric ozone data obtained from ozonesondes launched at Irene: (**a**) Monthly mean and standard deviation of the total tropospheric ozone column obtained from ozonesondes between 1998 and 2018; (**b**) Monthly mean ozone mixing ratio from 1.5 to 16.5 km above sea level and monthly mean lapse-rate tropopause obtained from ozonesondes between 1998 and 2018 (dashed black line).

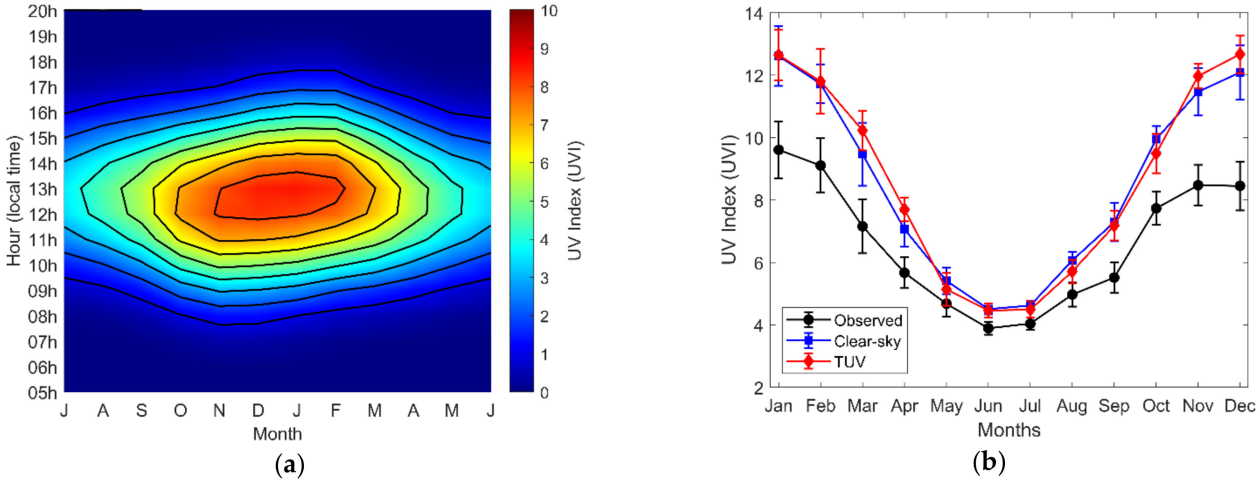

Figure 4. Solar Ultraviolet Index (UVI) observations for Bolepi House, Pretoria from 2009 to 2018. (**a**) Monthly and hourly averages of UVI for July to June; and (**b**) UVI at solar noon for observed all-sky and clear-sky UVI compared to modelled clear-sky UVI for January to December (red line).

The seasonal peak in tropospheric ozone (Figure 3a) is in agreement with previously published work [9,12,20] and occurred in the austral spring when STE enhanced tropospheric ozone concentrations due to the Brewer–Dobson circulation and coincided with the peak of the biomass burning season [57]. Tropospheric ozone formation favors drier conditions that occur near the end of the dry season which further contribute to the seasonal peak in tropospheric ozone [18,58]. Although the main biomass burning region is to the north and east of Irene, the anti-cyclonic air mass from the biomass burning region as well as the emission of ozone precursors from coal-fired power stations affect tropospheric ozone at Irene [12,58].

3.3. Observed and Modelled UVI Levels

Hourly solar UVB radiation data were used to determine monthly and hourly averages of UVI. The observed clear-sky UVI levels were compared to modelled clear-sky UVI levels. The hourly and monthly averages (Figure 4a) showed that UVI is at a maximum during the summer months and highest daily between 12:00 and 14:00 local time. This was further demonstrated by the solar noon UVI values for all-sky and clear-sky conditions (Figure 4b). The higher observed clear-sky solar noon UVI values—with respect to the all-sky UVI values—indicated that the clear-sky determination method was able to remove the effect of clouds on UVI.

The monthly averaged relative difference between the TUV model and observed clear-sky UVI at solar noon ranged between −4% and 29% with an annual relative difference of 7%. Between November and April, the modelled clear-sky values were higher than the observed clear-sky UVI. The monthly-averaged relative difference between the TUV model and observed all-sky UVI ranged between 18% and 87%. The largest difference between the modelled and observed UVI occurred during summer months and may be related to the increase in cloud cover associated with convection during summer months due to synoptic-scale circulation.

Comparisons with observed and modelled UVI in the Southern Hemisphere showed a small relative difference of approximately 10% on clear-sky days [59,60]. To our knowledge, this is the first study in South Africa to compare modelled and observed surface UVI and investigates the effect of atmospheric parameters on surface UVR over South Africa. The TUV model simulations may vary from the observed surface UVI due to factors such as the vertical distribution of aerosols, using AE for 340–440 nm and the climatological ozone and temperature profiles derived by McPeters and Labouw [49] that were used in the simulations. Future research could use satellite lidar observations from the Cloud-Aerosol Lidar with Orthogonal Polarization (CALIOP) instrument to investigate the vertical distribution of aerosols. Furthermore, an ozone and temperature profile specific to Irene could be utilized by using data from ozonesondes and satellites.

3.4. Anomalous AOD over Pretoria

Between August 2017 and October 2017, 31% of AOD observations from the AERONET station at the CSIR were one-standard-deviation above the respective monthly average. The AOD and UVI observations were compared during this period (i.e., August to October 2017) to determine if the anomalously high AOD resulted in lower surface UVR. AOD had seasonal peaks in February and September (Figure 2). Between August and October 2017 (Figure 5a), 24 days were one-standard-deviation above the monthly AOD average. Between 2 September and 2 October 2017, the majority of AOD observations were well above one-standard-deviation from the monthly mean. Between 3 October and 18 October 2017, AOD was below one-standard-deviation from the monthly average. Figure 5b shows the daily and monthly averages of the modelled clear-sky UVI. Between 2 September and 2 October 2017 when AOD was anomalously high, UVI was below one standard deviation from the monthly mean. In October 2017, when AOD was below the monthly average, the corresponding UVI values were above the monthly average.

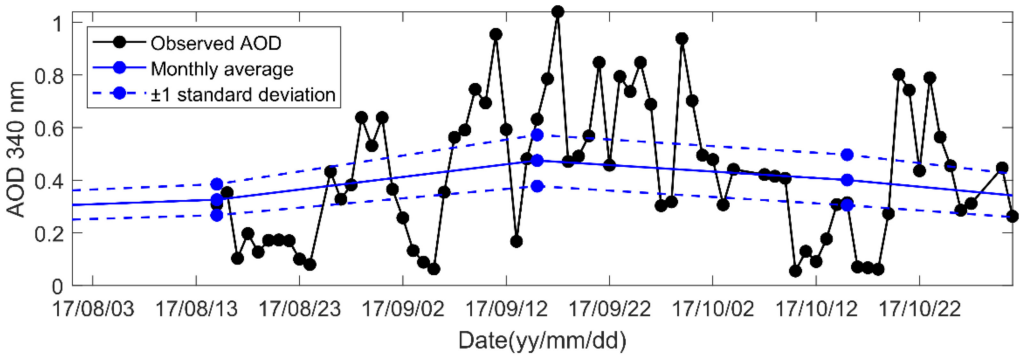

(**a**)

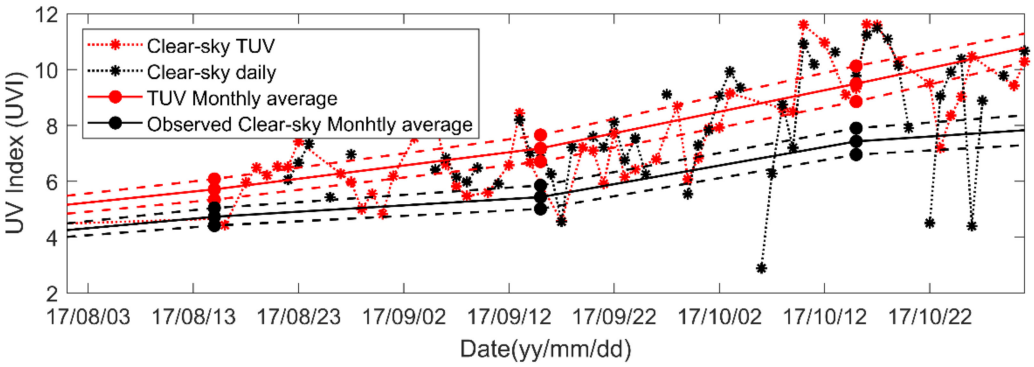

(**b**)

Figure 5. (**a**) Daily AOD values at 340 nm from August to October 2017 as recorded by the AERONET station at the CSIR and the monthly AOD averages and standard deviations (during the 2011–2018 period); (**b**) Daily modelled clear-sky UVI and modelled and observed clear-sky monthly averages and standard deviations from August to October 2017.

From August to October 2017, higher AOD observations occurred simultaneously to lower UVI values and vice versa. This inverse relationship between AOD and UVI—with anomalously high AOD values—has been observed in previous studies [61,62]. Using dispersion modelling, future research may trace the origin of specific biomass burning episodes and investigate the radiative effect over Pretoria.

3.5. Effect of Aerosols and Tropospheric Ozone

To assess the sensitivity of surface solar UVR to aerosols and tropospheric ozone, the TUV model was used to simulate surface solar UVR in four different scenarios and modelled UVI was compared to ground-based observations. The simulations were initialized for the period August to October (2011–2017) with and without the biomass burning component of aerosols and tropospheric ozone. The biomass burning component used the monthly averages of tropospheric ozone and aerosols optical properties (AOD, AE, and SSA) between August and October, while the background level used the monthly averages of tropospheric ozone and aerosol optical properties between November and July as described in Section 2.2.

Table 1 presents the relative difference (%) between the modelled and observed clear-sky UVI in each of the simulations over the three months. The aerosol and tropospheric ozone columns in Table 1 indicate whether the background level or biomass burning emissions were used in the respective simulations. The first simulation (Simulation 1) was a reference simulation and included the aerosol and tropospheric ozone levels between August and October as seen in Figures 2 and 3a. In this simulation, the modelled clear-sky UVI was 3% than observed clear-sky UVI during September months. In Simulation 2, when aerosols and tropospheric ozone from biomass burning were not included, the modelled

clear-sky UVI was 11% higher in September months compared to the observed clear-sky UVI; a change of approximately 14% compared to the reference simulation. In Simulation 3, where tropospheric ozone from biomass burning was excluded and the background level was used, the modelled clear-sky UVI was 2% lower than the observed which was similar to Simulation 1. In Simulation 4, where aerosols from biomass burning were excluded, the modelled UVI was 10% higher than the observed UVI and was similar to Simulation 2 where both aerosols and tropospheric ozone from biomass burning were excluded. Simulations 2, 3, and 4 indicated that increases in aerosols and tropospheric ozone contributed to the reduction in UVR flux reaching the surface and that aerosols from biomass burning have a larger radiative effect.

Table 1. Relative differences (%) between modelled and observed UVI from Tropospheric Ultraviolet-Visible (TUV) model simulations with and without aerosols and tropospheric ozone for August to October (2011 to 2017) and the average relative difference between August and October (ASO).

	Aerosol	Tropospheric ozone	RD—August	RD—September	RD—October
Simulation 1	BB *	BB	−4	−3	−7
Simulation 2	BGL **	BGL	−2	11	2
Simulation 3	BB	BGL	−4	−2	−6
Simulation 4	BGL	BB	−2	10	1

* BB—biomass burning, ** BGL—background level.

Although the changes in Simulation 3 were small compared to the reference simulation, increases in tropospheric ozone may result in decreases in UVR at the surface due to Rayleigh scattering of denser air in the lower levels as shown by other studies [63,64]. Positive decadal trends in tropospheric ozone have been identified over Pretoria [65,66] and these trends may further contribute to the radiative effect of tropospheric ozone.

Future research should investigate the radiative impact of nitrogen dioxide as well as tropospheric aerosols and tropospheric ozone on UVI levels at the surface. Furthermore, research should be done at all SZAs and not be limited to solar noon. Although the three stations (i.e., CSIR, Irene and Bolepi House) were located relatively close to each other, factors such as cloud cover and albedo may have differed between the stations and this could have influenced the comparison between observed and modelled UVI data.

4. Conclusions

The aim of this study was to investigate the effect of aerosols and tropospheric ozone on surface UVR over Pretoria during the biomass burning season. The study modelled surface UVR with and without aerosols and tropospheric ozone from biomass burning and compared the modelled UVR to surface observations. The aerosol loadings and atmospheric composition were affected by biomass burning which reached a peak near the end of the dry winter season. Over Pretoria, AOD reached a maximum value of 0.46 in September and tropospheric ozone reached a maximum of 45 DU in October. The study area was predominantly affected by fine aerosol particles which increased in size during the biomass burning when AOD was at a maximum.

A comparison between modelled and observed clear-sky UVI levels at solar noon showed a small relative difference of 7% on clear-sky days. Between August and October 2017, anomalously high AOD levels were observed over Pretoria. Investigation of this event showed that higher AOD values corresponded with lower UVR levels. In the TUV model simulation—which excluded aerosols and tropospheric ozone from biomass burning—a change of 9% relative to the reference simulation was observed. Furthermore, in the simulation that excluded aerosols from biomass burning there was a relative difference similar to the simulation that excluded both aerosols and tropospheric ozone. This demonstrated that the radiative effect of aerosols was larger than the radiative effect of tropospheric ozone. Future research on the radiative effect of aerosols and trace gases,

particularly in regions that are affected by emissions from biomass burning, is considered important.

Author Contributions: Conceptualization, D.J.d.P., C.Y.W., H.B., K.L., and T.P.; methodology, D.J.d.P., C.Y.W., H.B., and T.P. formal analysis, D.J.d.P.; writing—Original draft preparation, D.J.d.P., C.Y.W., H.B., and T.P.; writing—Review and editing, D.J.d.P., C.Y.W., H.B., K.L., and T.P. All authors have read and agreed to the published version of the manuscript.

Funding: D.J.d.P. received a doctoral scholarship from the University of Pretoria and a scholarship from the French Embassy in South Africa. C.Y.W. receives funding from the South African Medical Research Council, the National Research Foundation of South Africa, and the University of Pretoria. The APC was funded by LACy (Laboratoire de l'Atmosphère et des Cyclones).

Institutional Review Board Statement: Not applicable.

Informed Consent Statement: Not applicable.

Data Availability Statement: The datasets used in this study are freely available from the relevant sources.

Acknowledgments: The authors would like to thank the South African Weather Service for providing UVB and SHADOZ network for ozone sounding data. Furthermore, we would like to thank AERONET for the aerosol data. Authors acknowledge the French Embassy in Pretoria, the South-African PROTEA programme and the CNRS-NRF International Research Project ARSAIO (Atmospheric Research in Southern Africa and Indian Ocean), for supporting research activities.

Conflicts of Interest: The authors declare no conflict of interest.

References

1. Fioletov, V.; Kerr, J.B.; Fergusson, A. The UV index: Definition, distribution and factors affecting it. *Can. J. Public Health* **2010**, *101*, I5–I9. [CrossRef] [PubMed]
2. Bais, A.F.; Zerefos, C.S.; Meleti, C.; Ziomas, I.C.; Tourpali, K. Spectral measurements of solar UVB radiation and its relations to total ozone, SO2, and clouds. *J. Geophys. Res. Atmos.* **1993**, *98*, 5199–5204. [CrossRef]
3. Lerche, C.; Philipsen, P.; Wulf, H. UVR: Sun, lamps, pigmentation and vitamin D. *Photochem. Photobiol. Sci.* **2017**, *16*, 291–301. [CrossRef] [PubMed]
4. Heald, C.L.; Ridley, D.A.; Kroll, J.H.; Barrett, S.R.H.; Cady-Pereira, K.E.; Alvarado, M.J.; Holmes, C.D. Contrasting the direct radiative effect and direct radiative forcing of aerosols. *Atmos. Chem. Phys.* **2014**, *14*, 5513–5527. [CrossRef]
5. Rap, A.; Scott, C.E.; Spracklen, D.V.; Bellouin, N.; Forster, P.M.; Carslaw, K.S.; Schmidt, A.; Mann, G. Natural aerosol direct and indirect radiative effects. *Geophys. Res. Lett.* **2013**, *40*, 3297–3301. [CrossRef]
6. Pfeifer, M.; Koepke, P.; Reuder, J. Effects of altitude and aerosol on UV radiation. *J. Geophys. Res. Atmos.* **2006**, *111*. [CrossRef]
7. Tesfaye, M.; Sivakumar, V.; Botai, J.; Mengistu Tsidu, G. Aerosol climatology over South Africa based on 10 years of Multiangle Imaging Spectroradiometer (MISR) data. *J. Geophys. Res. Atmos.* **2011**, *116*. [CrossRef]
8. Duflot, V.; Dils, B.; Baray, J.L.; De Mazière, M.; Attié, J.L.; Vanhaelewyn, G.; Senten, C.; Vigouroux, C.; Clain, G.; Delmas, R. Analysis of the origin of the distribution of CO in the subtropical southern Indian Ocean in 2007. *J. Geophys. Res. Atmos.* **2010**, *115*. [CrossRef]
9. Thompson, A.M.; Witte, J.C.; Hudson, R.D.; Guo, H.; Herman, J.R.; Fujiwara, M. Tropical tropospheric ozone and biomass burning. *Science* **2001**, *291*, 2128–2132. [CrossRef]
10. Piketh, S.J.; Annegarn, H.J.; Tyson, P.D. Lower tropospheric aerosol loadings over South Africa: The relative contribution of aeolian dust, industrial emissions, and biomass burning. *J. Geophys. Res. Atmos.* **1999**, *104*, 1597–1607. [CrossRef]
11. Sinha, P.; Jaeglé, L.; Hobbs, P.V.; Liang, Q. Transport of biomass burning emissions from southern Africa. *J. Geophys. Res. Atmos.* **2004**, *109*. [CrossRef]
12. Diab, R.D.; Thompson, A.M.; Mari, K.; Ramsay, L.; Coetzee, G.J.R. Tropospheric ozone climatology over Irene, South Africa, from 1990 to 1994 and 1998 to 2002. *J. Geophys. Res.* **2004**, *109*. [CrossRef]
13. Randles, C.A.; Ramaswamy, V. Direct and semi-direct impacts of absorbing biomass burning aerosol on the climate of southern Africa: A Geophysical Fluid Dynamics Laboratory GCM sensitivity study. *Atmos. Chem. Phys.* **2010**, *10*, 9819–9831. [CrossRef]
14. Edwards, D.P.; Emmons, L.K.; Gille, J.C.; Chu, A.; Attié, J.-L.; Giglio, L.; Wood, S.W.; Haywood, J.; Deeter, M.N.; Massie, S.T.; et al. Satellite-observed pollution from Southern Hemisphere biomass burning. *J. Geophys. Res. Atmos.* **2006**, *111*. [CrossRef]
15. Kumar, K.R.; Sivakumar, V.; Reddy, R.R.; Gopal, K.R.; Adesina, A.J. Inferring wavelength dependence of AOD and Ångström exponent over a sub-tropical station in South Africa using AERONET data: Influence of meteorology, long-range transport and curvature effect. *Sci. Total Environ.* **2013**, *461–462*, 397–408. [CrossRef]
16. Vakkari, V.; Kerminen, V.-M.; Beukes, J.P.; Tiitta, P.; van Zyl, P.G.; Josipovic, M.; Venter, A.D.; Jaars, K.; Worsnop, D.R.; Kulmala, M.; et al. Rapid changes in biomass burning aerosols by atmospheric oxidation. *Geophys. Res. Lett.* **2014**, *41*, 2644–2651. [CrossRef]

17. Monks, P.S.; Archibald, A.T.; Colette, A.; Cooper, O.; Coyle, M.; Derwent, R.; Fowler, D.; Granier, C.; Law, K.S.; Mills, G.E.; et al. Tropospheric ozone and its precursors from the urban to the global scale from air quality to short-lived climate forcer. *Atmos. Chem. Phys.* **2015**, *15*, 8889–8973. [CrossRef]
18. Klonecki, A.; Levy, H., II. Tropospheric chemical ozone tendencies in CO-CH4-NOy-H2O system: Their sensitivity to variations in environmental parameters and their application to a global chemistry transport model study. *J. Geophys. Res. Atmos.* **1997**, *102*, 21221–21237. [CrossRef]
19. Cooper, O.R.; Parrish, D.D.; Ziemke, J.; Cupeiro, M.; Galbally, I.E.; Gilge, S.; Horowitz, L.; Jensen, N.R.; Lamarque, J.-F.; Naik, V. Global distribution and trends of tropospheric ozone: An observation-based review. *Elem. Sci. Anthr.* **2014**. [CrossRef]
20. Sivakumar, V.; Ogunniyi, J. Ozone climatology and variability over Irene, South Africa determined by ground based and satellite observations. Part 1: Vertical variations in the troposphere and stratosphere. *Atmósfera* **2017**, *30*, 337–353. [CrossRef]
21. Adesina, A.J.; Kumar, K.R.; Sivakumar, V.; Griffith, D. Direct radiative forcing of urban aerosols over Pretoria (25.75° S, 28.28° E) using AERONET Sunphotometer data: First scientific results and environmental impact. *J. Environ. Sci.* **2014**, *26*, 2459–2474. [CrossRef]
22. NASA Goddard Space Flight Center, Goddard Earth Sciences Data and Information Services Center. AERONET Aerosol Optical Depth Data. Available online: https://aeronet.gsfc.nasa.gov/cgi-bin/data_display_aod_v3?site=Pretoria_CSIR-DPSS&nachal=2&level=3&place_code=10 (accessed on 25 November 2020).
23. Dubovik, O.; Holben, B.; Eck, T.F.; Smirnov, A.; Kaufman, Y.J.; King, M.D.; Tanré, D.; Slutsker, I. Variability of Absorption and Optical Properties of Key Aerosol Types Observed in Worldwide Locations. *J. Atmos. Sci.* **2002**, *59*, 590–608. [CrossRef]
24. NASA Goddard Space Flight Center, Goddard Earth Sciences Data and Information Services Center. Version 2 AOD Descriptions. Available online: https://aeronet.gsfc.nasa.gov/new_web/data_description_AOD_V2.html (accessed on 25 November 2020).
25. Eck, T.F.; Holben, B.N.; Reid, J.S.; Dubovik, O.; Smirnov, A.; O'neill, N.T.; Slutsker, I.; Kinne, S. Wavelength dependence of the optical depth of biomass burning, urban, and desert dust aerosols. *J. Geophys. Res. Atmos.* **1999**, *104*, 31333–31349. [CrossRef]
26. Schuster, G.L.; Dubovik, O.; Holben, B.N. Angstrom exponent and bimodal aerosol size distributions. *J. Geophys. Res. Atmos.* **2006**, *111*. [CrossRef]
27. Eck, T.F.; Holben, B.N.; Dubovik, O.; Smirnov, A.; Goloub, P.; Chen, H.B.; Chatenet, B.; Gomes, L.; Zhang, X.-Y.; Tsay, S.-C.; et al. Columnar aerosol optical properties at AERONET sites in central eastern Asia and aerosol transport to the tropical mid-Pacific. *J. Geophys. Res. Atmos.* **2005**, *110*. [CrossRef]
28. O'Neill, N.T.; Eck, T.F.; Holben, B.N.; Smirnov, A.; Dubovik, O.; Royer, A. Bimodal size distribution influences on the variation of Angstrom derivatives in spectral and optical depth space. *J. Geophys. Res. Atmos.* **2001**, *106*, 9787–9806. [CrossRef]
29. Holben, B.; Eck, T.; Slutsker, I.; Smirnov, A.; Sinyuk, A.; Schafer, J.; Giles, D.; Dubovik, O. *Aeronet's Version 2.0 Quality Assurance Criteria*; SPIE: Bellingham, WA, USA, 2006; Volume 6408.
30. NASA Goddard Space Flight Center, Goddard Earth Sciences Data and Information Services Center. AERONET Inversion Products (Version 3). Available online: https://aeronet.gsfc.nasa.gov/new_web/Documents/Inversion_products_for_V3.pdf (accessed on 25 November 2020).
31. Moosmüller, H.; Sorensen, C.M. Single scattering albedo of homogeneous, spherical particles in the transition regime. *J. Quant. Spectrosc. Radiat. Transf.* **2018**, *219*, 333–338. [CrossRef]
32. Thompson, A.M.; Witte, J.C.; Sterling, C.; Jordan, A.; Johnson, B.J.; Oltmans, S.J.; Fujiwara, M.; Vömel, H.; Allaart, M.; Piters, A.; et al. First Reprocessing of Southern Hemisphere Additional Ozonesondes (SHADOZ) Ozone Profiles (1998–2016): 2. Comparisons With Satellites and Ground-Based Instruments. *J. Geophys. Res. Atmos.* **2017**, *122*, 13000–13025. [CrossRef]
33. Witte, J.C.; Thompson, A.M.; Smit, H.G.J.; Fujiwara, M.; Posny, F.; Coetzee, G.J.R.; Northam, E.T.; Johnson, B.J.; Sterling, C.W.; Mohamad, M.; et al. First reprocessing of Southern Hemisphere ADditional OZonesondes (SHADOZ) profile records (1998–2015): 1. Methodology and evaluation. *J. Geophys. Res. Atmos.* **2017**, *122*, 6611–6636. [CrossRef]
34. Witte, J.C.; Thompson, A.M.; Smit, H.G.J.; Vömel, H.; Posny, F.; Stübi, R. First Reprocessing of Southern Hemisphere ADditional OZonesondes Profile Records: 3. Uncertainty in Ozone Profile and Total Column. *J. Geophys. Res. Atmos.* **2018**, *123*, 3243–3268. [CrossRef]
35. WMO. A three-dimensional science. *WMO Bull.* **1957**, *6*, 134–138.
36. Coetzee, G.J.R. *Pretoria Solar UVB Radiation Data*; SAWS: San Antonio, TX, USA, 2020.
37. SolarLight. Available online: https://solarlight.com/wp-content/uploads/Meters_Model-501-UVB.pdf (accessed on 7 March 2020).
38. Heckman, C.J.; Chandler, R.; Kloss, J.D.; Benson, A.; Rooney, D.; Munshi, T.; Darlow, S.D.; Perlis, C.; Manne, S.L.; Oslin, D.W. Minimal Erythema Dose (MED) Testing. *JoVE* **2013**, e50175. [CrossRef] [PubMed]
39. McKinlay, A.F.; Diffey, B.L. A reference action spectrum for ultraviolet erythema in human skin. *CIE J.* **1987**, *6*, 17–22.
40. Nollas, F.; Luccini, E.; Carbajal, G.; Orte, F.; Wolfran, E.; Hülsen, G.; Gröbner, J. *Report of the Fifth Erythemal UV Radiometers Intercomparison: Buenos Aires, Argentina, 2018*; World Meteorological Organisation: Geneva, Switzerland, 2019.
41. Cadet, J.-M.; Bencherif, H.; Portafaix, T.; Lamy, K.; Ncongwane, K.; Coetzee, G.J.R.; Wright, C.Y. Comparison of Ground-Based and Satellite-Derived Solar UV Index Levels at Six South African Sites. *Int. J. Env. Res. Public Health* **2017**, *14*, 1384. [CrossRef] [PubMed]
42. Bodeker, G.E.; McKenzie, R.L. An algorithm for inferring surface UV irradiance including cloud effects. *J. Appl. Meteorol.* **1996**, *35*, 1860–1877. [CrossRef]

43. du Preez, D.J.; Ajtić, J.V.; Bencherif, H.; Bègue, N.; Cadet, J.M.; Wright, C.Y. Spring and summer time ozone and solar ultraviolet radiation variations over Cape Point, South Africa. *Ann. Geophys.* **2019**, *37*, 129–141. [CrossRef]
44. Madronich, S. UV radiation in the natural and perturbed atmosphere. In *Environmental Effects of UV*; Tevini, M., Ed.; Lewis Publisher: Boca Raton, FL, USA, 1993.
45. Stamnes, K.; Tsay, S.-C.; Wiscombe, W.; Jayaweera, K. Numerically stable algorithm for discrete-ordinate-method radiative transfer in multiple scattering and emitting layered media. *Appl. Opt.* **1988**, *27*, 2502–2509. [CrossRef]
46. Palancar, G.G.; Lefer, B.L.; Hall, S.R.; Shaw, W.J.; Corr, C.A.; Herndon, S.C.; Slusser, J.R.; Madronich, S. Effect of aerosols and NO_2 concentration on ultraviolet actinic flux near Mexico City during MILAGRO: Measurements and model calculations. *Atmos. Chem. Phys.* **2013**, *13*, 1011–1022. [CrossRef]
47. Bhartia, P.K. *OMI/Aura TOMS-Like Ozone and Radiative Cloud Fraction L3 1 Day 0.25 Degree X 0.25 Degree V3*; NASA Goddard Space Flight Center Goddard Earth Sciences Data and Information Services Center: Greenbelt, MD, USA, 2012. [CrossRef]
48. Krotkov, N.A.; Lamsal, L.N.; Marchenko, S.V.; Celarier, E.A.; Bucsela, E.J.; Swartz, W.H.; Joiner, J. *OMI/Aura NO2 Cloud-Screened Total and Tropospheric Column L3 Global Gridded 0.25 Degree X 0.25 Degree V3*; NASA Goddard Space Flight Center, Goddard Earth Sciences Data and Information Services Center: Greenbelt, MD, USA, 2019. [CrossRef]
49. McPeters, R.D.; Labow, G.J. Climatology 2011: An MLS and sonde derived ozone climatology for satellite retrieval algorithms. *J. Geophys. Res. Atmos.* **2012**, *117*. [CrossRef]
50. Cunnold, D.M.; Wang, H.J.; Thomason, L.W.; Zawodny, J.M.; Logan, J.A.; Megretskaia, I.A. SAGE (version 5.96) ozone trends in the lower stratosphere. *J. Geophys. Res. Atmos.* **2000**, *105*, 4445–4457. [CrossRef]
51. Elterman, L. UV, Visible and IR attenuation for altitudes to 50 km. *Environ. Res. Pap.* **1968**, *285*.
52. Kinne, S. The MACv2 aerosol climatology. *Tellus B Chem. Phys. Meteorol.* **2019**, *71*, 1–21. [CrossRef]
53. Griffiths, P.T.; Keeble, J.; Shin, Y.M.; Abraham, N.L.; Archibald, A.T.; Pyle, J.A. On the Changing Role of the Stratosphere on the Tropospheric Ozone Budget: 1979–2010. *Geophys. Res. Lett.* **2020**, *46*, e2019GL086901. [CrossRef]
54. Mkololo, T.; Mbatha, N.; Sivakumar, V.; Bègue, N.; Coetzee, G.; Labuschagne, C. Stratosphere–Troposphere Exchange and O3 Variability in the Lower Stratosphere and Upper Troposphere over the Irene SHADOZ Site, South Africa. *Atmosphere* **2020**, *11*, 586. [CrossRef]
55. Kumar, K.R.; Sivakumar, V.; Yin, Y.; Reddy, R.R.; Kang, N.; Diao, Y.; Adesina, A.J.; Yu, X. Long-term (2003–2013) climatological trends and variations in aerosol optical parameters retrieved from MODIS over three stations in South Africa. *Atmos. Environ.* **2014**, *95*, 400–408. [CrossRef]
56. Power, H.C.; Willmott, C.J. Seasonal and interannual variability in atmospheric turbidity over South Africa. *Int. J. Clim.* **2001**, *21*, 579–591. [CrossRef]
57. Thompson, A.M.; Balashov, N.V.; Witte, J.C.; Coetzee, J.G.R.; Thouret, V.; Posny, F. Tropospheric ozone increases over the southern Africa region: Bellwether for rapid growth in Southern Hemisphere pollution? *Atmos. Chem. Phys.* **2014**, *14*, 9855–9869. [CrossRef]
58. Balashov, N.V.; Thompson, A.M.; Piketh, S.J.; Langerman, K.E. Surface ozone variability and trends over the South African Highveld from 1990 to 2007. *J. Geophys. Res. Atmos.* **2014**, *119*, 4323–4342. [CrossRef]
59. Cadet, J.-M.; Portafaix, T.; Bencherif, H.; Lamy, K.; Brogniez, C.; Auriol, F.; Metzger, J.-M.; Boudreault, L.-E.; Wright, C.Y. Inter-Comparison Campaign of Solar UVR Instruments under Clear Sky Conditions at Reunion Island (21° S, 55° E). *Int. J. Environ. Res. Public Health* **2020**, *17*, 2867. [CrossRef]
60. Lamy, K.; Portafaix, T.; Brogniez, C.; Godin-Beekmann, S.; Bencherif, H.; Morel, B.; Pazmino, A.; Metzger, J.M.; Auriol, F.; Deroo, C.; et al. Ultraviolet radiation modelling from ground-based and satellite measurements on Reunion Island, southern tropics. *Atmos. Chem. Phys.* **2018**, *18*, 227–246. [CrossRef]
61. Andrada, G.C.; Palancar, G.G.; Toselli, B.M. Using the optical properties of aerosols from the AERONET database to calculate surface solar UV-B irradiance in Córdoba, Argentina: Comparison with measurements. *Atmos. Environ.* **2008**, *42*, 6011–6019. [CrossRef]
62. Wenny, B.N.; Saxena, V.K.; Frederick, J.E. Aerosol optical depth measurements and their impact on surface levels of ultraviolet-B radiation. *J. Geophys. Res. Atmos.* **2001**, *106*, 17311–17319. [CrossRef]
63. Brühl, C.; Crutzen, P.J. On the disproportionate role of tropospheric ozone as a filter against solar UV-B radiation. *Geophys. Res. Lett.* **1989**, *16*, 703–706. [CrossRef]
64. Madronich, S.; Wagner, M.; Groth, P. Influence of Tropospheric Ozone Control on Exposure to Ultraviolet Radiation at the Surface. *Environ. Sci. Technol.* **2011**, *45*, 6919–6923. [CrossRef] [PubMed]
65. Clain, G.; Baray, J.-L.; Delmas, R.; Diab, R.; de Bellevue, J.L.; Keckhut, P.; Posny, F.; Metzger, J.-M.; Cammas, J.-P. Tropospheric ozone climatology at two Southern Hemisphere tropical/subtropical sites, (Reunion Island and Irene, South Africa) from ozonesondes, LIDAR, and in situ aircraft measurements. *Atmos. Chem. Phys.* **2009**, *9*, 1723–1734. [CrossRef]
66. Bencherif, H.; Toihir, A.M.; Mbatha, N.; Sivakumar, V.; du Preez, D.J.; Bègue, N.; Coetzee, G.J.R. Ozone Variability and Trend Estimates from 20-Years of Ground-Based and Satellite Observations at Irene Station, South Africa. *Atmosphere* **2020**, 11. [CrossRef]

Chapter 6 Results: Skin cancer risks associated with solar UVR exposure

6.1 Paper overview

Excessive exposure to solar UVR is a major contributing factor to the development of melanoma and keratinocyte cancer which includes BCC and SCC (Armstrong et al., 2001). Globally, the incidence rates of melanoma and keratinocyte cancers have increased (Apalla et al., 2017). South Africa is no exception and has one of the highest incidence rates of keratinocyte cancer, particularly among the fair skin population groups, in the world (Norval et al., 2014). Generally, the incidence rates of keratinocyte cancer among individuals with higher skin phototypes (FST IV/V) are lower compared to individuals with lower skin phototypes (FST I/II) (Diffey, 2018).

Skin phototype and occupation are important factors contributing to the overall skin cancer risk of an individual. Previous risk assessment studies do not account for different skin phototypes. Therefore, this manuscript aimed to assess the keratinocyte cancer risks for an indoor and outdoor worker in Cape Town using hypothetical exposure scenarios. The risk assessment included a novel approach to include individuals of different FSTs.

The widely used FST classification was not developed to determine skin cancer risks and is limited by the interdependency between susceptibility to burn and the ability to tan. Using a new SCP classification (Holm-Schou et al., 2019), South African population statistics and a previously-published FST classification of the South African population (Wilkes et al., 2015) were used to determine a risk ratio which was used to determine the BCC and SCC risk of individuals with different FSTs.

The lifetime risk was determined for an adult individual who works indoor and for an adult individual who works outdoors. Both individuals were deemed to have the same exposure until the age of 18 years which was based on the hypothetical exposure scenario of a school child aged 10 years. In the hypothetical scenarios, the exposure of the indoor worker was limited to lunchtimes on weekdays while the

exposure for the outdoor worker was assumed to be eight hours per weekday. A typical year was considered, i.e., no pandemic and lockdown conditions were applied.

The risk assessment of a typical indoor adult and outdoor adult worker found that irrespective of FST, outdoor workers had approximately 1.6 times more risk of BCC or SCC compared to an indoor worker of the same FST. Furthermore, individuals of FST I and FST II are most at risk, especially if they are outdoor workers.

6.2 Thesis contribution

This paper contributes to the fourth objective of this thesis which was to perform a keratinocyte cancer risk assessment for indoor and outdoor workers in the City of Cape Town, South Africa.

Using a quantitative risk calculation, the risk assessment was able to identify population groups that were at risk of developing BCC or SCC based on their exposure to solar UVR. These at-risk population groups included outdoor workers and individuals with fairer skin phototypes. The findings from risk assessment studies can be used to identify at-risk population groups for targeted skin cancer prevention campaigns.

6.3 Contribution of candidate

D. Jean du Preez was responsible for the data analysis, model simulations and writing the manuscript. All the co-authors contributed to the conceptualization, discussion, and final manuscript preparations.

The research presented in this chapter used hypothetical exposure scenarios and therefore ethical clearance was obtained for secondary data source from the University of Pretoria.

6.4 Publication status

du Preez, D.J., Wright, C.Y., Diffey, B.L., Roomaney, R.A. & Bencherif, H. (2021). Estimation of potential keratinocyte cancer risks from excess solar UVR exposure to inform sun exposure awareness programmes. In preparation.

6.5 References

Apalla, Z., Lallas, A., Sotiriou, E., Lazaridou, E., & Ioannides, D. (2017). Epidemiological trends in skin cancer. *Dermatology practical & conceptual, 7*(2), 1. doi:10.5826/dpc.0702a01

Armstrong, B. K., & Kricker, A. (2001). The epidemiology of UV induced skin cancer. *Journal of photochemistry and photobiology B: Biology, 63*(1-3), 8-18.

Diffey, B. L. (2018). Time and Place as Modifiers of Personal UV Exposure. *International Journal of Environmental Research and Public Health, 15*(6). doi:10.3390/ijerph15061112

Holm-Schou, A.-S. S., Philipsen, P. A., & Wulf, H. C. (2019). Skin cancer phototype: A new classification directly related to skin cancer and based on responses from 2869 individuals. *Photodermatology, photoimmunology & photomedicine, 35*(2), 116-123. doi:10.1111/phpp.12432

Norval, M., Kellett, P., & Wright, C. Y. (2014). The incidence and body site of skin cancers in the population groups of South Africa. *Photodermatology, photoimmunology & photomedicine, 30*(5), 262-265. doi:10.1111/phpp.12106262

Wilkes, M., Wright, C. Y., du Plessis, J. L., & Reeder, A. (2015). Fitzpatrick skin type, individual typology angle, and melanin index in an African population: Steps toward universally applicable skin photosensitivity assessments. *JAMA dermatology, 151*(8), 902-903. doi:10.1001/jamadermatol.2015.0351

6.6 Manuscript 4

Estimation of potential keratinocyte cancer risks from excess solar UVR exposure to inform sun exposure awareness programmes

D. Jean du Preez*[1,2], Caradee Yael Wright [1,3] , Brian L. Diffey [4] , Rifqah Abeeda Roomaney [5] , Hassan Bencherif [2,6]

[1]. Department of Geography, Geoinformatics and Meteorology, University of Pretoria, Pretoria, South Africa, [2]. Laboratoire de l'Atmosphère et des Cyclones (UMR 8105 CNRS, Université de La Réunion, MétéoFrance), 97744 Saint-Denis de La Réunion, France, [3]. Environmental and Health Research Unit, South African Medical Research Council, Pretoria, South Africa, [4]. Dermatological Sciences, Newcastle University, Newcastle Upon Tyne, United Kingdom, [5]. Burden of Disease Research Unit, South African Medical Research Council, Cape Town, South Africa, [6]. School of Chemistry and Physics, University of Kwa-Zulu Natal, Durban, South Africa.

*Corresponding author e-mail: dupreez.dj@tuks.co.za (D. Jean du Preez)

ABSTRACT

Solar ultraviolet radiation (UVR) exposure has been associated with adverse health effects including skin cancer. The risk of developing skin cancer is dependent on several factors related to sun exposure and personal characteristics such as Fitzpatrick skin phototype (FST). Using quantitative risk tools, the personal risks of developing basal cell carcinoma or squamous cell carcinoma were determined for two hypothetical scenarios (i.e., indoor and outdoor adult workers) for residents of Cape Town, South Africa. An indoor and an outdoor worker of FST I were more at risk of developing either cancer compared to an indoor worker of FST V. The potential risks associated with high levels of solar UVR exposure for different scenarios suggest that prevention programmes should be tailored for at-risk population groups such as indoor and outdoor workers with lightly pigmented skin.

INTRODUCTION

Exposure to solar ultraviolet radiation (UVR) and skin phototype are important factors in the development of skin cancer (1). Personal exposure to solar UVR is dependent on environmental factors as well as individual involvement in outdoor endeavours such as occupational or recreational activities (2).

Globally, the incidence of keratinocyte skin cancer has increased over time and can be attributed to environmental factors and personal sun exposure habits of individuals (3). Furthermore, this increase can also be due to the increased awareness of individuals and improved access to public health services (4). The development of keratinocyte cancer, both Basal cell carcinoma (BCC) and squamous cell carcinomas (SCC) (1) are linked to exposure to solar UVR. The development of BCC is liked to intermittent UVR exposure and has a higher incidence compared to SCC which is linked to chronic UVR exposure (5, 6).

Besides exposure to solar UVR, skin phototype is one of the key factors in the development of skin cancer. The Fitzpatrick skin phototype (FST) classification (Table 1) assesses the ability of an individual to tan and tendency to burn to classify individuals into one of six categories (7).

South Africa receives high levels of solar UVR throughout the year (8). The Western Cape province in South Africa is no exception and receives a mean daily exposure dose of 60 Standard Erythemal Dose (SED) units (1 SED = 100 Jm^{-2}) in December calculated using daily data between 2009 and 2018 (9). Furthermore, keratinocyte cancer is among the top ten

cancers in South Africa (10) and is likely to be underreported as has been found in other countries (11, 12).

Table 1. ***Fitzpatrick skin phototype classification (7). Standard Erythemal Dose (SED), where 1 SED is equal to 100 Jm^{-2}.***

FST	Skin characteristics	Standard dose for erythema (SED)
I	Extremely sensitive, white skin, light eyes, freckles	2 - 3
II	Overly sensitive, white skin, blonde hair, hazel/brown eyes	2.5 - 3.5
III	Moderately sensitive, light brown skin, brown hair, brown eyes	3 - 5
IV	Dark hair, light brown skin, dark eyes	4.5 - 6
V	Variable sensitivity, brown skin, brown eyes, dark brown or black hair	6 - 10
VI	Brown eyes, black skin, dark brown or black hair	10 - 20

Given the high surface solar UVR and high incidence of keratinocyte cancer in South Africa, this study aimed to determine a relative risk ratio for different skin phototypes and aimed to demonstrate how it could be used in skin cancer risk assessments. The study findings are important for tailoring skin cancer prevention and sun protection campaigns for identified at-risk population groups in Cape Town and probably the Western Cape province of South Africa.

DATA AND METHODS

To conduct a BCC and SCC risk assessment for individuals of different phototypes, first, a relative risk ratio had to be determined for each phototype. Once the relative risk ratio had been determined, it could be applied in a risk assessment using two hypothetical exposure scenarios.

FST weighting factor: To calculate a relative risk ratio for different phototypes that would be relevant to the South African population, the population statistics, the incidence rates of BCC and SCC for male and female in South Africa were used along with the skin cancer phototype (SCP) classification.

A study in 2014 classified South Africans according to their FST using individual typology angle (ITA) data from a sample group (13). These data showed that the South African population is spread across all FST categories. Using these findings and the population group (i.e., Black African, Indian/Asian, Coloured and White groups) estimates for South Africa in 2014 (14), the percentage of the South African population in each FST group were estimated (Table 2).

The South African National Cancer Registry Report for 2014 provided the age-standardised incidence rate of cancers per 100 000 by population group and gender (i.e., male and female) (14) (Table 3). Using the incidence of BCC and SCC by population group, the rate ratios were calculated for each population group using the Black African population as the reference group (Table 3). The rate ratios were calculated by dividing the incidence in each population group by the incidence of the Black African population.

Table 2. ***Population percentage (%) per population group and FST.***

	Black African		Indian/Asian		Coloured		White	
	Male	**Female**	**Male**	**Female**	**Male**	**Female**	**Male**	**Female**
FST I	0.0	0.0	0.0	0.0	0.0	0.0	4.9	4.9
FST II	0.0	0.0	0.2	0.1	3.3	3.3	3.1	3.2
FST III	0.4	0.4	0.4	0.3	0.0	0.0	0.35	0.34
FST IV	5.4	5.4	1.1	1.0	2.7	2.8	0.0	0.0
FST V	66.7	66.6	0.9	0.9	2.7	2.8	0.0	0.0
FST VI	7.8	7.8	0.0	0.0	0.0	0.0	0.0	0.0
Total	80.3	80.2	2.6	2.4	8.7	8.9	8.4	8.5

Tables 2 and 3 indicate population percentage in each FST group and the incidence of keratinocyte cancer relative to the Black African population, respectively. The next step was to determine the relative risk ratio for each phototype using the odds ratios from the SCP. These odds ratios relate skin phototype to skin cancer incidence.

Holm-Schou et al. proposed the SCP as the commonly used FST does not directly relate skin phototype to skin cancer incidence (15). The SCP was determined by using keratinocyte cancer incidence rates in Denmark, measurements of the melanin content in the skin and a questionnaire that independently asked the question of ability to tan and tendency to burn (15). In this study, a "weighted skin type" was calculated for each population group using the

population percentage per FST in Table 2. The "weighted skin type" and the rate ratios from Table 3 were linearly interpolated for the lowest weighted FST using the odds ratio from Holm-Schou et al (15). These interpolated values were the relative risk ratios that could then be used in a risk assessment study for individuals of different phototypes (Table 4).

Table 3. ***BCC and SCC incidence rates per 100 000 from the 2014 cancer registry of South Africa and the rate ratio of BCC and SCC for male and female using the Black African population as the reference group (noted as *).***

	Black African*		**Indian / Asian**		**Coloured**		**White**	
	Male	Female	Male	Female	Male	Female	Male	Female
BCC incidence	3.5	2.2	6.9	5.4	64.5	32.7	223.2	138.0
SCC incidence	3.5	2.0	3.2	2.6	29.9	11.5	84.5	38.8
Rate ratio - BCC	1.0	1.0	1.9	2.5	18.4	14.8	63.8	62.5
Rate ratio - SCC	1.0	1.0	0.9	1.2	8.5	5.6	24.1	19.1

Keratinocyte cancer risk assessment: The BCC and SCC cancer risk assessments were performed for each FST group using the relative risk ratio (Table 4) and for two hypothetical exposure scenarios. The scenarios included an indoor and outdoor worker in each FST group for both male and female. The risks were determined for the face area using a published risk assessment model of anatomically distributed solar UVR (16, 17).

Solar UVR data: Solar UVR data were used to determine the daily dose that an individual would receive based on their exposure scenario. The South African Weather Service (SAWS) has a network of surface UVR monitoring stations around South Africa. Data from the Cape

104 Town International Airport (33.97°S 18.6°E) (Fig. 1) station were obtained for a 10-year
105 period from 2009 to 2018. The station is in the Western Cape province of South Africa at 42 m
106 above sea level. The region is characterised by winter rainfall and hot, dry summers.

107 **Table 4.** ***A relative risk ratio of BCC and SCC for each FST based on incidence and population demographics***
108 ***of South Africa.***

FST	Relative risk ratio			
	BCC		SCC	
	Male	Female	Male	Female
I	68.2	66.8	25.7	20.4
II	58.4	57.2	22.0	17.5
III	33.0	32.3	12.5	9.9
IV	12.7	12.5	4.8	3.8
V	1.0	1.0	1.0	1.0

109 A Solar Light 501 UVB radiometer was used to measure solar UVR between 280 nm
110 and 315 nm and the instrument provides an analogue voltage output proportional to the
111 measured radiation. Due to financial constraints, the instrument was last calibrated in January
112 2012 (18). A comparison study found large differences between satellite and ground-based
113 erythemal UVR levels during certain periods. Annually there was a strong correlation between
114 the two datasets and during which period data availability was between 70 % and 85 % (19).

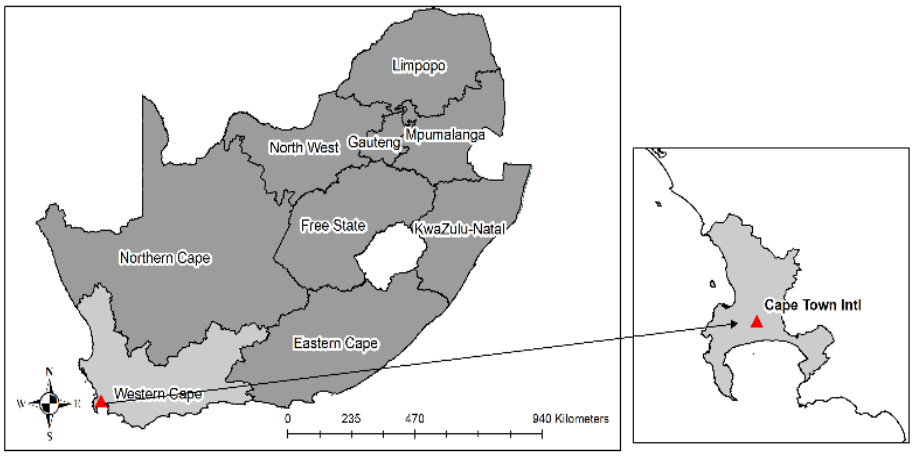

Figure 1. ***Map indicating the location of Cape Town International Airport and the City of Cape Town (light grey).***

The hourly UVR data from the radiometer was given in Minimal Erythemal Dose (MED) units. One MED unit is equal to 210 $J.m^{-2}$ and this was converted to SED, where 1 SED is equal to 100 $J.m^{-2}$. To convert this instrument-weighted UVB (280-315 nm) to erythemal-UVB (280-320 nm), a correction factor was used. For each hourly data point, the hourly solar zenith angle (SZA) and corresponding daily total column ozone value were used to select the correction factor from the calibration matrix. The calibration matrix is an estimate of the spectral and angular response functions of similar instruments (20). The instrument-weighted UVB were multiplied by the relevant correction factor to obtain the erythemal UVB before being converted to SED.

Risk calculations: To estimate the BCC and SCC risk, the daily dose was determined for each scenario by using an exposure fraction and relative risk ratio (Eq. 1). The exposure fraction accounted for the fraction of ambient UVR received on the face as keratinocyte cancers often develop on this anatomic site (among others) (21). The exposure fraction varies with SZA and assuming that the face receives a constant exposure, the exposure fraction was assumed to be one-sixth of the ambient erythemal exposure on weekdays in urban

environments. On weekends the exposure fraction was assumed to be one-quarter of the ambient erythemal exposure. (21). In the case of missing data, the relevant hourly and monthly average was used.

$$Daily\ dose = \sum UV_{ambient} \times EF \times FST \qquad \text{(Eq. 1)}$$

Where $\Sigma\ UV_{ambient}$ is the sum of the ambient UVR recorded by the radiometer for the duration of the time spent outdoors in each scenario and is multiplied by the fraction of UVR received by the face as well as the relative risk ratio.

The daily dose was calculated for 2013 as the UVR data was 85% complete and the lifetime risk was calculated for an adult of the age of 65 years since the highest number of new cases of BCC in 2014 in South Africa was recorded between the ages of 65-69 years for men and 70-74 for women. (14). Using the daily dose calculated in Equation 1 for each scenario, the annual was determined. The risk of BCC and SCC was calculated using the power-law equation (Eq. 2) for each FST (16). The relative risk for each

$$\text{Risk} \propto (\text{cumulative dose at age T})^{\beta-1} \sum [\text{annual dose at age (T-t)}]t^{\alpha-\beta} \qquad \text{(Eq. 2)}$$

Where T is the age and t is an integer between 0 and T. The constants α and β are based on the cumulative incidence and a biological amplification factor, respectively.

The values of α and β used in Equation 2 were different for the BCC and SCC risk assessments. For the BCC risk assessment, α and β were 3.2 and 1.7, respectively. For the SCC risk assessment, α and β were 5.1 and 2.3, respectively (22). The annual dose used in Equation 2 was based on the observed data from 2013 but the annual dose changed for the

149 childhood years as an individual is unlikely to receive a constant erythemal UVR dose
150 throughout his / her lifetime. Children have significantly more days with risky sun behaviour
151 compared to adults (23). Therefore two life stages were included: the first for childhood and
152 adolescence combined, and the second for adulthood. In Equation 2, a singular exposure dose
153 was used up until a predetermined age when exposure patterns were likely to change (defined
154 here as the age of 18 years) (17, 24).

155 In the childhood / adolescence stage, the exposure dose was based on the hypothetical
156 exposure of a school child (Table 5). Time spent outdoors during lunch breaks and after school
157 activities were included in the exposure scenario. The risk for the school child was not
158 calculated because keratinocyte cancer in children is rare (25). In the adulthood phase, two
159 different scenarios were used namely a hypothetical exposure scenario for indoor and outdoor
160 workers, respectively (Table 5). The scenario of an indoor adult worker during weekdays was
161 limited to their lunchtime because the exposure during their daily commute by car or public
162 transport was assumed to be low (26-28). The outdoor adult worker scenario was based on the
163 exposure of an individual who spends most of the weekdays outdoors and has the longest
164 exposure times.

165 The two adult scenarios were based on the results of previous sun exposure studies (29)
166 and similar to those used in other risk assessments conducted in the United Kingdom and
167 Australia (24, 30). These studies used exposure durations of five or more hours per day on
168 weekends and holidays and a similar approach was applied here. The scenarios in this study
169 assumed the worst-case, where no sun protection was used and the exposures on public
170 holidays and annual holidays were assumed to be the same as on weekends.

171

172 **Table 5.** ***The hypothetical personal exposure scenarios with exposure periods on weekdays, weekends and***
173 ***annual holidays.***

Occupation	Weekday exposure	Weekend exposure	Annual holiday
Childhood / adolescence	10:00-11:00 12:00-13:00 14:00-16:00	09:00-12:00 13:00-15:00	25 Mar-9 Apr 23 Jun-15 Jul 29 Sep-7 Oct 8 Dec–8 Jan
Indoor adult worker	13:00-14:00	10:00-15:00	17 Dec-13 Jan
Outdoor adult worker	07:00-11:00 12:00-18:00	09:00-14:00	2 Aug-21 Aug

174 # RESULTS

175 ## Solar Erythemal UVB climatology

176 The hourly erythemal UVR data were used to determine the monthly and hourly mean values.
177 This illustrated the seasonal and diurnal cycle of erythemal UVR at Cape Town (Fig. 2). During
178 the austral summer months of December, January, and February, solar erythemal UVR is at a
179 maximum, with daily maximums between 8 SED/h and 10 SED/h occurring between 13:00 and
180 15:00 local time.

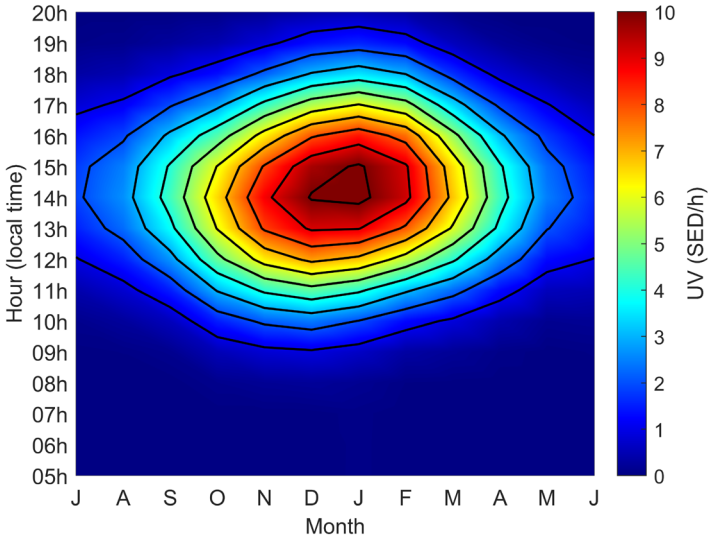

Figure 2. Exposure dose rates as a function of time of the day and month averaged over the period 2008-2018 for Cape Town International Airport, South Africa.

Due to the relatively high latitudinal position of Cape Town (i.e., 34°S) solar erythemal UVB of 4 to 5 SED/h can be observed as late as 17:00 local time during summer months. During the austral winter, solar erythemal UVB is at a minimum with a daily maximum of 3 to 4 SED/h between 13:00 and 15:00 local time. The daily erythemal UVR maximum occurred at solar noon provided clouds did not attenuate incoming solar UVR.

Keratinocyte cancer risk assessments results

The BCC and SCC risks were calculated for the facial area of the indoor and outdoor adult worker using the exposure fraction and the relevant risk ratio for each FST and gender.

BCC risk assessment: In the risk assessment of BCC for the indoor and outdoor worker (Table 6), indicate the relative risk for each FST group relative to the indoor worker of FST V for that gender (i.e. A male outdoor worker of FST I is relative to the male indoor worker of FST V). Overall, indoor and outdoor workers of FST I-IV are more at risk compared to an indoor

worker of FST V irrespective of gender. Furthermore, the male and female outdoor workers in each FST group were more at risk compared to an indoor worker of the same FST group. The relative risk for a male and female outdoor worker of FST I was 20.

Table 6. BCC relative risk for indoor and outdoor workers in each FST group.

	Relative skin cancer risk per FST				
	I	**II**	**III**	**IV**	**V**
Indoor - Male	13	10	4	1	1
Outdoor - Male	20	16	6	1	1
Indoor - Female	13	10	4	1	1
Outdoor - Female	20	15	6	1	1

SCC risk assessment: In the risk assessment of SCC for the indoor and outdoor worker (Table 7), showed a similar overall pattern compared to the relative risk for BCC risk where lower FST types had more risk compared to higher FST types. The relative risk difference between FST I and FST V in SCC are much lower than compared to BCC. This is due to the lower incidence of BCC compared to SCC.

DISCUSSION

Understanding the role that skin phototype plays in the development of keratinocyte cancer can identify at-risk population groups. Given the range of FSTs and incidence of skin cancer in

South Africa, a risk assessment model was altered to consider different FSTs in what we consider to be the first application of its kind. For their lifetime, the indoor and outdoor worker received solar UVR exposure for 47 707 hours and 76 471 hours, respectively. The lifetime dose received irrespective of skin type of 82 0212 SED and 106 2826 SED for the indoor and outdoor worker respectively.

Table 7. SCC relative risk for indoor and outdoor workers in each FST group.

	Relative skin cancer risk per FST				
	I	**II**	**III**	**IV**	**V**
Indoor - Male	18	12	3	1	1
Outdoor - Male	32	22	6	2	2
Indoor - Female	10	7	2	1	1
Outdoor - Female	19	13	4	2	1

Previous studies have shown that occupation plays an important role in determining the solar UVR exposure dose received by an individual (31-34) and the relative risks of keratinocyte cancer (35-37). Zink et al. (35) recently found that outdoors workers, such as gardeners, mountain guides and farmers had higher keratinocyte cancer incidence compared with indoor workers; despite this, many workers (and their employees) do not consider the occupational risk of developing skin cancer from excess sun exposure (11). In South Africa, there are no national limits for occupational solar UVR exposure (38). Given the known

occupational risk of excess solar UVR exposure, such limits are important to reduce the risks posed to individuals in outdoor occupations.

The lifetime dose received on the face of the outdoor worker was approximately 1.3 times greater than that of the indoor worker. In comparison, Austrian outdoor workers received between 2 and 2.5 times the annual dose of indoor workers (39). The difference can be attributed to the anatomical site used in the risk assessment as well as the exposure patterns and clothing worn.

The risk assessment for BCC and SCC for indoor and outdoor working adults suggested that an outdoor worker is more at risk of developing BCC or SCC than an indoor worker. The largest difference in relative risk (Table 6 and 7) was between BCC and SCC.

The largest difference in relative risk was seen in the lower FST groups. Where the relative risk of an outdoor worker was approximately 1.7 times that of an indoor worker. Among Australian mail, delivery personnel were found to be between 1.1 and 5.5 times greater risk of keratinocyte skin cancer compared to indoor workers (30). The higher relative risk of an outdoor worker of FST I-III compared to an indoor worker, suggest that sun exposure and skin phototype play an important role in estimate BCC and SCC risks. Several studies confirm the higher prevalence of keratinocyte cancers among individuals with lower FST (40, 41). For example, in southern Spain, individuals from northern Europe with lower FST were more prone to keratinocyte skin cancer than the local Spanish population who have a higher FST (42).

From the National Cancer Registry of South Africa, the incidence of both BCC and SCC is lower in females than males across FST groups. This pattern has been observed around

the world where the include of keratinocyte cancer is higher in men than in women (43, 3). Females, in general, had a lower risk of both BCC and SCC and investigating the risks of females relative to males would improve the understanding of cancer risks posed to each gender.

Limitations: The risk assessment model included two different exposure scenarios but did not account for changes in personal exposure due to seasonal weather (which is likely to affect an individual's outdoor behaviour and solar UVR exposure patterns), or differences in the personal solar UVR exposure of males and females. Furthermore, individual factors such as personal preference for sun protection and annual summer holiday destinations further impact UVR exposure (44) and risk (45-47).

The calibration of the biometer was noted as a limitation although the data have been used in recently published studies (9, 19). The National Cancer Registry (NCR) of South Africa is an invaluable dataset but under-reporting of cancer has been identified from the private healthcare sector which services a small percentage of the population (48).

CONCLUSION*:* Using population statistics, cancer incidence rates and known ratios that relate skin cancer to skin phototype allowed for the development of a "weighting factor" that could be used to assess the BCC and SCC risk of individuals with different skin phototypes. Estimating the risk of BCC and SCC among indoor and outdoor adult workers of different FSTs living in Cape Town revealed that outdoor adult workers, as well as individuals of FST I – III, were more at risk for developing both BCC and SCC compared to any other outdoor or indoor workers. Occupational sun protection awareness and skin cancer prevention campaigns

should be developed to advise workers to take precautions such as using clothing, hats, shade, sunscreen and avoiding exposure during peak ambient solar UVR periods.

ACKNOWLEDGMENTS: This work was undertaken in the framework of the French South-African International Research Project ARSAIO (Atmospheric Research in Southern African and Indian Ocean). D. Jean du Preez received a doctoral scholarship from the University of Pretoria, the National Research Foundation (NRF) and the French embassy in South Africa. Caradee Y. Wright receives funding from the South African Medical Research Council and the National Research Foundation (NRF).

REFERENCES

1. Armstrong, B. K. and A. Kricker (2001) The epidemiology of UV induced skin cancer. *Journal of photochemistry and photobiology B: Biology* **63,** 8-18.
2. Diffey, B. L. (2018) Time and Place as Modifiers of Personal UV Exposure. *Int. J. Environ. Res. Public Health* **15**.
3. Apalla, Z., A. Lallas, E. Sotiriou, E. Lazaridou and D. Ioannides (2017) Epidemiological trends in skin cancer. *Dermatology practical & conceptual* **7,** 1.
4. Welch, H. G., B. L. Mazer and A. S. Adamson (2021) The Rapid Rise in Cutaneous Melanoma Diagnoses. *New England Journal of Medicine* **384,** 72-79.
5. Watson, M., D. M. Holman and M. Maguire-Eisen (2016) Ultraviolet Radiation Exposure and Its Impact on Skin Cancer Risk. *Seminars in Oncology Nursing* **32,** 241-254.
6. Wright, C. Y., M. Norval, T. Kapwata, D. J. du Preez, B. Wernecke, B. M. Tod and W. I. Visser (2019) The Incidence of Skin Cancer in Relation to Climate Change in South Africa. *Atmosphere* **10,** 634.
7. Fitzpatrick, T. B. (1988) The Validity and Practicality of Sun-Reactive Skin Types I Through VI. *Archives of Dermatology* **124,** 869-871.
8. Lucas, R. M., M. Norval and C. Y. Wright (2016) Solar ultraviolet radiation in Africa: a systematic review and critical evaluation of the health risks and use of photoprotection. *Photochemical & Photobiological Sciences* **15,** 10-23.
9. Cadet, J.-M., H. Bencherif, D. J. du Preez, T. Portafaix, N. Sultan-Bichat, M. Belus, C. Brogniez, F. Auriol, J.-M. Metzger, K. Ncongwane, G. J. R. Coetzee and C. Y. Wright (2019) Solar UV Radiation in Saint-Denis, La Réunion and Cape Town, South Africa: 10 years Climatology and Human Exposure Assessment at Altitude. *Atmosphere* **10,** 589.
10. NICD (2014) Cancer in South Africa 2014. National Cancer Registry.

11. Gobba, F., A. Modenese and S. M. John (2019) Skin cancer in outdoor workers exposed to solar radiation: a largely underreported occupational disease in Italy. *Journal of the European Academy of Dermatology and Venereology* **33,** 2068-2074.
12. Sella, T., I. Goren, V. Shalev, H. Shapira, J. Zandbank, J. Rosenblum, M. G. Kimlin and G. Chodick (2015) Incidence trends of keratinocyte skin cancers and melanoma in Israel 2006–11. *Br. J. Dermatol* **172,** 202-207.
13. Wilkes, M., C. Y. Wright, J. L. du Plessis and A. Reeder (2015) Fitzpatrick skin type, individual typology angle, and melanin index in an African population: Steps toward universally applicable skin photosensitivity assessments. *JAMA dermatology* **151,** 902-903.
14. StatsSA (2014) Mid-year population estimates. Statistics South Africa.
15. Holm-Schou, A.-S. S., P. A. Philipsen and H. C. Wulf (2019) Skin cancer phototype: A new classification directly related to skin cancer and based on responses from 2869 individuals. *Photodermatol. Photoimmunol. Photomed.* **35,** 116-123.
16. Schothorst, A., H. Slaper, R. Schouten and D. Suurmond (1985) UVB doses in maintenance psoriasis phototherapy versus solar UVB exposure. *Photo-dermatology* **2,** 213-220.
17. Slaper, H. and J. C. Van der Leun (1987) Human exposure to ultraviolet radiation: quantitative modelling of skin cancer incidence. *Human Exposure to Ultraviolet Radiation***,** 155-171.
18. SolarLight Available at: https://solarlight.com/wp-content/uploads/Meters_Model-501-UVB.pdf. Accessed on 7 March 2019.
19. Cadet, J.-M., H. Bencherif, T. Portafaix, K. Lamy, K. Ncongwane, G. J. R. Coetzee and C. Y. Wright (2017) Comparison of Ground-Based and Satellite-Derived Solar UV Index Levels at Six South African Sites. *Int. J. Environ. Res. Public Health* **14,** 1384.
20. Nollas, F., E. Luccini, G. Carbajal, F. Orte, E. Wolfran, G. Hülsen and J. Gröbner (2019) Report of the fifth erythemal UV radiometers intercomparison: Buenos Aires, Argentina, 2018.
21. Diffey, B. L. (2017) *Sun Protection: A risk management approach.* IOP Publishing, Bristol, UK.
22. NRPB (1995) Health Effects from Ultraviolet Radiation. In *Report of an Advisory Group on Non-ionising Radiation*, Vol. 6.
23. Thieden, E., P. A. Philipsen, J. Sandby-Møller, J. Heydenreich and H. C. Wulf (2004) Proportion of lifetime UV dose received by children, teenagers and adults based on time-stamped personal dosimetry. *Journal of Investigative Dermatology* **123,** 1147-1150.
24. Diffey, B. L. (1992) Stratospheric ozone depletion and the risk of non-melanoma skin cancer in a British population. *Physics in Medicine & Biology* **37,** 2267.
25. Fogel, A. L., K. Y. Sarin and J. Teng (2017) Genetic diseases associated with an increased risk of skin cancer development in childhood. *Current Opinion in Pediatrics* **29,** 426-433.
26. Baczynska, K., M. Khazova and J. O'hagan (2019) Sun exposure of indoor workers in the UK–survey on the time spent outdoors. *Photochemical & Photobiological Sciences* **18,** 120-128.

27. Schmalwieser, A. W., C. Enzi, S. Wallisch, F. Holawe, B. Maier and P. Weihs (2010) UV exposition during typical lifestyle behavior in an urban environment. *Photochem. Photobiol* **86,** 711-715.
28. Thieden, E., A.-S. S. Holm-Schou, P. A. Philipsen, J. Heydenreich and H. C. Wulf (2019) Adult UVR exposure changes with life stage – a 14-year follow-up study using personal electronic UVR dosimeters. *Photochemical & Photobiological Sciences* **18,** 467-476.
29. Guy, C. and R. Diab (2002) A health risk assessment of ultraviolet radiation in Durban. *S. Afr. Geogr. J.* **84,** 208-213.
30. Vishvakarman, D. and J. Wong (2003) Description of the use of a risk estimation model to assess the increased risk of non-melanoma skin cancer among outdoor workers in Central Queensland, Australia. *Photodermatol. Photoimmunol. Photomed.* **19,** 81-88.
31. Modenese, A., L. Korpinen and F. Gobba (2018) Solar radiation exposure and outdoor work: an underestimated occupational risk. *Int. J. Environ. Res. Public Health* **15,** 2063.
32. Grandahl, K., P. Eriksen, K. S. Ibler, J. P. Bonde and O. S. Mortensen (2018) Measurements of Solar Ultraviolet Radiation Exposure at Work and at Leisure in Danish Workers. *Photochem. Photobiol* **94,** 807-814.
33. Peters, C. E., E. Pasko, P. Strahlendorf, D. L. Holness and T. Tenkate (2019) Solar Ultraviolet Radiation Exposure among Outdoor Workers in Three Canadian Provinces. *Ann. Work Expo. Health* **63,** 679-688.
34. Moldovan, H. R., M. Wittlich, S. M. John, R. Brans, G. S. Tiplica, C. Salavastru, S. T. Voidazan, R. C. Duca, E. Fugulyan, G. Horvath, A. Alexa and A. I. Butacu (2020) Exposure to solar UV radiation in outdoor construction workers using personal dosimetry. *Environ. Res* **181,** 108967.
35. Zink, A., L. Tizek, M. Schielein, A. Böhner, T. Biedermann and M. Wildner (2018) Different outdoor professions have different risks – a cross-sectional study comparing non-melanoma skin cancer risk among farmers, gardeners and mountain guides. *Journal of the European Academy of Dermatology and Venereology* **32,** 1695-1701.
36. Paulo, M. S., B. Adam, C. Akagwu, I. Akparibo, R. H. Al-Rifai, S. Bazrafshan, F. Gobba, A. C. Green, I. Ivanov, S. Kezic, N. Leppink, T. Loney, A. Modenese, F. Pega, C. E. Peters, A. M. Prüss-Üstün, T. Tenkate, Y. Ujita, M. Wittlich and S. M. John (2019) WHO/ILO work-related burden of disease and injury: Protocol for systematic reviews of occupational exposure to solar ultraviolet radiation and the effect of occupational exposure to solar ultraviolet radiation on melanoma and non-melanoma skin cancer. *Environment International* **126,** 804-815.
37. Peters, C. E., J. Kim, C. Song, E. Heer, V. H. Arrandale, M. Pahwa, F. Labrèche, C. B. McLeod, H. W. Davies, C. B. Ge and P. A. Demers (2019) Burden of non-melanoma skin cancer attributable to occupational sun exposure in Canada. *International Archives of Occupational and Environmental Health* **92,** 1151-1157.
38. Wright, C. Y., M. C. Ramotsehoa, J. L. Du Plessis, M. Wittlich and C. E. Peters (2017) Solar UV radiation-induced non-melanoma skin cancer as an occupational reportable disease: international experience to inform South Africa. *Occupational Health Southern Africa* **23,** 10-17.

39. Milon, A., J. L. Bulliard, L. Vuilleumier, B. Danuser and D. Vernez (2014) Estimating the contribution of occupational solar ultraviolet exposure to skin cancer. *Br. J. Dermatol* **170,** 157-164.
40. Climstein, M., J. Furness, W. Hing and J. Walsh (2016) Lifetime prevalence of non-melanoma and melanoma skin cancer in Australian recreational and competitive surfers. *Photodermatol. Photoimmunol. Photomed.* **32,** 207-213.
41. Diepgen, T. L. and V. Mahler (2002) The epidemiology of skin cancer. *Br. J. Dermatol* **146,** 1-6.
42. Aguilar Bernier, M., F. Rivas Ruiz, M. De Troya Martín and N. Blázquez Sánchez (2012) Comparative epidemiological study of non-melanoma skin cancer between Spanish and north and central European residents on the Costa del Sol. *Journal of the European Academy of Dermatology and Venereology* **26,** 41-47.
43. Madan, V., J. T. Lear and R.-M. Szeimies (2010) Non-melanoma skin cancer. *The Lancet* **375,** 673-685.
44. Thieden, E., P. A. Philipsen, J. Heydenreich and H. C. Wulf (2004) UV radiation exposure related to age, sex, occupation, and sun behavior based on time-stamped personal dosimeter readings. *Archives of dermatology* **140,** 197-203.
45. Diffey, B. L. (2008) A behavioral model for estimating population exposure to solar ultraviolet radiation. *Photochem. Photobiol* **84,** 371-375.
46. Downs, N. J., T. Axelsen, A. V. Parisi, P. W. Schouten and B. R. Dexter (2020) Measured UV Exposures of Ironman, Sprint and Olympic-Distance Triathlon Competitors. *Atmosphere* **11,** 440.
47. Downs, N. J., P. W. Schouten, A. V. Parisi and J. Turner (2009) Measurements of the upper body ultraviolet exposure to golfers: non-melanoma skin cancer risk, and the potential benefits of exposure to sunlight. *Photodermatol. Photoimmunol. Photomed.* **25,** 317-324.
48. Singh, E., J. Underwood, C. Nuttey, C. Babb, M. Sengayi and P. Kellett (2015) South African National Cancer Registry: Effect of withheld data from private health systems on cancer incidence estimates. *S. Afr. Med. J.* **105**.

Chapter 7 Summary, limitations and recommendations

Previous research has shown that decreases in stratospheric ozone in the Southern Hemisphere can be due to the dilution of the Antarctic polar vortex in the austral spring. This can result in anomalously high UVR at the surface and has been observed over South America and Australia. The research presented in Chapter 3 investigated the relationship between atmospheric ozone and surface UVR. The research further investigated the origin of ozone-poor air masses present over Cape Point and their impact on surface UVR. The findings and recommendations from Chapter 3 are summarised below:

- The results indicated that the strongest inverse relationship between stratospheric ozone and UVR occurs at SZA 25° and that decreases in stratospheric ozone resulted in increased UVR at the surface.
- Using a dynamical transport model, decreases in stratospheric ozone observed over Cape Point were identified to originate from the sub-tropical regions rather than from the Antarctic polar vortex.

The relationship between surface UVR and atmospheric parameters is complex and could be further invested at specific SZAs. The radiative effect of aerosols at Cape Point should be invested as well. Investigating the relationship between latitude and the polar vortex could indicate why South Africa is not impacted by the Antarctic ozone hole. Although this study did not investigate the effect of ozone recovery on ozone anomalies, understanding how ozone recovery has affected ozone anomalies and the recovery of stratospheric ozone over South Africa would contribute to valuable knowledge in this area of research. Additionally, investigating the role of the subtropical barrier on the transport of ozone from the subtropics to the midlatitudes would improve our understanding of the transport of ozone over Southern Africa.

The volcanic plume from the 2011 PCCVC eruption increased the aerosol loading and impacted surface UVR stations around South America. The dispersion of the volcanic plume across the Southern Hemisphere has been widely demonstrated but the impact on South Africa has not investigated. The research presented in Chapter 4 aimed to address this by investigating the impact on AOD and surface UVB at

Cape Point, South Africa. The findings and recommendations from Chapter 4 are summarised below:

- The volcanic plume from the PCCVC eruption in June 2011 was located near Cape Point several days after the eruption. At the time when the plume was located near Cape Point, ground-based observation of AOD increased. The increases were above the climatological monthly mean and the increase in AOD could be attributed to the passage of the plume.
- Small changes in surface UVR were observed between 20°S and 60°S which may be due to the large SZAs (>65°) which occur during the austral winter.
- Using a vertical aerosol profile and additional chemical species would improve the FLEXPART simulations. Furthermore, using the aerosol profiles would enable the accurate estimation of surface UVR in radiative transfer models.

The radiative effect of aerosols over Southern African has been demonstrated in previous research but has not included the radiative effect of tropospheric ozone. With tropospheric ozone levels increasing globally, it is important to understand its impact on surface UVR. The research presented in Chapter 5 investigated the radiative effect of aerosols and tropospheric ozone during the biomass burning season over Irene. Using the TUV radiative transfer model, the sensitivity of surface UVR to aerosols and tropospheric ozone from biomass burning was assessed in relation to the background levels of aerosols and tropospheric ozone. The findings and recommendations from Chapter 5 are summarised below:

- By comparing observed UVR and modelling UVR from different simulations, the sensitivity study showed that aerosols from biomass burning have a much larger radiative effect compared to tropospheric ozone from biomass burning.
- The simulations indicated that aerosol emitted from biomass burning can impact surface UVR by as much as 14% while tropospheric ozone from biomass burning has a radiative effect of approximately 1%.
- Future research on this topic should make use of vertical profiles of aerosols and ozone to improve the radiative transfer model simulations.

Skin cancer incidence rates and previous research have indicated that sun exposure and FST plays an important role in determining the BCC or SCC risk of an individual. While previous research has included various exposure scenarios, these studies did not account for individuals with different FSTs. The research presented in Chapter 6, estimated the relative risk of developing BCC or SCC among indoor and outdoor adult workers of different FSTs working in Cape Town. In this research, a "weighing factor" was determined and applied in a risk assessment of individuals with different FSTs. The findings and recommendations from Chapter 6 are summarised below:

- The risk assessment indicated that outdoor workers of any FST were at greater risk compared to their indoor working counterparts.
- Individuals of FST I – III were more at risk compared to an individual of FST V.
- The risk assessment assumed the worst-case scenario where individuals did not use any sun protection such as sunscreen or hats and their exposure remained constant throughout the year. The constant exposure is unlikely due to changes in weather conditions and personal habits and should be accounted for in future research.
- This risk assessment focused on BCC and SCC risk in relation to solar UVR exposure as the incidence of these cancers are much higher compared to melanoma cancer. Furthermore, the relation between melanoma cancer and solar UVR exposure is more complex and therefore should be the focus of future research. This should include the melanoma cancer risk assessment for different phototypes (i.e., FSTs).

The results presented in this thesis demonstrate the relationship between atmospheric parameters and solar UVR at the surface over South Africa. Understanding the influence of atmospheric parameters on surface UVR can lead to the identification of days with increased surface UVR and a relevant warning for the general public. Furthermore, population groups with the highest risk of keratinocyte cancer can be targeted for awareness campaigns.